UNIVERSITY OF WARMIA AND MAZURY IN OLSZTYN

Technical Sciences

17(2) 2014

PUBLISHER UWM

OLSZTYN 2014

The Technical Sciences is indexed and abstracted in BazTech (http://baztech.icm.edu.pl) and in IC Journal Master List (http://journals.indexcopernicus.com)

The Journal is also available in electronic form on the websites
http://www.uwm.edu.pl/techsci (subpage Issues)
http://wydawnictwo.uwm.edu.pl (subpage Czytelnia)

The print edition is the primary version of the Journal

PL ISSN 1505-4675

Address
ul. Jana Heweliusza 14
10-718 Olsztyn-Kortowo, Poland
tel.: +48 89 523 36 61
fax: +48 89 523 34 38
e-mail: wydawca@uwm.edu.pl

Ark. wyd. 8,0, ark. druk. 6,5, nakład 95 egz.
Druk – Zakład Poligraficzny UWM w Olsztynie
zam. nr 369

Contents

Technical Sciences 17(2), 2014, 87–103

EUROPEAN VERTICAL REFERENCE FRAME EVRF2007

***Adam Łyszkowicz*[1], *Anna Bernatowicz*[2]**

[1] Chair of Land Surveying and Geoinformatics
University of Warmia and Mazury in Olsztyn
[2] Chair of Land Surveying
Koszalin University of Technology

Received 3 March 2014, accepted 26 April 2014, available on line 4 May 2014

K e y w o r d s: Vertical reference system and frame, levelling networks, tide corrections.

A b s t r a c t

In Poland at the end of 2013 was completed implementation of the *European Vertical Refrence Frame* EVRF2007 in the country. This frame is the result of twenty years of works of the Subcommittee EUREF IAG. The paper in a condensed way describes the successive stages of development of the EVRF2007 frame in order to allow the readers to understand its essence.

In the first part of the work are given definitions and how the EVRF2000 frame has been implemented and then is described how the system has been improved. Then the EVRF2007 is characterized with particular attention paid to the vertical movements of the earth crust and tidal corrections.

Introduction

Height reference system is defined by the reference surface (geoid) and height. If the reference surface and height depend on the Earth's gravity field, such system is called a physical height system. If it is not related to the gravity, it is the geometrical height system. Normal and orthometric heights, obtained from the levelling and gravity measurements, are typical physical height systems.

The level surface (geoid) in respect to which the heights are defined, in practice is defined by the mean sea level, which is estimated at one or more tide gauge stations. The tide gauge stations of the national European height systems are located at various seas: the Baltic Sea, the North Sea, the Mediterranean Sea, the Black Sea and the Atlantic Ocean. Differences in mean

* Correspondence: Adam Łyszkowicz, Katedra Geodezji Szczegółowej, Uniwersytet Warmińsko-Mazurski, ul. Heweliusza 12, 10-724 Olsztyn, phone 48 89 523 48 78, e-mail: adaml@uwn.edu.pl

sea levels of these seas come to several decimeters, what causes that heights in different countries related to different surfaces differ amongst themselves.

First definition of the European Vertical Reference System (EVRS)

In order to unify the local vertical systems in Europe, in 2000 the *European Vertical Reference System, EVRS* was defined (IHDE and AUGATH 2000) as follows:

– The vertical datum in this system is the equipotential surface for which the Earth gravity field potential W_0 is equal to the normal potential of the mean Earth ellipsoid U_0

$$W_0 = U_0 = \text{const} \tag{1}$$

– The height component is the difference ΔW_P between the potential W_P of the Earth gravity field in the considered points P and the potential W_0 of the EVRS zero level. The potential difference – ΔW_P is also called a geopotential number C_P and its equivalent is the normal height,

– The EVRS is a zero tidal system accordingly to the IAG Resolution.

Practical realization of the EVRF2000

The practical realization of any height system is a vertical frame (datum). The first practical realization of the EVRS was result of the adjustment of the UELN-95/98 network.

The starting point of the UELN-95 project was levelling data from Western Europe so called the UELN-73 network, which was adjusted once more in 1986. Afterward the new data were included to the UELN-73 network from the precise levelling campaigns from the Czech Republic, Hungary, Slovenia, Poland and Slovakia also eastern part of Germany (former GDR). The UELN-95 network was then adjusted, step by step, as a nodal network of the geopotencial heights referred to the Normaal Amsterdams Peil NAP at Amsterdam (tide) gauge (LANG, SACHER 1995, SACHER at al. 1999). A consequence of this the geopotential number of NAP is zero:

$$C_{\text{NAP}} = 0 \tag{2}$$

and in practice the EVRF2000 datum is fixed through the geopotential number and the equivalent normal height of the reference point of the UELN No. 000A2530/13600 located near to the gauge in Amsterdam (Table 1).

Table 1

Characteristic of EVRF2000 reference point

Station name	UELN number	Position in ETRS89	Height in UELN 95/98		Gravity in IGSN71
		ellipsoidal latitude and longitude	geopotential number in m^2s^{-2}	normal height in m	in ms^{-2}
Reference point 000A2530 Netherlands	13600	52° 22' 53' 4°54' 34'	7.0259	0.71599	9.81277935

Source: IHDE, AUGATH (2000)

In January 1999 the results of the adjustment of the network have been passed on to the participating countries in the project under the name the UELN-95/98 (Fig. 1). In addition to the results of the adjustment also report prepared by the UELN Data Centre was handed over. It describes the adjustment method and the manner of calculating normal heights. A year later, after the EUREF symposium in Tromso in 2000, the realization of the UELN-95/98 solution as the *European Vertical Reference Frame* (EVRF2000) was accepted.

Fig. 1. UELN-95 network, December 1998

Source: ADAM et al. (2000).

New definition of the European Vertical Reference System

Realization of the *European Vertical Reference Frame* EVRF2000 has provided heights in Europe with the accuracy of a few decimeters. This accuracy is satisfying only for the GIS users. In order to improvement the EVRS system a revision of the EVRS2000 realization, conventions and parameters was made (IHDE, AUGAT 2000).

As a result of the work carried out in 2008 a new definition of the *European Vertical System* named EVRS2007 was given (IHDE et al. 2008). According to this definition EVRS is a geopotential reference system related to the Earth gravity field and rotates with the Earth. In this system positions of points are defined by geopotential values in relation to the reference potential and by corresponding coordinates (*X, Y, Z*) defined in a *Terrestrial Reference System* (TRS).

On the contrary the *European Vertical Reference Frame* (EVRF) is a collection of physical points with precisely determined differences of geopotential in respect to a reference potential W_0 at a defined epoch. Positions of the points are defined by the coordinates (*X, Y, Z*) in a specific spatial coordinate system attached to a *Terrestrial Reference System*. Therefore the EVRF is the realization of the EVRS at a defined epoch. Accordingly to this definition the *European Vertical Reference System* is a kinematic height system.

Definition of this system fulfils the following conventions (IHDE at al. 2008):

– The vertical datum is equipotential surface for which the gravity potential W_0 is constant, (formula (1)), and which is a potential in the level of the Normaal Amsterdams Peil.

– The unit of length of the EVRS is the meter (SI) and the unit of time is second (SI). This scale is consistent with the TCG time coordinate for a local geocentric frame, in agreement to IAU and IUGG (1991) resolutions. The TCG time is obtained by appropriate relativistic modeling.

– The height components are the differences ΔW_P between the potential W_P of the Earth gravity field through the considered point *P,* and the potential W_0 of the EVRS conventional zero level. The potential difference $-\Delta W_P$ also is designated as the geopotential number C_P. Normal heights are equivalent with geopotential numbers, provided that the reference gravity field is specified.

– The EVRS is a zero tidal system, in agreement with the IAG Resolutions No. 9 and 16 adopted in Hamburg in 1983.

Practical realization of the EVRF2007

Since the adjustment of the UELN 95/98 network in January 1999 and adoption of this solution as the EVRF2000 a significant number of new data have been delivered to the UELN Data Centre (SACHER et al. 2008). Between others fourteen counties carried out new campaigns of part or entire precise levelling networks (Fig. 2).

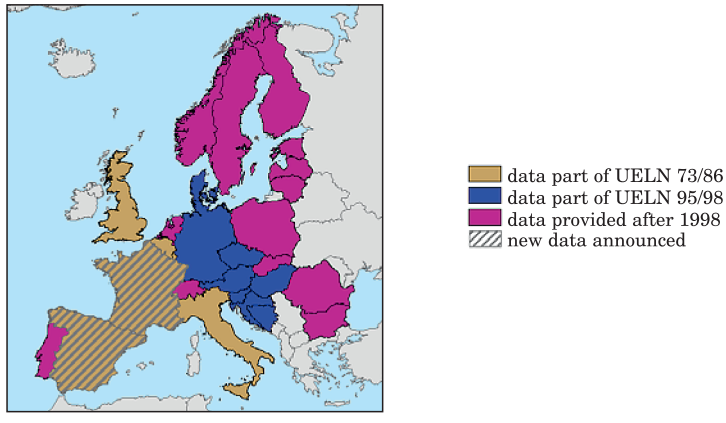

Fig. 2. Geographical range of the UELN network
Source: SACHER et al. (2008).

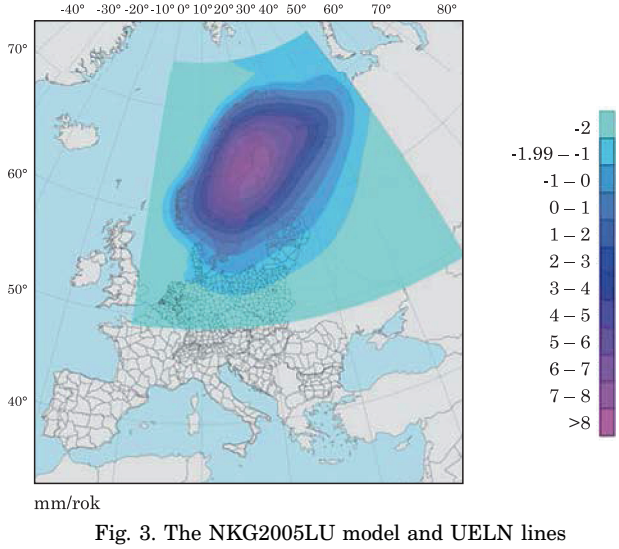

Fig. 3. The NKG2005LU model and UELN lines
Source: SACHER et al. (2008)

Therefore Data Center had to realize a new variant of the *European Vertical System* as the EVRF2007. All countries participating in this project were asked to provide their current data. The results of measurements of precise levelling networks gathered in the UELN Data Centre come from very different epochs (Fig. 2). In order to refer all observations to one epoch, data from levelling were reduced due to the vertical movements of the Earth's crust. These corrections were introduced only to data of Finland, Norway, Sweden, Denmark, Germany (northern part), Poland, Lithuania, Latvia, and Estonia. The necessary corrections to the reduction were calculated from the land uplift model developed by (ÅGREN, SVENSSONN 2007) (Fig. 3).

The EVRF2000 vertical datum is determined by the geopotential number and the equivalent normal height of the reference point no 000A2530 (Tab. 1). Because this point is not included in the current levelling network of the Netherlands, therefore in new EVRF realization it could not be taken into account (no longer available) as a datum point. In order to keep in Europe the level of the EVRF2000 datum, the new UELN adjustment was fitted to the EVRF2000 solution by selecting several fixed points and introducing them in the new adjustment. This was realized by introducing the following condition:

$$\sum_{i=1}^{n}(C_{P_{i2007}} - (C_{P_{i2000}}) = 0 \tag{3}$$

The chosen points should be on the stable part of the European plate. In December 2006, all the participating countries in the UELN project were asked for proposals for reference points in order to proper adjustment of the network. Figure 4 presents the positions of proposed reference points.

Then several variants of adjustment of the network were performed with different selections of data sets of reference points. Change in heights caused by different reference points was from 1 to 5 mm. In the final adjustment were only used 13 of 20 proposed reference points. Seven points were rejected for a variety of reasons.

For example, the Netherlands had proposed three reference points from which one has changed height considerably in comparison to the EVRF2000 solution. United Kingdom proposed two reference points but finally they were not used in adjustment, because the country is located on the island and is connected to the continental network only by one uncertain levelling line. After a planned inclusion a levelling line through the tunnel, significant height variations in these reference points are to be expected. There was a similar problem with the reference points of France, Spain and Portugal. After

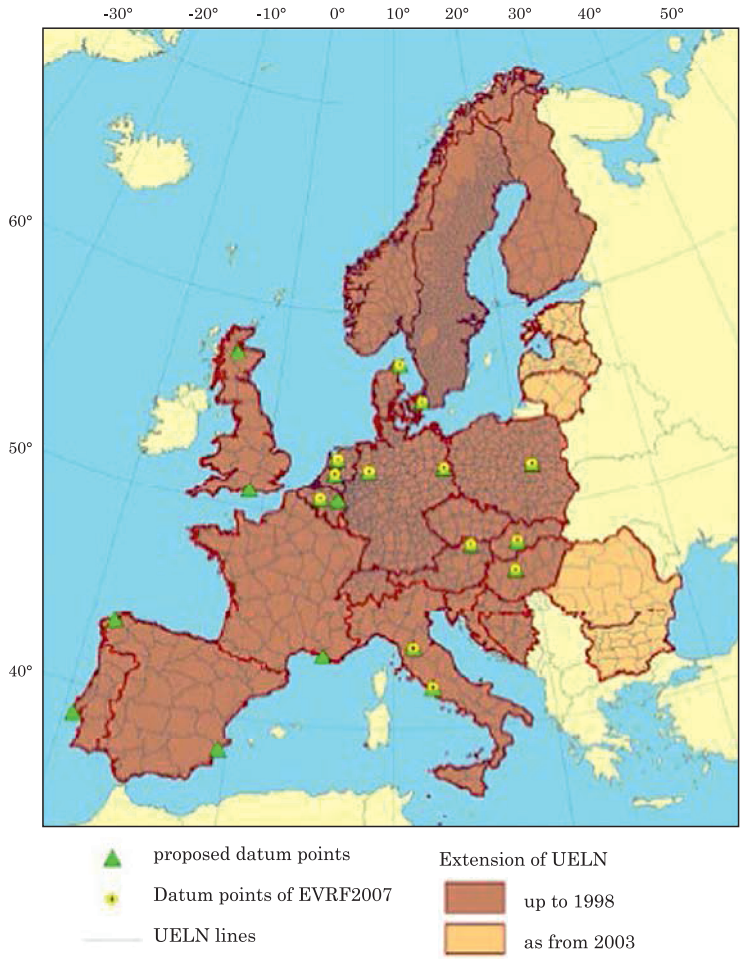

Fig. 4. Proposed and used reference points
Source: SACHER et al. (2008).

including the new data from these countries, variations in the reference points could be large and therefore also these proposed reference points have been rejected.

Influence of tidal corrections on reference level

In the formula (3) which is the condition which should be included into the new adjustment of the levelling network a system of tidal corrections must be

specified. In the new UELN adjustment consisting of geopotential differences it was assumed that the zero tidal system was used.

Despite the fact that the system EVRS2000 is also defined as a zero-tide system, mostly data that have been used in UELN-95/98 adjustment were not reduced for tidal effects, and therefore adjusted geopotential numbers $C_{95/98}$ referred approximately to mean tidal system. This means that the geopotential numbers of reference benchmarks, on which is based the adjustment of EVRF2007, are related to mean tidal system.

A separate problem is the tidal system of the NAP datum in EVRF2007. It could be concluded that since the NAP originally was determined from observations of the mean sea level (the mean high tide at Amsterdam in 1684), the reference level of the EVRF2007 defined by the NAP should relate to a mean-tide system. On the other hand EVRS2007 is defined as a zero tidal system which implies that its NAP datum should be in zero tide system. As the authors of the vertical system intend to keep the numerical values of the bench marks in EVRF2007 as close as possible to the EVRF2000, therefore adopted NAP datum should be in zero tide system. The condition for datum of the height reference frame can be written in the following form:

$$\sum_{i=1}^{n} [C_{P_i 2007} - (C_{P_i 95/98} + W_2(\varphi_{P_i}) - W_2(\varphi_{NAP}))] = 0 \tag{4}$$

where $C_{P_i 95/98}$ is the geopotential number of the EVRF2007 reference point P_i adopted for calculation of EVRF2007, $W_2(\varphi_{P_i})$ is its correction from the mean tide system to the zero tide system, a $W_2(\varphi_{NAP})$ is the same type correction but for reference point 000A2530 in EVRF2000.

Reference ellipsoid and normal gravity field

EVRS2007 system is defined by the gravity potential and geopotential numbers determined by results of levelling and measured gravity accelerations. None of these quantities depend on the size of the reference ellipsoid and the reference ellipsoid is not part of the definition of EVRS, as long as we are dealing with geopotential numbers.

However, to convert the geopotential numbers into normal heights, it is necessary a normal gravity field and geodetic latitude. For this reason normal gravity field of the GRS80 ellipsoid is adopted. Normal gravity at the ellipsoid GRS80 is computed from (MORITZ 1980):

$$\gamma_0 = 9.7803267715 \left(\begin{array}{c} 1 + 0.0052790414 \sin^2 \varphi + 0.0000232718 \sin^4 \varphi \\ + 0.0000001262 \sin^6 \varphi + 0.0000000007 \sin^8 \varphi \end{array} \right) \quad (5)$$

where φ is the geodetic latitude in ETRS89.

The normal height H_P^N is computed from:

$$H_P^N = \frac{C_P}{\bar{\gamma}} \quad (6)$$

where $\bar{\gamma}$ is the average value of normal acceleration along the line of the vertical between the GRS80 ellipsoid and the telluroid. The mean value of the normal gravity is calculated from the formula:

$$\bar{\gamma} = \gamma_0 \left(1 - (1 + f + m - 2f \sin^2 \varphi) \frac{H}{a} + \frac{H^2}{a^2} \right) \quad (7)$$

where H is the approximate height the point P.

Tidal corrections

The EVRS involves both geopotential and geometric quantities (station position). Therefore their variations in time, caused by geodynamical phenomena such as tides of solid earth and ocean have significant impact on the EVRS. The IERS Convention (McCarthy and Pétit 2003) defines exactly the size of both positions and geopotential and there is no need to duplicate it for the purpose of EVRS. One particular aspect has to be carefully considered, namely the treatment of the permanent tide.

The gravitational forces of the Moon and Sun cause tides not only seas and oceans but also the Earth's crust. The value of tide changes over time so there are diurnal, semi-diurnal or long period tides. It turns out that the average value of tides measured over a long period of time is not equals to zero. This average unchangeable in time value is called permanent tide. Because the permanent tide is larger at the Equator and smaller in the polar areas this causes additional slight flattening of the Earth.

Tides change the gravity acceleration of the Earth and affect the position of the geoid. Therefore, the definitions of geodetic coordinate systems, heights and gravity systems should take into account the tidal effects.

The existence of a permanent tide causes complications when defining how to take account tidal corrections in measured gravity acceleration in precise levelling and GNSS observations. There are known different ways of handling the permanent tide in these observations (EKMAN 1989) which leads to the *non-tidal*, *mean* and *zero tidal* corrections (MÄKINEN 2008).

In the *non-tidal* system, from gravity field the tidal potential variable in time and the permanent tidal potential are removed. The results that so improved gravity acceleration does not coincide to its mean value and geoid computed from such gravity data does not coincide with the mean sea level. Therefore Honkasalo proposed that the permanent tide should be restored to characteristics of the gravity field of the Earth. This approach has led to the concept of the *mean tidal* system and mean gravity and mean geoid.

Another approach is a *zero tidal system*. This system refers to the situation when characteristics of gravity field generating by the Sun and the Moon are eliminated and deformation of the earth crust caused by permanent tide is retained.

Resolution No 16 of the International Association of Geodesy recommends to use in the positioning systems, gravity and precise levelling *zero tidal system* to determine tidal corrections.

In the next chapter will be raised three issues. The first issue is about numerical values for the permanent tide, the second is about obtaining geopotential differences in zero-tide system from the mixed tidal systems of levelling in the UELN data and the last one is considering the fact that coordinates in the ETRS89 and ITRFxx gives the (conventional) tide-free position.

Numerical values for the permanent tide

The formula limited to the second degree of the development of the tidal potential in a series of spherical harmonics is:

$$W_2 = B\left(\frac{r}{R}\right)^2 P_2(\sin\varphi) = B\left(\frac{r}{R}\right)^2\left(\frac{3}{2}\sin^2\varphi - \frac{1}{2}\right) = A\left(\frac{r}{a}\right)^2\left(\sin^2\varphi - \frac{1}{3}\right) \quad (8)$$

where r, φ are the geocentric radius and latitude, R is a scaling factor for distance, the coefficients A and B depend on the chose of R, and $P_2(\ )$ is the second-degree Legendre polynomial and a is a semi-major axis of ellipsoid GRS80.

IERS convention of 2003 (MCCARTHY, PÉTIT 2003, section 7.1.3) says that the amplitude of W_2 Cartwright-Tayler-Edden normalization is 0.31460 m

(as the symbol H_0). Transforming it into the formula above and using the parameters given in the Section 6.5 of paper (MCCARTHY, PÉTIT 2003) we have:

$$W_2 = A\left(\frac{r}{a}\right)^2\left(\sin^2\varphi - \frac{1}{3}\right) \tag{9}$$

which gives $A = -2.9166\ \mathrm{m^2 s^{-2}}$.

The value $H_0 = 0.31460$ given in the IERS Conventions and used to determine the coefficient A refers to the epoch 2000.0. The Conventions does not provide any change of this magnitude over time. Recently obtained a high-accuracy tidal expansion (KUDRYATSEV 2004) gives the coefficient A in the epoch 2000.0 slightly different than in the Convention. The difference is less than $0.0001\ \mathrm{m^2 s^{-2}}$ and the change this ratio is $-0.0009\ \mathrm{m^2 s^{-2}}$ /century.

For the GRS80 ellipsoid there is a practical formula for W_2 as a function of geodetic latitude φ and height above ellipsoid h:

$$W_2(\varphi, h) = (1 + 0.31 \cdot 10^{-6} m^{-1} h)(0.9722 - 2.8841 \sin^2\varphi - 0.0195 \sin^4\varphi)\ [\mathrm{m^2 s^{-2}}] \tag{10}$$

where h is the height above the ellipsoid. In order to make practical use of the equation (10) in the EVRS we can neglect the impact of topography expressed by h and then this formula has the form:

$$W_2(\varphi) = 0.9722 - 2.8841 \sin^2\varphi - 0.0195 \sin^4\varphi\ [\mathrm{m^2 s^{-2}}] \tag{11}$$

Error due to negligence of height h is less than $0.001\ \mathrm{m^2 s^{-2}}$. Equation (11) determines the permanent tide-generating potential. Because geopotential numbers have the opposite sign than potential differences, thus equation (11) is the value that should be added to the geopotential numbers in the mean tidal system to obtain geopotential numbers in the zero tidal system.

In the case of normal height $W_2(\varphi)/\gamma_0(\varphi)$ should be calculated where $\gamma(\varphi)$ is normal gravity on the ellipsoid GRS80.

$$H_2(\varphi) = W_2(\varphi)/\gamma_0(\varphi) = +99.40 - 295.41 \sin^2\varphi - 0.42 \sin^4\varphi\ [\mathrm{mm}] \tag{12}$$

Equation (12) gives the values that should be added to normal heights in the mean tidal system in order to obtain normal heights in zero tidal system. In this case, this should not be a normal acceleration on ellipsoid but the mean normal acceleration along the plumb line (7).

In the case of point P at 5 km elevation, using directly the formula (12) instead converting the geopotential numbers from one system to the other and then converting these numbers to normal heights, gives the error no greater than 0.15 mm (IHDE et al. 2008).

The permanent tide in 3-D coordinates calculated using IERS Conventions

Typically the 3-D position of a bench mark computed from GSNN observations is in a tide-free system. It serves to compute potential values from geopotential models. Contrary the potential values from spirit levelling and gravity measurements are in zero-tide system. In order to obtain both potential values in the same tidal system the 3-D coordinates have to be transform into zero-tide system. For this reason, a suitable correction must be added to these coordinates to change them in the mean-tide system. The correction which has to be added to these coordinates in non-tidal system depends on how they were entered in the past. There are minor differences in the tidal correction proposed by the IERS various Conventions published in 1992, 1996 and 2003.

Corrections due to the mean tide (IERS, 2003, Convention) are given to the nearest 0.1 mm. Authors (IHDE et al. 2008) have recalculated these corrections with higher accuracy and have received the following formula:

$$\Delta\hat{r} = \{[-120.61+0.12P_2(\sin\varphi)]P_2(\sin\varphi)\}\hat{r}+\{[-25.21-0.06P_2(\sin\varphi)]\sin 2\varphi\}\hat{n} \tag{13}$$

where $\hat{r}$ is the unit vector from the geocenter to the point on the surface of the Earth, $\hat{n}$ is the unit vector, φ is the geocentric latitude, a $P_2(.)$ is the second-degree Legendre polynomial.

For further calculations we need the projection of the vector Δr in equation (13) onto the ellipsoidal normal. Near the surface of the ellipsoid GRS80 we have

$$h_T(\varphi) = 60.34 - 179.01 \sin^2\varphi - 1.82^4 \tag{14}$$

Definition of the EVRS2000 system which says that the EVRS is a zero tidal system, in agreement with the IAG resolutions, this part of the definition was not completely realized until now. To the data computed by the UELN center there were not applied reductions because of the permanent tides. The

countries participating in the project provided data in different tidal systems, therefore it was assumed that the EVRS2000 is a mixed system. It is now known that it is mostly mean-tide system.

In 2004, within the framework of the project of the Geodetic Information and Service System CRS (SACHER et al. 2005) to all European countries, was sent a questionnaire on national height systems. There was also a question about the tidal system of these national heights. Most of the countries responded that their height systems are in the mean tidal system. Some countries that have used other national systems provided data in required by UELN tidal system (the Netherlands and Scandinavia). Poland and Denmark delivered a new data in the non-tidal system to the UELN data center. There is, however, no information about the tidal system from Italy. It can be assumed that the data of Czech Republic and Latvia are in the mean tidal system because these countries have participated, in the late seventies, in the common adjustment of the East European countries in that system. It can be also expected that the data from Bosnia-Herzegovina, Croatia are in the same tidal system, since they come from a common network of the former Yugoslavia.

In order to realize the EVRS definition concerning the tidal system, in the measuring table of the UELN data base, there was created an additional column which shows the geopotential difference in the zero tidal system. To solve the problem of the reduction of the reference points, in a first step their geopotential numbers were corrected by following correction to move them from the mean-tide system to the zero-tide system (MÄKINEN 2008):

$$\Delta = -0.2884 \sin^2 \varphi - 0.00195 \sin^4 \varphi + 0.09722 \text{ kgal m} \qquad (15)$$

The result of the applied treatment were a value ranged between -0.030 (Italy) and -0.108 kgal · m (Denmark). In order to minimize the differences to the EVRF2000 solution also was added the constant value +0.08432 kgal · m which is the value of the tidal correction of point 13600 (000A2530) with opposite sign.

This is equivalent to the assumption that the level of reference of the NAP is EVRF2000 zero tidal system in accordance with the definition of EVRS2000 (IHDE et al. 2008). Figure 6 shows the differences in the adjusted geopotential numbers in EVRF2007 and in the EVRF2000.

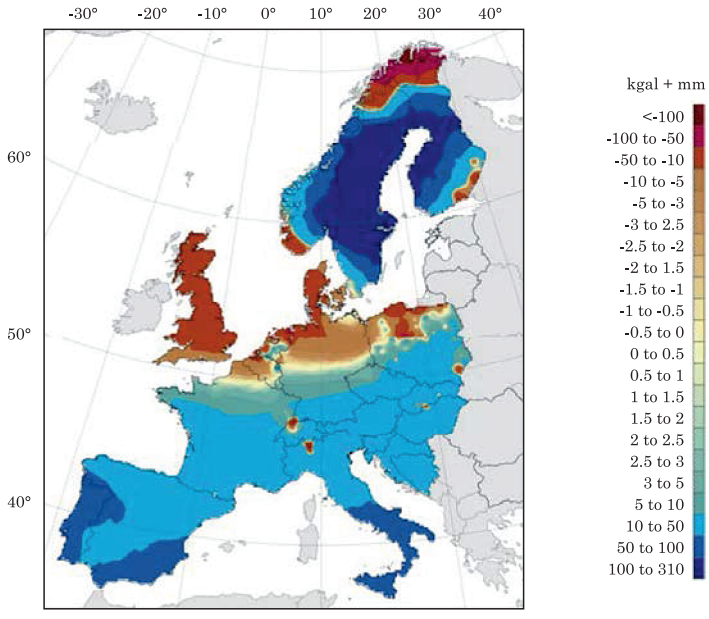

Fig. 5. Differences between EVRF2007 and EVRF2000
Souce: SACHER et al. (2008).

Characteristics of adjusted parameters

The vertical datum of EVRF2007 is realized on the basis of 13 reference points and their location is presented in Figure 4. The geopotential numbers of these points from the EVRF2000 and reduced to the zero tidal system adjustment by following formula (EKMAN 1989, MÄKINEN 2008):

$$C_{2007} - C_{95/98} - 0.2884 \sin^2 \varphi - 0.00195 \sin^4 \varphi + 0.09722 + 0.08432 \text{ [kgal m]} \tag{16}$$

served for independent adjustment.

Differences of geopotential numbers were reduced to zero-tide system using the formula:

$$\Delta C_Z = \Delta C_M - 0.2884 (\sin^2 \varphi_2 - \sin^2 \varphi_1) \;] \; 0.00195 (\sin^4 \varphi_2 - \sin^4 \varphi_2) \text{ [kgal m]} \tag{17}$$

and referred to the epoch 2000 through the use of the land uplift model NKG2005LU. This was data from Poland, Finland, Norway, Sweden, Denmark, Germany, Lithuania, Latvia and Estonia.

Table 2 shows the comparison of the parameters obtained from the EVRF2000 and EVRF2007 adjustment while.

Table 1

Characteristics of parameters of the adjustment

Parameter	EVRF2000	EVRF2007
Number of reference points:	1	13
Number of unknowns:	3063	8133
Number of measurements:	4263	10568
Number of condition equations:	0	1
Degrees of freedom:	1200	2436
A-posteriori standard deviation referred to 1 km levelling distance in [kgal · mm]:	1.10	1.12
Mean value of the standard deviation of the adjusted geopotential numbers (=^ heights), [kgal mm]:	19.6	16.2
Average redundancy:	0.281	0.231

Source: SACHER et al. (2008)

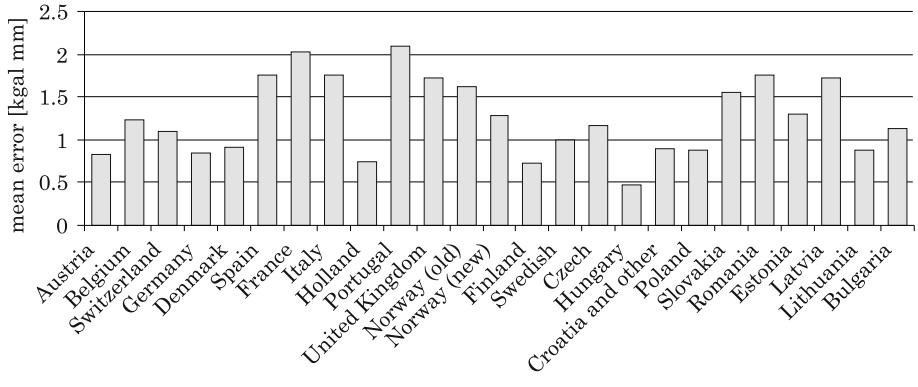

Fig. 6. Standard deviations for EVRF2007 derived for each country on the basis of the separate groups of observations in kgal · mm

From Figure 6 it follows that the accuracy of precise levelling network measured in Poland between 1999–2001 is high and is characterized by mean error 0.88 kgal · mm (~ 0.88 mm) and in terms of accuracy is as good as accuracy of networks from the Netherlands, Denmark, Germany and Lithuania.

The results of evaluation of EVRS

Just before the EUREF Symposium in Brussels in 2008 preliminary results of the network adjustment with the report were passed on to the countries participating in the project. Since then there was no an agreement on the exchange of data between the countries, therefore, each of the countries received only his own part of adjustment of levelling network. Representatives most of the countries taking part in the UELN during this symposium agreed to exchange the full results with each other.

Each country received two files saved in Excel spreadsheet. The first one contained data with reference points i.e. number of internal identification in the country, adjusted geopotential numbers and normal heights and their standard deviation. The second file contained survey data at the beginning and end point of the measured line, weight, correction, standardized correction, redundancy number, adjusted geopotential differences and their standard deviations. The files also contain the end points of border connections with neighboring country.

Finally, at the EUREF Symposium June 2008, the EVRF2007 was adopted as new realization of the EVRS. Resolution No. 3 suggested to the European Commission adoption of EVRF2007 as a vertical reference for pan-European geoinformation systems.

After the presentation of the preliminary results of the adjustment, some minor updated data from Norway as well as some additional measurements related to the EUVN_DA project were included. The final results of the EVRF2007 were delivered to all participating countries in UELN project in autumn 2008.

References

ADAM J., AUGATH W., BROUWER F., ENGELHARDT G., GURTNER W., HARSSON B.G., IHDE J., INEICHEN D., LANG H., LUTHARDT J., SACHER M., SCHLUTER W., SPRINGER T., WOPPELMAN G. 2000. *Geodesy beyond 2000 – the challenges of the first decade.* International Geodesy Symposia, 121.

ÅGREN J., SVENSSON R. 2007. *Postglacial Land Uplift Model and System Definition for the New Swedish Height System RH 2000.* LMV-Rapport 2007: 4, p. 124.

EKMAN M. 1989*, Impacts of geodynamic phenomena on systems of height and gravity,*. Bulletin Geodesique, 63: 281–296.

IERS Conventions. 2003. Eds. D. DENNIS, D. MCCARTHY, G. PETIT, IERS Technical Note, 32.

IERS Conventions. 2003. Eds. D.D. MCCARTHY, G. PETTIT G. IERS Technical Note, 32. Verlag des Bundesamts fur Kartographie und Geodasie, Frankfurt am Main.

IHDE J., AUGATH W. 2000. *The Vertical Reference System for Europe.* Veröffentlichungen der Bayerischen Kommission für die Internationale Erdmesssung der Bayerischen Akademie der Wissenschaften, Astronomisch – Geodatisch Arbeiten, Heft 61, München, pp. 99–110.

IHDE J., MÄKINEN J., SACHER M. 2008. *Conventions for the Definition and Realization of a European Vertical Reference System (EVRS).* EVRS Conventions 2007. Draft.

Information System EVRS: http://www.bkg.bund.de/ nn_164806/geodIS/ EVRS/EN/EVRF2000/ evrf2000_node.html_nnn=true

KUDRAYATSEV S.M. 2004. *Improved harmonic development of the Earth tide-generating potential*. Journal of Geodesy, 77: 829–838.

MÄKINEN J. 2008. *The treatment of permanent tide.* In EUREF products. Paper presented at the Symposium of the IAG Sub-commission for Europe (EUREF) in Brussels, June 17–21.

SACHER M,. IHDE J., LIEBSCH G., MÄKINEN J. 2008. *EVRF2007 as Realization of the European Vertical Reference System*. Presented at the Symposium of the IAG Sub-commission for Europe (EUREF) in Brussels, June 18–21,

SACHER M., LIEBSCH G., IHDE J, 2007. *Status of EVRS2007.* Presented at the Symposium of the IAG Sub-commission for Europe (EUREF) in London, June 6-9. Submitted to the proceedings.

SACHER M., IHDE J., LANG H. 1999. *Results of the Adjustment of the United European Levelling Network 1995 (UELN-95/98).* Report by the UELN data centre, Bundesamt für Kartographie und Geodasie – Leipzig, Germany.

SACHER M., IHDE J., LIEBSCH G., LUTHARDT J. 2005. *Steps on the Way to UELN05 and Enhancements of the Web-based Geodetic Information and Service System.* Report on the Symposium of the IAG Sub-Commission for Europe.

Technical Sciences 17(2), 2014, 105–121

MODELING OF THE STRESS-DEFORMED STATE AND CRACKING INREINFORCED CONCRETE STRUCTURES USING ANSYS MECHANICAL

***Vitaliy Stepanovich Dorofeev*[1], *Vasiliy Mikhaylovich Karpyuk*[2], *Oleksandr Stepanovich Neutov*[1], *Stepan Filipovich Neutov*[2]**

[1] Department of Reinforced Concrete and Masonry Structures
[2] Department of Strength of Materials
Odessa State Academy of Civil Engineering and Architecture, Ukraine

Received 11 June 2013, accepted 5 June 2014, available on line 10 June 2014

K e y w o r d s: concrete beam, stress-strain state, finite-element modeling, ANSYS.

A b s t r a c t

The article presents the results of reinforced concrete beams modeling under short-term loading with the use of the ANSYS Mechanical software. The obtained parameters were compared with the experimental ones. The comparison showed a satisfactory concordance of the parameters. In case of the discrepancies, the authors suggest that they are due to the idealization of material properties and structural model of the finite method. The paper is divided into the following chapters: Introduction, Literature Review, Research Significance, Element Types, Real Constants, Material Properties Modeling, Geometric Modeling, Loads and Boundary Conditions, Cracking and Failure and Conclusions. Each of the five conclusions in the last chapter offers a summary of the presented experimental research.

Introduction

Frequently, providing required load bearing capacity of reinforced concrete beams support areas under complexstress-deformed state is a design driver. Nevertheless, behavior and response of these structure elements in case of high level loads (est. (0.7 – 0.9 V_{ult}) still remain underexplored. That is why, systematic experimental and theoretical research aimed at improvement of the existing and development of modern computational models of support areas in reinforced concrete elements is of essential importance. Various methods have been used to study the response of structural components. Natural experi-

* Correspondence: Stepan Filipovich Neutov, Didrikhsonast., Odessa, 65029, Ukraine, e-mail: neutov.alex@gmail.com, phone +38 0 634 193 089

ments, while producing real time response, are extremely time consuming and quite costly. As for calculation methods, we must mention, that despite all theirefforts (and first of all, price), it is rather unsafe to use them alone for investigation at load levels near 0.9 of ultimate load. Thus, using FEA, such as MacroFe, Ansys, along with natural experiments,is one of the most effective ways to do this task.

In the design of frame concrete structures, it is very important to construct support areas properly. Their combined stress-deformed state makes this task rather difficult. The most common methods used for computational support areas are based on analogies or statistic data and do not describe the real behavior fully.

The aim of this experimental research is to study combinedstress-deformed state of reinforced concrete beams support areas using finite element modeling with ANSYS Mechanical. Authors intended to investigate possibility of modeling the multifactor experiment, and, at the same time, to focus on the behavior of RC beams support areas, shear cracking, stress distribution in shear and longitude reinforcement under short-term loading.

Material and methods

The data presented herein are basis for the five-factor three-level experimental investigation of reinforced concrete beams support areas under steady loading. Full-sized Hartley-5-type experiment plan includes 27 series. Due to

Table 1

Plan of experiment

Series N	Natural values of the factors				
	a/h_0	C, MPa	Shear reinf. at support sect. [%]	Bottom longt. reinf. [%]	Top longt. reinf. [%]
17	3	C20/25	0.0029 (2Ø4 mm)	0.0176 (2Ø14 mm)	0.0090 (2Ø10 mm)
18	1	C20/25	0.0029 (2Ø4 mm)	0.0176 (2Ø14 mm)	0.0090 (2Ø10 mm)
19	2	C30/35	0.0029 (2Ø4 mm)	0.0176 (2Ø14 mm)	0.0090 (2Ø10 mm)
20	2	C12/15	0.0029 (2Ø4 mm)	0.0176 (2Ø14 mm)	0.0090 (2Ø10 mm)
21	2	C20/25	0.0045 (2Ø5 mm)	0.0176 (2Ø14 mm)	0.0090 (2Ø10 mm)
22	2	C20/25	0.0016 (2Ø3 mm)	0.0176 (2Ø14 mm)	0.0090 (2Ø10 mm)
23	2	C20/25	0.0029 (2Ø4 mm)	0.0230 (2Ø16 mm)	0.0090 (2Ø10 mm)
24	2	C20/25	0.0029 (2Ø4 mm)	0.0129 (2Ø12 mm)	0.0090 (2Ø10 mm)
25	2	C20/25	0.0029 (2Ø4 mm)	0.0176 (2Ø14 mm)	0.0129 (2Ø12 mm)
26	2	C20/25	0.0029 (2Ø4 mm)	0.0176 (2Ø14 mm)	0.0058 (2Ø8 mm)
27	2	C20/25	0.0029 (2Ø4 mm)	0.0176 (2Ø14 mm)	0.0090 (2Ø10 mm)

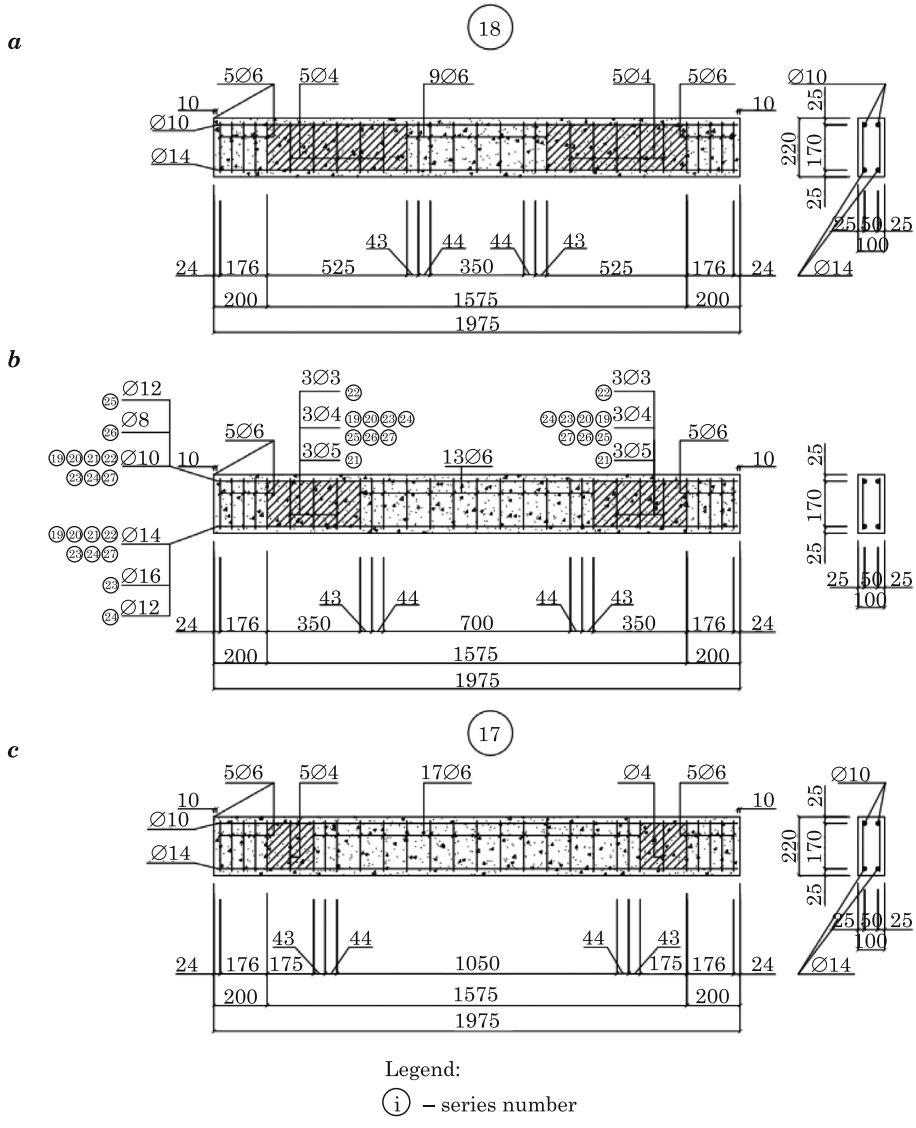

Fig. 1. Beam design: *a* – 18 series, *b* – 19–27 series, *c* – 17 series

considerable complexity of the long-time experiment we decided to use series from 17 to 27 with only one factor variation at one series. Beams of all series are designed to getdestroyedalong support areas. Experimental plan with a description ofexperimental factors and variation levels is shown in Table 1.

Construction scheme of authors' experimental RC beam (DOROFEYEV et al. 2010, 2012) used as calibration model is shown in Figure 1. Simplified scheme that was used to simulate the experimental beam is shown in Figure 2.

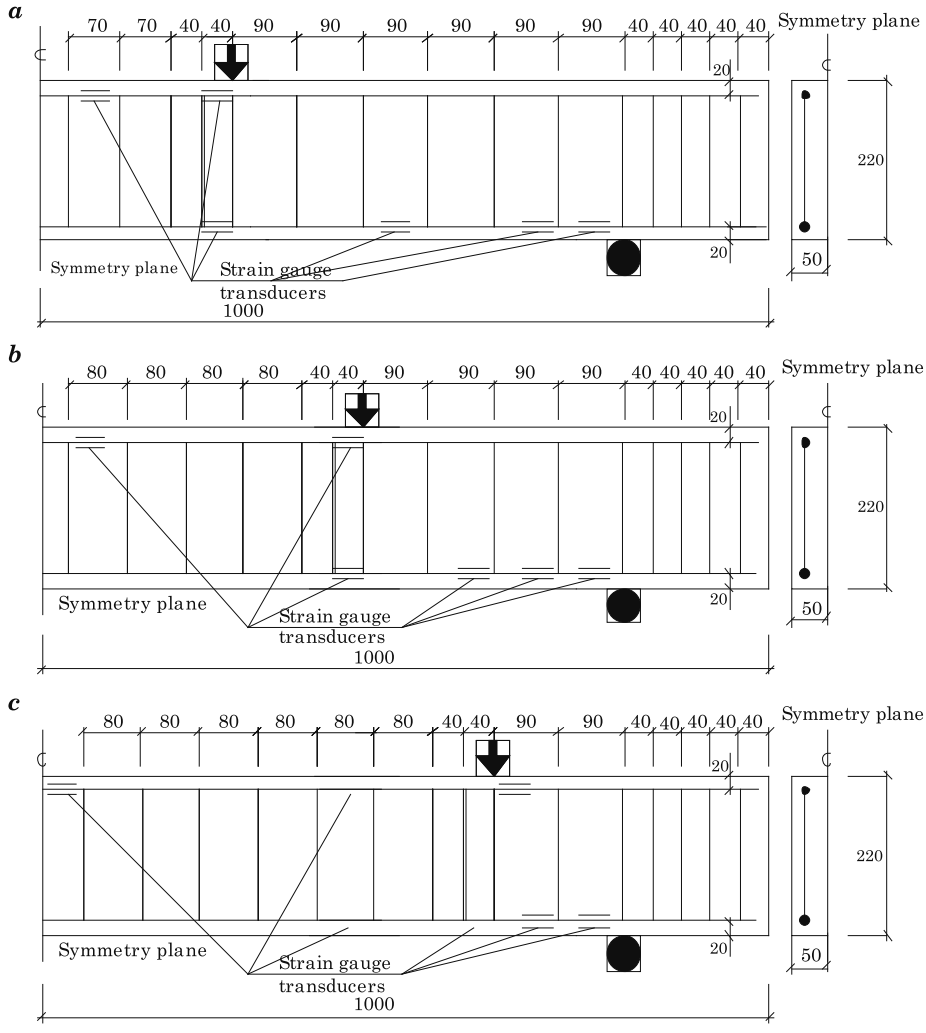

Fig. 2. Model design andstrain gauge transducer scheme: *a* – 18 series, *b* – 19–27 series, *c* – 17 series

The element types for this model are shown in Table 2. The Solid 65 element was used to model the concrete. This element is capable of plastic deformation, cracking in three orthogonal directions, crushing, creep and shrinkage. A Solid 45 element was used for steel load plates and supports of the beam. Both these elements have eight nodes with three degrees of freedom at each node. A Link8 element was used to model steel reinforcement. This is 3D spar element and it has two nodes with three degrees of freedom. Also, it is capable of plastic deformation.

Table 2

Elements and real constants used for model

No	Purpose	Element type	Real constants			
1	concrete	solid 65	rebar direction	*x*	*y*	*z*
			reinf. material	0	0	0
			ρ, %	0	0	0
			orient. angle	0	0	0
			orient. angle	0	0	0
2	bottom longitude reinforcement	link 8	cross-sect. area [m^2]		1.702E-4	
			initial strain		0	
3	top longtitudereinforcement	link 8	cross-sect. area [m^2]		0.785E-4	
			lnitial strain		0	
4	shear reinf. in pure flexure zones	link 8	cross-sect. area [m^2]		0.2827E-4	
			initial strain		0	
5	shear reinf. in support areas	link 8	cross-sect. area [m^2]		0.1257E-4	
			initial strain		0	

Real constants for this model are shown in Table 2. Solid 65 elements requireconstants for rebar assuming a smeared model. In that case, valuesfor Material Number (refers to material model), Volume Ratio and Orientation Angles should be set. Value of zero isentered for all real constants, because discrete reinforcement model is used. For shear, top and bottom reinforcement cross sectional areas and initial strain are defined.

Parameters needed to define material models are shown in Table 3. Complex material model for each element is needed (ANSYS theory reference). The Solid 65 element requires linear isotropic and multilinear isotropic material properties to properly model concrete. The multi-linearisotropic material uses the vonMises failure criterion along with Willam and Warnke model (WILLAM, WARNKE 1974). Modulusof elasticity and Poisson's ratio were assumed according to C20/25 concrete properties. The uniaxial compressive stress-strain relationship for the concrete was obtained using the following equations (DBN – V.2.6-98:2009) with parameters for C20/25 concrete:

$$\sigma_c = f_{(ck)} \sum_{k=1}^{5} a_k \left(\frac{\varepsilon}{\varepsilon_{bR}} \right)^k \tag{1}$$

where

$f_{(ck)}$ – design value of concrete compressive strength;

a_k – the coefficients of the polynomial depending on the parameters, which are used to describe the stress-strain curve;

ε – concrete strain deformation;

ε_{bR} – concrete strain deformation corresponding to the maximum stress value.

Table 3

Material models

Material No	Material	Element type	Material properties		
1	concrete	solid 65	linear isotropic		
			E_x, MPa	3×10^4	
			V_{xy}	0.2	
			multilinear isotropic		
			point num.	ε	σ, MPa
			1	0.000246	7.65
			2	0.000492	15.3
			3	0.00102	19.3
			4	0.00181	25.2
			5	0.00324	13.2
			6	0.00420	5.10
			concrete		
			const1	1	
			const2	0.9	
			const3	0.9	
			const4	51.0	
			const5	-1	
2	support and load plates	solid 45	linear isotropic		
			E_x, MPa	2×10^5	
			υ_{xy}	0.3	
3	longitude reinf.	link 8	linear isotropic		
			E_x, MPa	2×10^5	
			υ_{xy}	0.3	
			multilinear isotropic		
			point num.	ε	σ, MPa
			1	0.00125	250
			2	0.0025	495
			3	0.025	500
4	shear reinf. in pure flexure zones	link 8	linear isotropic		
			E_x, Mpa	2×10^5	
			υ_{xy}	0.3	
			bilinear isotropic		
			yield stress	240	
			tang mod.	145	
5	shear reinf. in support areas	link 8	linear isotropic		
			E_x, MPa	2×10^5	
			υ_{xy}	0.3	
			bilinear isotropic		
			yield stress	410	
			tang mod.	145	

Implementation of Willam and Warnke concrete model requires nine constants to be defined:

1. Shear transfer coefficients for an open crack.
2. Shear transfer coefficients for a closed crack.
3. Uniaxial tensile cracking stress.
4. Uniaxial crushing stress (positive).
5. Biaxial crushing stress (positive).
6. Ambient hydrostatic stress state for use with constants 7 and 8.
7. Biaxial crushing stress (positive) under the ambient hydrostatic stress state.
8. Uniaxial crushing stress (positive) under the ambient hydrostatic stress state.
9. Stiffness multiplier for cracked tensile condition.

Concrete failure surface is described with the following equation

$$\frac{1}{z}\frac{\sigma_a}{f_{cu}} + \frac{1}{r(\Theta)}\frac{\tau_a}{f_{cu}} = 1 \tag{2}$$

where:

f_{cu} – uniaxial compressive strength;
z – apex of the surface;
δ_a, τ_a – average stress components;
Θ – lode angle;
$r(\Theta)$ – quantity, which indicates the locus of the boundary of the stress surface in the deviatoric stress plane.

The reinforcement elements require linear isotropic andmultilinearisotropic material models to be defined. Material of steel load plates and supports of the beam requires only linear isotropic material model.

Concrete, load plates and support element were modeled using volume elements. And the reinforcement was modeled using spar elements. Experimental beam hadtwo symmetry planes and therefore only one quarter of the beam was modeled. Finite element model of concrete and reinforcement with mesh size of 1 cm are shown in Figure 3.

Displacement boundary conditions must be set to constrain the model. To model the symmetry, nodes on the plane must be constrained in the perpendicular direction (UX = 0 and UZ = 0 constraints). The support was modeled in such a way that a roller was created. A constraint in the UY and UZ (applied as constant values of 0) directions was given to the single line of nodes on the plate. The one tenth of the actual force, F, applied across its centerline at the each node. Main calculation parameters are shown in Table 4.

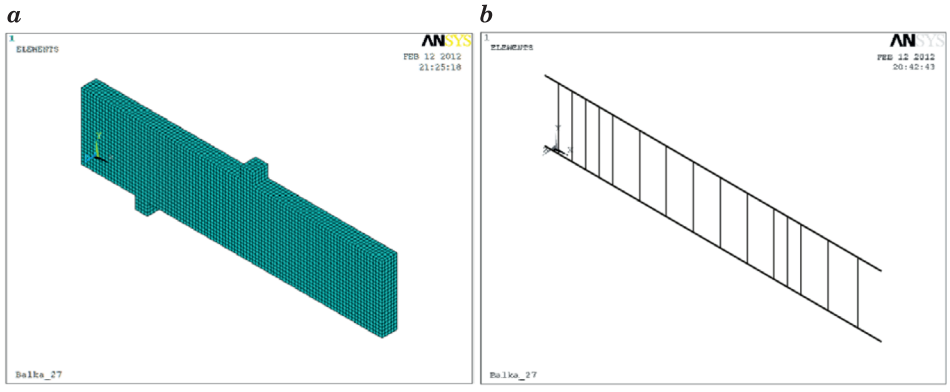

Fig. 3. Mesh of the whole beam (*a*) mesh of the reinforcement (*b*)

Table 4

Calculation options

Main parameters	
Analysis type	Static
Displacement control	big displ.
Prestress effects	off
Time at the end of loadstep	P
Number of substeps	10^6
Automatic time stepping	on
Nonlinear alghoritm and convergence criteria parameters	
Line search	on
Equiv. Plasric strain	1.0
Full Newton-Rapson option with unsym. matrices	on
Maximum number of iterations	10
Element from control	off
Checking elements	No
Convergence criteria	forces
Tolerance	0.5

Results and Discussion

Crack modeling along with cracking of experimental beam for the most characteristic stages of loading is shown in Figure 4. Ultimate, normal and inclined cracking loads for beam series (17-27) obtained both from natural experiment and modeling using ANSYS are shown in Table 5. We must state, firstly, that cracking load for the model is smaller than for experimental beam;

secondly, that cracks in the model develop more intensively, due to cracking criteria used in Willam-Warnke model. Experiment results indicate that cracking process, both in a simulated beam and corresponding experimental one, begins from the pure flexure zone at the load level close to 0.3 V_{ult}. Inclined cracks appear in the support areas later, at the loads about. This process is significantly affected by concrete class, percentage of transversal and longitude reinforcement.

Comparing whole cracking pattern in model and experimental beam at the load about 0.8 V_{ult} we must state their similarity, as well as equal crack heights. Figures 5 and 6 show the experimental values of midspan deflections and longitude reinforcement deformations of the series 22 and the results of their simulations, where 22–1(1) means "22 series, 1st beam, left side of experimen-

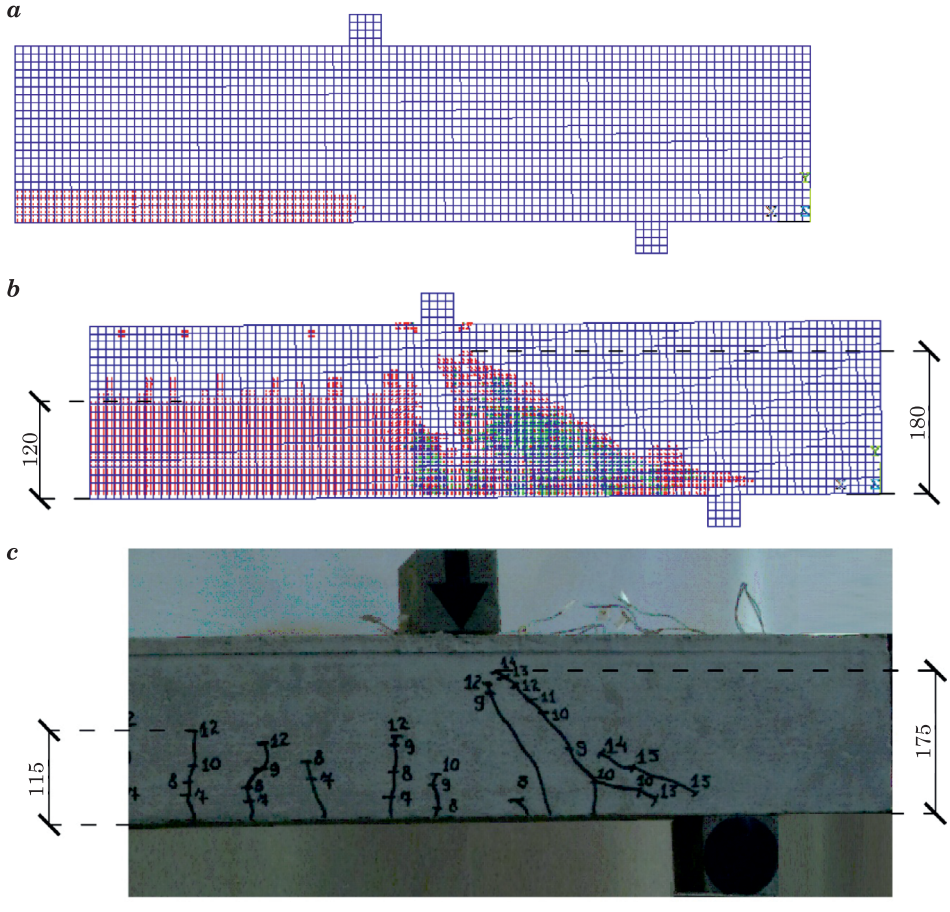

Fig. 4. Modeling of crack at load levels: 0.3 V_{ult} (*a*), 0.8 V_{ult} (*b*); appearance and crack opening in the experimental sample (*c*)

tal beam" and 22–1(2) means "22 series, 1st beam, right side of experimental beam" respectively. It is obvious, that up to, congruence is more than satisfactory. Further increasing discrepancy is due to method limitations.

Table 5

Failure and cracking loads

Series	Model			Experiment		
	V_{ult} [kN]	$M_{(cr)}$ (normal cracks at pureflexure zone) [kNm]	$F_{(cr)}$ (inclined cracks at the support area) [kN]	V_{ult} [kN]	$M_{(cr)}$ (normal cracks at pureflexure zone) [kNm]	$F_{(cr)}$ (inclined cracks at the support area) [kN]
0–17	147	18	20	140	20	30
0–18	60	46	50	64	50	70
0–19	120	26	27	116	27	65
0–20	75	15	28	72	28	45
0–21	86	25	33	96	33	48
0–22	81	22	32	82	32	40
0–23	96	25	33	100	33	48
0–24	65	21	26	72	26	48
0–25	86	25	30	89	30	48
0–26	86	23	30	84	30	40
0–27	86	23	30	86	30	48

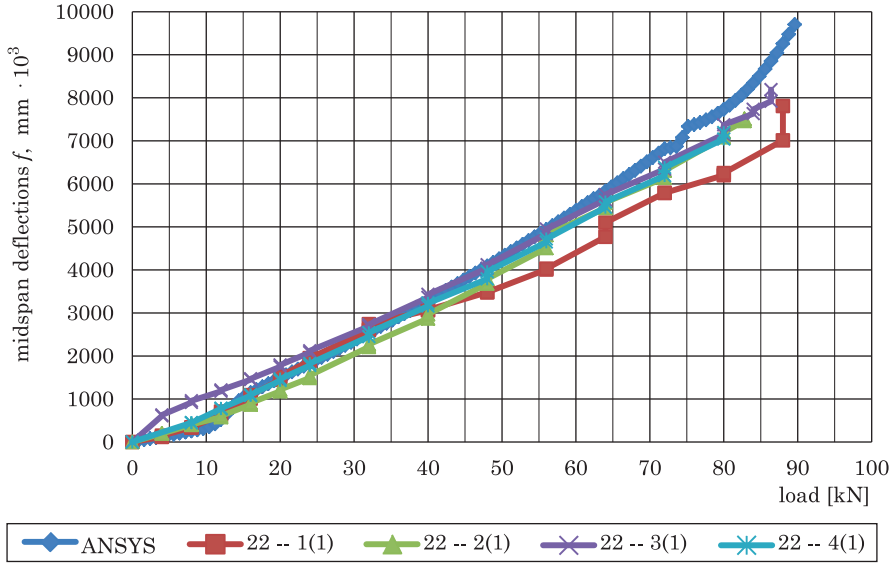

Fig. 5. Calculated and experimental values of beam midspan deflections

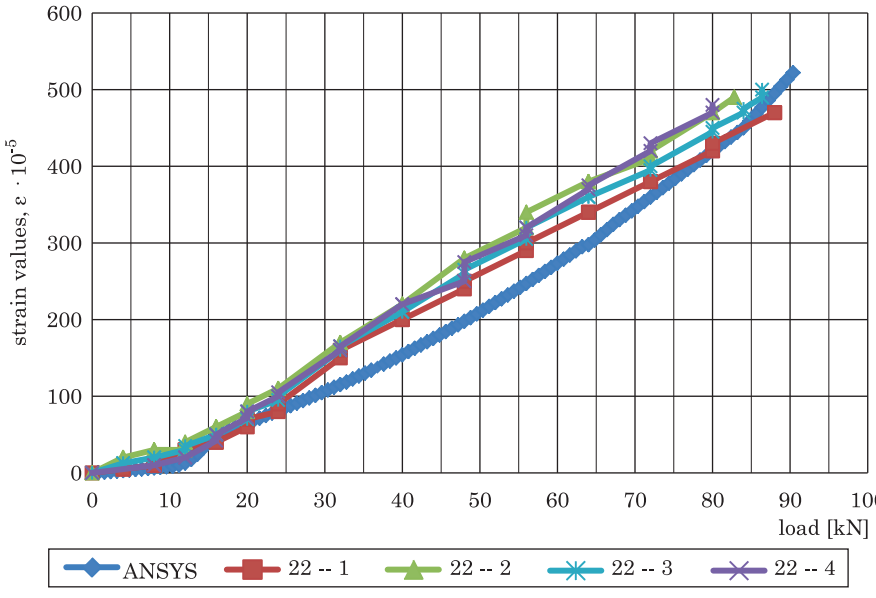

Fig. 6. Calculated and experimental strain values in bottom rebar sat mid span

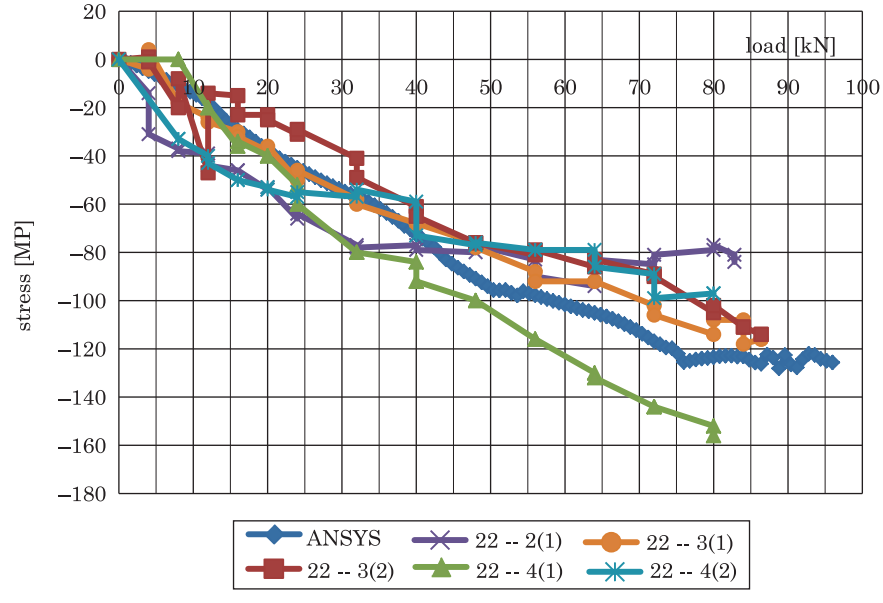

Fig. 7. Calculated and experimental stress values in top reinforcement near the load plate (at the end of support area)

Calculated values of longitude reinforcement stresses along with modeled values are shown in Figures 7–10. Experimental values have been obtained byprocessing the strain gauge transducer chain data, located on bottom and top longitude reinforcement both in pure flexure zone and support areas. It is fair to say that, in total, congruence of experimental and modeled stress-deformed state of top reinforcement is stable (Fig. 6 and 7).

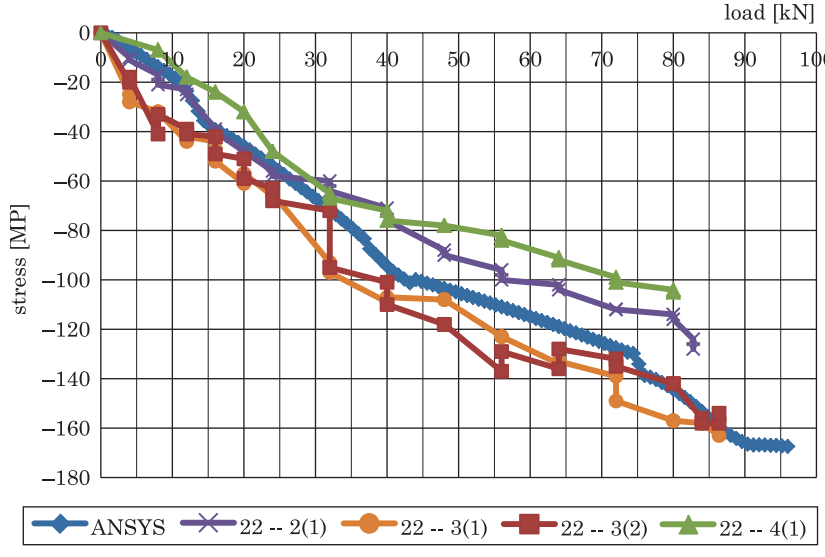

Fig. 8. Calculated and experimental stress values in top reinforcement in pure flexure zone

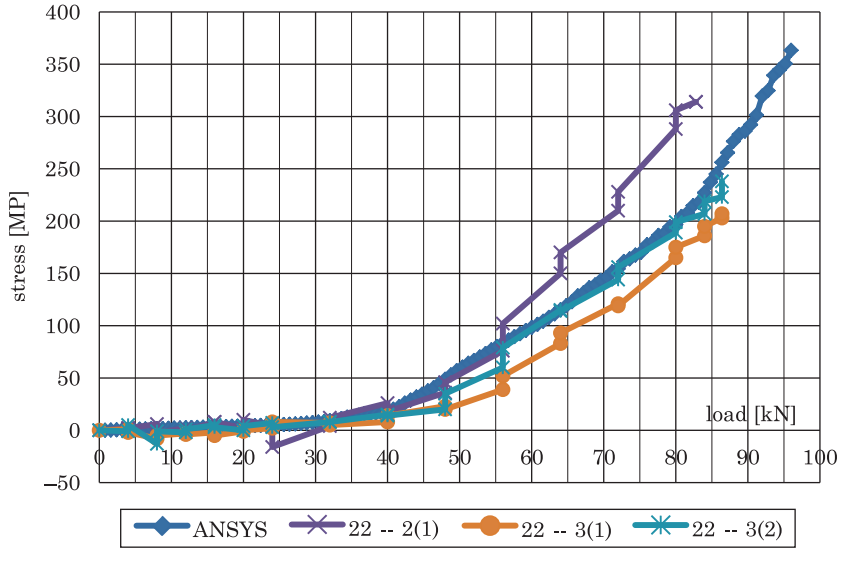

Fig. 9. Calculated and experimental stress values in bottom reinforcement near the support hinge

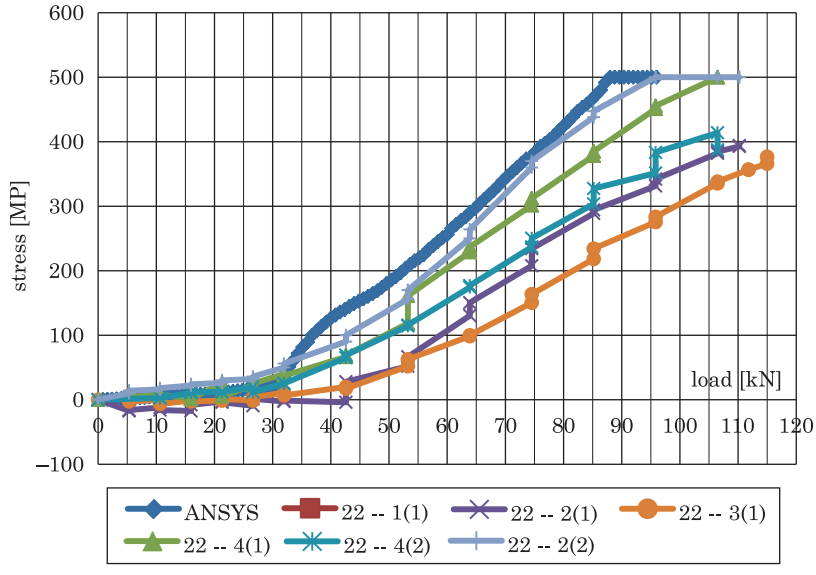

Fig. 10. Calculated and experimental stress values in bottom reinforcement at apoint located at a distance of 9 cm from the support (at the mouth of the critical inclined crack)

As for bottom reinforcement, they differ more significantly. In a greater degree this concerns pure flexure zone on loading, which is close to failure. Under these load levels cracking process in model is like an avalanche, leading to substantial strain growth. To a smaller extent it concerns bottom reinforcement in support areas, although model strain rate is biggerthan in natural beams. And, vice versa, modeled top reinforcement strain is less than experimental ones.

Stressed state of shear reinforcement was studied according to scheme, shown in Figure 11. Relations between load and modelled stresses in shear reinforcement bars in the support areas are shown in Figures 12, 13, 14.

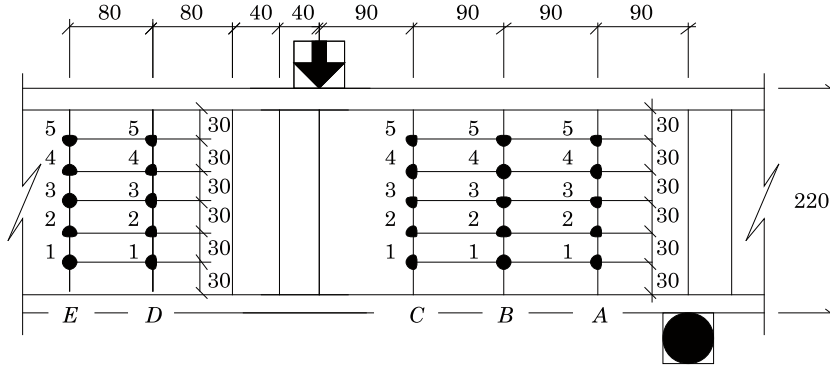

Fig. 11. Characteristic points of the shear reinforcement in the bars *A, B, C* in the support areas, *D, E* – in pure flexure zone

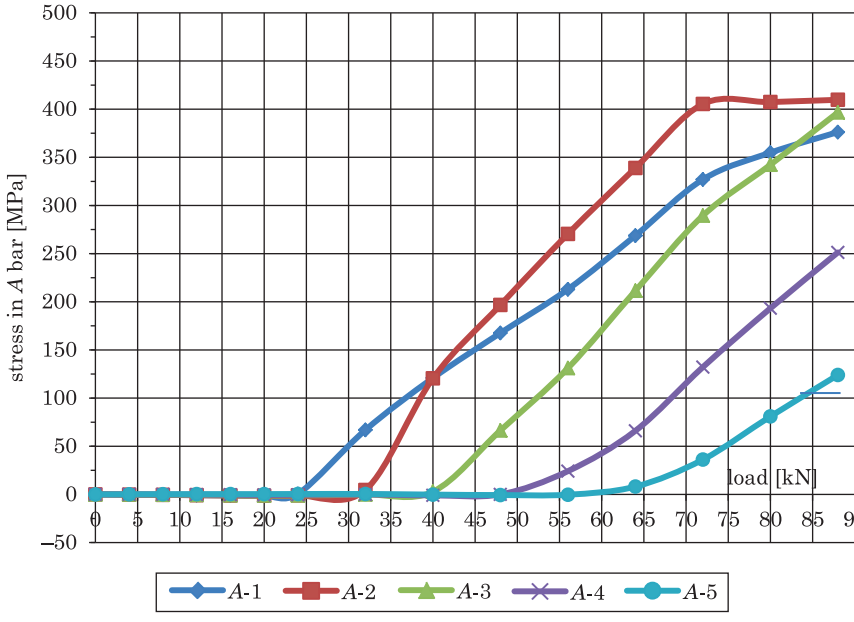

Fig. 12. Force-stress graph for the charecteristic points of the rebar *A*

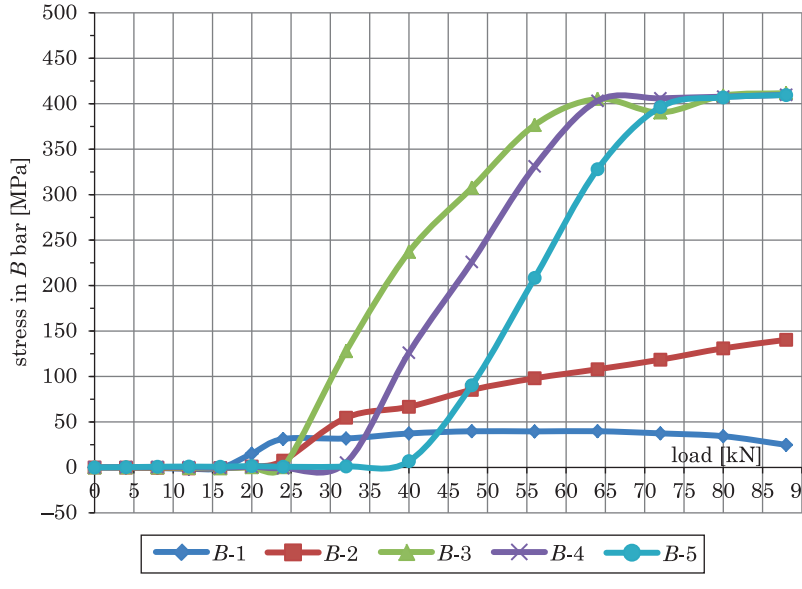

Fig. 13. Force-stress graph for the charecteristic points of the rebar *B*

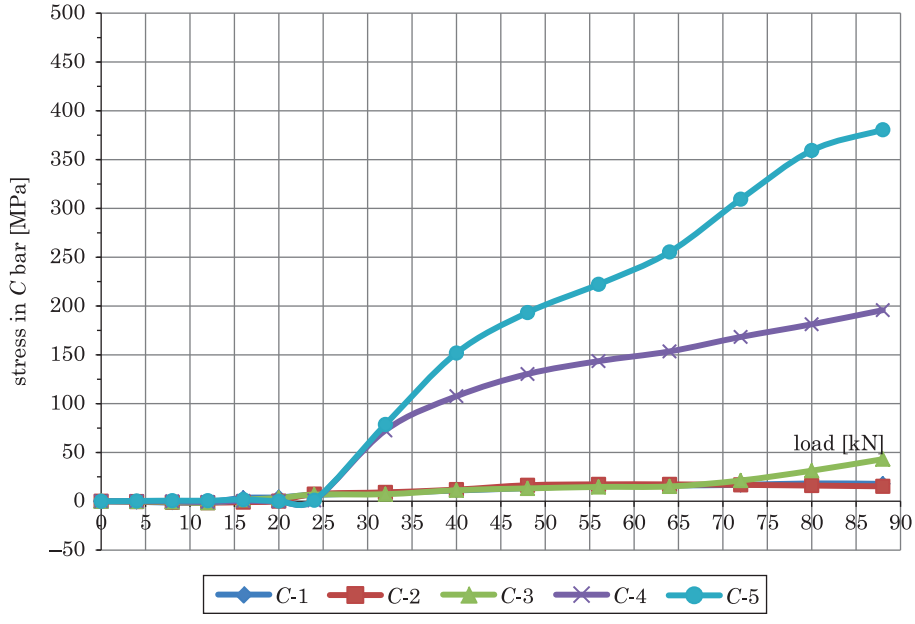

Fig. 14. Force-stress graph for the charecteristic points of the rebar *C*

As we can see, results shown in Figure 12, indicate that stresses in shear rebar *A* are unevenly distributed.Initially, the lowest point 1 is "turned on", then point 2, etc. Stresses in 5th point begin to grow sugnificantly only with load level about 0.75 V_{ult}. The most stressed point in *A* shear rebar is point 2. At load level about 0.80 V_{ult}, stresses in that point reach the yield strength. Point 1 is the second most stressed point, point 3 – the third one – its stresses reach yield strength at the time of failure.

Shear rebar *B*, which is located near midspan (Figure 13), is the most heavily loaded, as stresses reach yield strength in 3 of 5 of his characteristic points. It should be noted, that in these points stresses reach yield strength at load level about. Ultimate stresses in points 1, 2 reaches only 30 and 140 MPa respectively.

Shear reinforcement bar *C*, adjacent to the pure flexure zone, is the least loaded. Almost the entire height (points 1, 2, 3) stresses in their points are less than 50 MPa. Point 4 stress reaches 200 MPa. The most heavily loaded point in this rebar is point 5 (380 MPa), which is very close to the yield point. Modeling results which are shown in Figures 12–14, allow to indicate the direction and area of probable cracks occurrence (Figure 15). In order to do that we can draw a line across points in shear bars where stresses reach ultimate values. Cracking in the support area of experimental beam along with the first principal strain color map is shown in Figure 16. The results presented here indicate that modeled crack patterns practically coincide with the experimental ones.

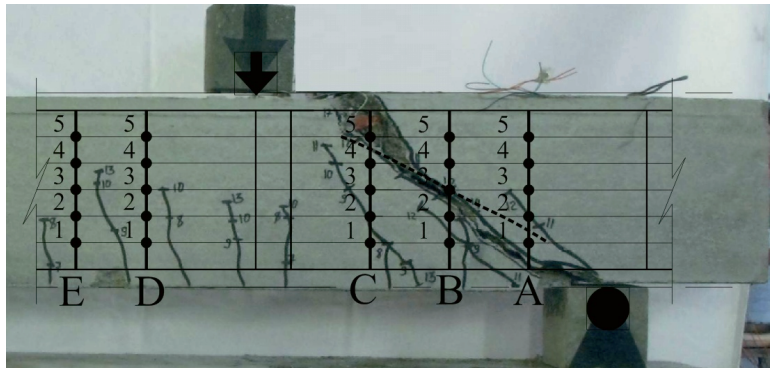

Fig. 15. Cracking and failure of experimental beam support area

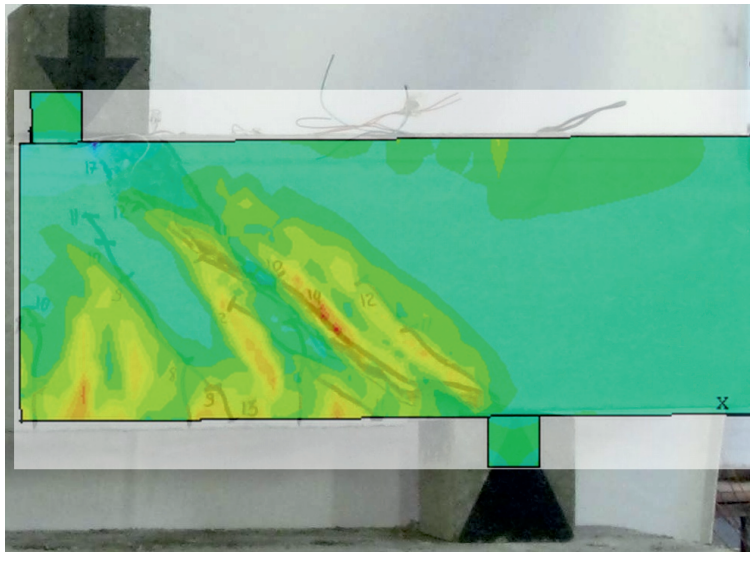

Fig. 16. Cracking in the support area along with the first principal strain color map

Conclusions

1. Failure mechanism modeling using FEA Ansys shows reliable results while received failure load is very close to experimental.

2. Modeled cracking load is also close to experimental. At the same time, it should be noted that cracking pattern in model is rather simplified compared to natural beams and crack growth rate in model is greater than in experimental beam due to restrictions of Willam-Warnke concrete model used in Ansys.

3. Modeled deflections and strains are almost the same as the experimental ones up to.

4. The stresses in top and bottom reinforcement bars received through modeling showed very good agreement and confirmed by direct measurements, actual cracking process in the test beams, as well as other experimental parameters. Discrepancies are due to the idealization of material properties and structural model of the finite element method.

5. Modeling of shear reinforcement provided that good agreementaccording to other parameters of stress-deformedstate can provide valuable data on the growth and change in the pattern of stresses in the shear reinforcement bars, which are difficult to get with a direct experiment. These data are indirectly confirmed as the development of the main crack in the experimental beam.

6. Modeling of the stress-deformed state of researched elements using FEA ANSYS unlike other approved local software systems (in particular, "Lyra", "SCAD", "Monomakh") gives an opportunity to predict the formation and development of both normal and inclined cracks on support areas of bending elements, and the possible mechanism of their failure.

References

ANSYS theory refence. 12th ed, SAS IP, Inc.

DBN – V.2.6-98:2009. Concrete and reinforced concrete structures. Fundamentals. 2011. Ukranian State Bulding Code. Kyiv, The Ministry of Regional Development and Construction.

DOROFEYEV V.S., KARPIUK V.M., NEUTOV A.S. 2010. *Experimental study of reinforced concrete beams support sections under steadyloading*. Journal of Odessa State Academy of Building and Architecture, 38, 255–262.

DOROFEYEV V.S., KARPIUK V.M., NEUTOV A.S.2010. *On the influence of structural factorson the carrying capacity of bendable concrete elements*. Journal of Odessa State Academy of Building and Architecture, 39(1): 186–199.

DOROFEYEV V.S., KARPIUK V.M., NEUTOV A.S. 2012. *On the simulation of the stress-deformed state of reinforced concrete beams in the FEA Ansys Mechanical*. Journal of Odessa State Academy of Building and Architecture, 46: 75–86.

KACHLAKEV D.I., MILLER T. H., YIM S., CHANSAWAT K., POTISUK T. 2001. *Finite Element Modeling of Reinforced Concrete Structures Strengthened With FRP Laminates*. Final Report FHWA-OR-RD-01-17, SPR 316, 111 pages plus appendices, United States Department of Transportation, Federal Highway Administration and Oregon DOT, Salem, Oregon.

SAIFULLAH I., NAZIR-UZ-ZAMAN M., UDDIN S.M. *Experimental and Analytical Investigation of Flexural Behavior of Reinforced Concrete Beam*. IJET, 11(02): 188–196.

VASUDEVAN G., KOTHANDARAMAN S. 2011. *Parametric study on Nonlinear Finite Element Analysis on flexural behaviour of RC beams using ANSYS*. International Journal of Civil and Structural Engineering, 2(1): 98–11.

WILLAM K.J., WARNKE E.P. 1974. *Constitutive model for triaxialbevior of concrete*. Proceedings of international associations of bridge and structural engeneering conference, Vol. 19, ISMES, Bergamo, Italy, pp. 174–191.

WOLANSKI A. J., B.S. 2004. *Flexural behaviour of reinforced and prestressed concrete beams using finite element analysis*. Master's Thesis, Marqutte University, Milwaukee, Wisconsin, p. 87.

Technical Sciences 17(2), 2014, 123–134

VARIABILITY IN AND CORRELATIONS AMONG SELECTED PHYSICAL PROPERTIES OF EUROPEAN LARCH (*LARIX DECIDUA* MILL.) SEEDS

***Zdzisław Kaliniewicz*[1], *Paweł Tylek*[2], *Andrzej Anders*[1], *Piotr Markowski*[1], *Tadeusz Rawa*[1]**

[1] Department of Heavy Duty Machines and Research Methodology
University of Warmia and Mazury in Olsztyn, Poland
[2] Department of Forest Work Mechanisation
University of Agriculture in Krakow, Poland

Received 01 April 2014, accepted 16 June 2014, available on line 18 June 2014

K e y w o r d s: seeds, physical properties, coefficients, correlation.

A b s t r a c t

Selected physical attributes of European larch seeds harvested from 2 seed plantations and 2 commercial seed stands in north-eastern Poland were determined. The physical properties of seeds were measured, and the results were used to calculate indicators of seed weight and the frictional and geometric properties of seeds. Physical attributes and indicators were compared by Student's t-test for independent samples, analysis of variance, correlation analysis and linear regression analysis. The average values of physical properties and indicators were determined at: critical transport velocity – from 5.93 to 6.13 $m \cdot s^{-1}$, thickness – from 1.25 to 1.43 mm, width – from 2.29 to 2.71 mm, length – from 3.71 to 4.57 mm, angle of sliding friction – from 27.85 to 31.98°, weight – from 4.03 to 6.14 mg, coefficient of sliding friction – from 0.54 to 0.63, arithmetic mean diameter – from 2.42 to 2.90 mm, geometric mean diameter – from 2.20 to 2.60 mm, aspect ratio – from 59.60 to 62.38%, sphericity index – from 57.27 to 59.40%, specific weight – from 1.81 to 2.33 $g \cdot m^{-1}$, volume – from 4.60 to 7.59 mm^3 and density – from 0.82 to 0.91 $g \cdot cm^{-3}$. The material harvested in seed plantations differed from seeds from commercial seed stands in all parameters, excluding critical transport velocity. Seed weight was most correlated with the remaining parameters. The highest value of the correlation coefficient and the equation with the highest value of the coefficient of determination were reported for the dependence between seed weight and seed length. Seed weight was also relatively highly correlated with seed width, therefore, the use of mesh screens with round openings and/or cylindrical grain graders is recommended in seed sorting processes.

Symbols:
D_a – arithmetic mean diameter, mm,
D_g – geometric mean diameter, mm,
m – seed weight, mg,
m_D – specific seed weight, $g \cdot m^{-1}$,

* Correspondence: Zdzisław Kaliniewicz, Katedra Maszyn Roboczych i Metodologii Badań, Uniwersytet Warmińsko-Mazurski, ul. Oczapowskiego 11/B112, 10-719 Olsztyn, phone: 48 89 523 39 34, e-mail: zdzislaw.kaliniewicz@uwm.edu.pl

R – aspect ratio, %,
SD – standard deviation of trait,
T, W, L – seeds thickness, width and length, mm,
v – critical transport velocity of seeds, $m \cdot s^{-1}$,
V – seed volume, mm^3,
x – average value of trait,
x_{max}, x_{min} – maximum and minimum value of trait,
γ – angle of static friction of seeds on steel, °,
μ – coefficient of static friction of seeds on steel,
ρ – seed density, $g \cdot cm^{-3}$,
Φ – sphericity index, %.

Introduction

Larch is a deciduous conifer that differs from other members of the pine family in that it sheds its needles in winter. The European larch (*Larix decidua* Mill.) is well adapted to the continental climate. In Poland, the optimal habitat for the species is found in the High Tatra Mountains. The European larch occurs sporadically in all Polish regions, mostly in artificial stands. The European larch and other larch species occupy approximately 2% of total forest area in Poland. The European larch is one of the most light-demanding trees of the temperate climate. The taxon has medium soil requirements, and it thrives on deep and medium-compact soils. The European larch grows best on soils with moderate moisture content and does not tolerate significant fluctuations in soil moisture (MURAT 2002, PUCHNIARSKI 2008, JAWORSKI 2011).

The European larch is a fast-growing species that can reach the height of 4.5 m already at the age of 5 years. The increase in height ends at the age of 15–25 years. Seeds can be harvested already from 15-year-old trees that grow in open spaces, whereas dense stands begin to produce seeds at the age of around 30 years. High seed yields are noted every 2–3 years or even every 6 years. Seeds mature in October-November, and cones are harvested between November and February before they release seeds (ZAŁĘSKI 1995, MURAT 2002, JAWORSKI 2011). In the natural habitat, seeds are released from the cone after repeated bending and flexing of the scales, and in extraction plants, seeds are removed from cones by a combination of thermal and mechanical extraction methods (ZAŁĘSKI 1995, ANISZEWSKA 2009, 2010). European larch seeds with moisture content of around 7% are suitable for short-term storage, but the moisture content of material intended for longer storage has to be further reduced (ZAŁĘSKI 1995).

European larch seeds do not require pre-sowing treatment, but soaking in water improves seed germination (ZAŁĘSKI 1995). According to the literature, (MIKOLA 1980, SABOR 1984, BONFIL 1998, CASTRO 1999, SEIWA 2000, KHAN, SHANKAR 2001, KHAN 2004, PARKER et al. 2006, SHANKAR 2006, QUERO et al.

2007, CASTRO et al. 2008, BURACZYK 2010), seed weight is one of the main physical properties that affect germination efficiency of most seed species. Seeds are difficult to sort based on this attribute. The correlations among seed weight and other physical properties were analyzed in this study, and the results were used to plan seed sorting processes.

The objective of this study was to determine the variations in and the correlations among the physical properties and the calculated indicators of European larch seeds obtained from seed plantations and commercial seed plants to increase the efficiency of seed sorting processes.

Materials and Methods

The experimental material comprised four batches of European larch from seed extraction plants in Jedwabno and Ruciane-Nida. Seeds were harvested in 2010 from selected seed stands and seed plantations in two forest regions of north-eastern Poland. The analyzed batches were harvested from the following tree stands:

a) registration No. MP/3/41221/05, region of origin – 157, municipality – Gardeja, geographic location – 53.67°N, 18.90°E, forest habitat – fresh mixed forest, age – 12 years (symbol: PN-12);
b) registration No. MP/3/41106/05, region of origin – 103, municipality – Braniewo, geographic location – 54.40°N, 19.83°E, forest habitat – fresh mixed coniferous forest, age – 25 years (symbol: PN-25);
c) registration No. MP/2/30944/05, region of origin – 202, municipality – Kowale Oleckie, geographic location 54.10°N, 22.25°E, forest habitat – fresh forest, age – 129 years (symbol: WDN-129);
d) registration number – MP/2/30988/05, region of origin – 206, municipality – Ruciane Nida, geographic location – 53.65°N, 21.53°E, forest habitat – fresh mixed forest, age – 150 years (symbol: WDN-150).

Seed batches were divided by halving (ZAŁĘSKI 1995). The analyzed material was halved, and one half was randomly selected for successive halving. The above procedure was applied to produce samples of around 100 seeds each. The analyzed seed batches had the following size: P-12 – 101, P-25 – 105, WDN-129 – 109, WDN-150 – 120.

Critical transport velocity of European larch seeds was determined in the Petkus K-293 pneumatic classifier, seed dimensions were determined with the use of the MWM 2325 workshop microscope (length and width) and a thickness gauge, the angle of sliding friction was measured on a horizontal plane with an adjustable angle of inclination equipped with a steel friction plate (GPS – Ra = 0.65 μm), and seed weight was determined on the WAA 100/C/2

laboratory scale. All measurements were performed according to the methods previously described by KALINIEWICZ et al. (2011) and KALINIEWICZ and POZNAŃSKI (2013).

The following indicators were determined for every seed:

– coefficient of static friction, based on the following general formula:

$$\mu = \tan\gamma \tag{1}$$

– arithmetic D_a and geometric mean diameter D_g, aspect ratio R and sphericity index Φ (MOHSENIN 1986):

$$D_a = \frac{T + W + L}{3} \tag{2}$$

$$D_g = (T \cdot W \cdot L)^{\frac{1}{3}} \tag{3}$$

$$R = \frac{W}{L} \cdot 100 \tag{4}$$

$$\Phi = \frac{(T \cdot W \cdot L)^{\frac{1}{3}}}{L} \cdot 100 \tag{5}$$

– specific weight (KALINIEWICZ 2013):

$$m_D = \frac{m}{D_g} \tag{6}$$

– volume, based on the coefficient determined experimentally by KALINIEWICZ et al. (2012b):

$$V = 0.42 \cdot T \cdot W \cdot L \tag{7}$$

– density:

$$\rho = \frac{m}{V} \tag{8}$$

The results were processed with the use of Statistica PL v. 10 application based on general statistical procedures, including Student's t-test for independent samples, one-way ANOVA, correlation analysis and linear regression

analysis (RABIEJ 2012). Statistical calculations were performed at the significance level of 0.05.

Results and Discussion

The parameters of the analyzed seeds are presented in Table 1. The lowest average values of seed thickness, width, length and mass, arithmetic and geometric mean diameter, specific weight and volume were reported in batch PN-25. The lowest seed plumpness was noted in batch PN-25, and the highest – in batch WDN-150. Seeds from selected seed stands were generally larger and heavier than the material harvested from seed plantations. Critical transport velocity values were generally consistent with those cited by KALINIEWICZ et al. (2012a) and somewhat higher than those noted by CZERNIK (1983b) and TYLEK (1999, 2004). The average seed dimensions and seed weight values were comparable to those reported by CZERNIK (1983a), TYLEK (2004) and KALINIEWICZ et al. (2012a). European larch seeds are similar in width to lodgepole pine seeds (JOHNSON et al. 2003), the seeds of selected rye varieties (ZDYBEL et al. 2009, KUSIŃSKA et al. 2010), oats, barley (HEBDA, MICEK 2007) and common

Table 1

Variations in the physical properties and the calculated indicators of the analyzed batches of European larch seeds in view of significant differences in the examined traits

Property/ indicator	Batch of seeds			
	PN-12 $\bar{x} \pm SD$	PN-25 $\bar{x} \pm SD$	WDN-129 $\bar{x} \pm SD$	WDN-150 $\bar{x} \pm SD$
v	6.13 ± 0.74^{a}	6.02 ± 0.47^{ab}	6.06 ± 0.57^{ab}	5.93 ± 0.57^{b}
T	1.29 ± 0.15^{c}	1.25 ± 0.14^{d}	1.37 ± 0.16^{b}	1.43 ± 0.16^{a}
W	2.43 ± 0.29^{c}	2.29 ± 0.30^{d}	2.62 ± 0.32^{b}	2.71 ± 0.29^{a}
L	3.90 ± 0.42^{c}	3.71 ± 0.47^{d}	4.36 ± 0.53^{b}	4.57 ± 0.62^{a}
γ	27.85 ± 5.79^{b}	31.52 ± 5.75^{a}	31.18 ± 6.30^{a}	31.98 ± 5.90^{a}
m	4.75 ± 1.51^{c}	4.03 ± 1.09^{d}	5.67 ± 1.48^{b}	6.14 ± 1.65^{a}
μ	0.54 ± 0.13^{b}	0.62 ± 0.15^{a}	0.62 ± 0.16^{a}	0.63 ± 0.14^{a}
D_a	2.54 ± 0.24^{c}	2.42 ± 0.27^{d}	2.78 ± 0.29^{b}	2.90 ± 0.31^{a}
D_g	2.30 ± 0.22^{c}	2.20 ± 0.23^{d}	2.50 ± 0.25^{b}	2.60 ± 0.25^{a}
R	62.38 ± 6.13^{a}	62.16 ± 5.89^{a}	60.43 ± 6.60^{b}	59.60 ± 5.52^{b}
Φ	59.11 ± 3.55^{a}	59.40 ± 3.18^{a}	57.48 ± 3.76^{b}	57.27 ± 3.96^{b}
m_D	2.03 ± 0.51^{b}	1.81 ± 0.36^{c}	2.24 ± 0.41^{a}	2.33 ± 0.46^{a}
V	5.25 ± 1.43^{c}	4.60 ± 1.42^{d}	6.74 ± 2.01^{b}	7.59 ± 2.13^{a}
ρ	0.91 ± 0.16^{a}	0.90 ± 0.15^{ab}	0.86 ± 0.13^{b}	0.82 ± 0.13^{c}

a, b, c, d – different letters point to significant differences in the value of a property (indicator) across seed batches

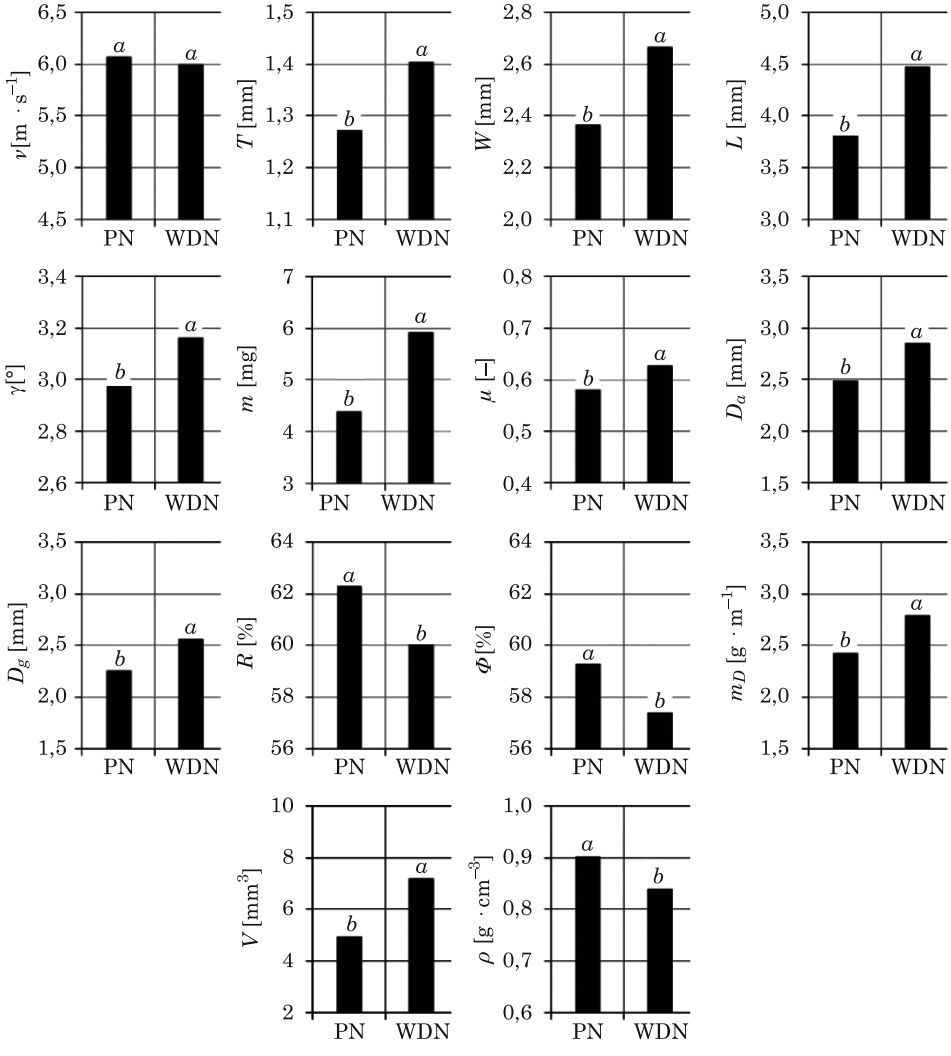

Fig. 1. Significance of differences among physical properties and indicators of European larch seeds: *a, b* – different letters indicate significant differences in the value of a property (indicator) across the analyzed seed batches

flax (PRADHAN et al. 2010). The average angle of sliding friction of European larch seeds, estimated in the range of 28° to 32°, resembles that of spelt seeds (CHOSZCZ et al. 2010) and sorry seeds (OMOBUWAJO et al. 2000). European larch seeds were similar to common flax seeds in their arithmetic and geometric mean diameter (PRADHAN et al. 2010), whereas their sphericity index resembled that of wheat (KALKAN, KARA 2011, KALINIEWICZ 2013, MARKOWSKI et al. 2013), *Chrysophyllum albidum* (OYELADE et al. 2005) and cocoa seeds (BART-PLANGE, BARYEH 2003).

The physical properties and the calculated indicators of seeds harvested from seed plantations (PN) and selected seed stands (WDN) are compared in Figure 1. The analyzed seeds differed in all parameters, excluding critical transport velocity. WDN seeds were more plump and were characterized by significantly greater thickness, width, length, weight, arithmetic and geometric mean diameter, specific weight and volume. They were also characterized by higher average angle of sliding friction and coefficient of sliding friction. The values of the aspect ratio and the sphericity index were lower in WDN seeds, which indicates that seeds harvested from seed stands were more slender that the material collected from seed plantations. The above also contributed to the lower density of WDN seeds.

A linear correlation analysis (Table 2) of selected properties that can be potentially applied in separation processes indicates that the angle of sliding friction was least correlated with the remaining attributes. Similar correlations with the angle of sliding friction and other physical parameters were observed in Scots pine seeds (KALINIEWICZ et al. 2011). Seed weight was most correlated with the remaining physical attributes, and the highest value of the correlation coefficient (0.823) was noted in a comparison of seed weight and seed length. The weight of European larch seeds was also significantly influenced by seed width and thickness. Similarly high correlation coefficients were noted in fir (CZERNIK 1993), Scots pine (SIVACIOĞLU 2010), Aleppo pine (MATZIRIS 1998) and black pine seeds (SIVACIOĞLU, AYAN 2010).

Table 2

Pearson's coefficients of correlation between selected parameters of European larch seeds

Grupa nasion	Property	T	W	L	γ	m	ρ
PN	v	**0.313**	**0.143**	0.106	-0.108	**0.580**	**0.595**
	T	1	**0.511**	**0.542**	**-0.196**	**0.603**	**-0.314**
	W		1	**0.702**	-0.081	**0.756**	-0.119
	L			1	-0.109	**0.721**	**-0.193**
	γ				1	**-0.145**	0.001
	m					1	**0.337**
WDN	v	**0.231**	0.074	0.076	**-0.214**	**0.460**	**0.556**
	T	1	**0.404**	**0.437**	**-0.306**	**0.566**	**-0.437**
	W		1	**0.714**	**-0.231**	**0.737**	**-0.330**
	L			1	**-0.226**	**0.800**	**-0.276**
	γ				1	**-0.343**	-0.003
	m					1	0.092
Total	v	**0.220**	0.066	0.039	**-0.169**	**0.423**	**0.575**
	T	1	**0.546**	**0.580**	**-0.173**	**0.655**	**-0.421**
	W		1	**0.772**	-0.075	**0.796**	**-0.291**
	L			1	-0.066	**0.823**	**-0.309**
	γ				1	**-0.155**	-0.035
	m					1	0.078

Values in bold indicate that the critical value of the correlation coefficient has been exceeded

Relatively high correlation coefficients were reported among seed dimensions and between seed weight and critical transport velocity. The noted values are somewhat different from those observed in European larch seeds by CZERNIK (1983a, 1983b), but they are similar to those reported in Scots pine (TURNA, GÜNEY 2009, KALINIEWICZ et al. 2011), black pine (SIVACIOĞLU, AYAN 2010), fir (CZERNIK 1993) and small-leaved lime seeds (KALINIEWICZ, POZNAŃSKI 2013).

According to the literature, seed weight influences seed germination and seedling development in the first year of life (MIKOLA 1980, SABOR 1984, BONFIL 1998, CASTRO 1999, SEIWA 2000, KHAN, SHANKAR 2001, KHAN 2004, PARKER et al. 2006, SHANKAR 2006, QUERO et al. 2007, CASTRO et al. 2008, BURACZYK 2010), and for this reason, only the dependences among seed weight and the remaining physical properties of European larch seeds were determined in this study (Table 3). In the correlation analysis, the equation with the highest value of the coefficient of determination (0.678) was reported in a comparison of seed weight and seed length. Relatively high values of the coefficient of determination were also noted for equations of seed weight as a function of the remaining parameters (width and thickness). It should also be noted that the above correlations were characterized by good fit to empirical data, implying that they can be effectively used to plan separation processes of European larch seeds. The results of the analysis can be applied to estimate the working parameters of seed separation machines based on aerodynamic and geometric attributes, mostly mesh screens (ZAŁĘSKI 1995, SARNOWSKA, WIĘSIK 1998).

Table 3

Correlations among seed weight and selected physical properties of European larch seeds

Equation	Coefficient of determination R^2	Standard error of estimate
$m = 1.190v - 1.985$	0.179	1.513
$m = 6.513T - 3.542$	0.429	1.261
$m = 3.904W - 4.657$	0.634	1.011
$m = 2.199L - 3.957$	0.678	0.948
$m = 0.042\gamma - 6.482$	0.024	1.649

For the needs of this analysis, it was assumed that European larch seeds comprised light ($m < 4.5$ mg), medium ($m = 4.5 \div 6.0$ mg) and heavy seeds ($m > 6.0$ mg). The distribution of seed fractions sorted based on seed thickness, width and length is presented in a histogram in Figure 2. The results indicate that seeds can be separated effectively based on differences in their width and length. A sieve separator incorporating a mesh screen with round openings measuring 2.6 mm in diameter can be used to separate 88% light seeds, 41% medium seeds and only 7% heavy seeds. A cylindrical grader with indentations

measuring 4.4 mm in diameter can potentially separate approximately 80% heavy seeds, 25% medium seeds and 2% light seeds.

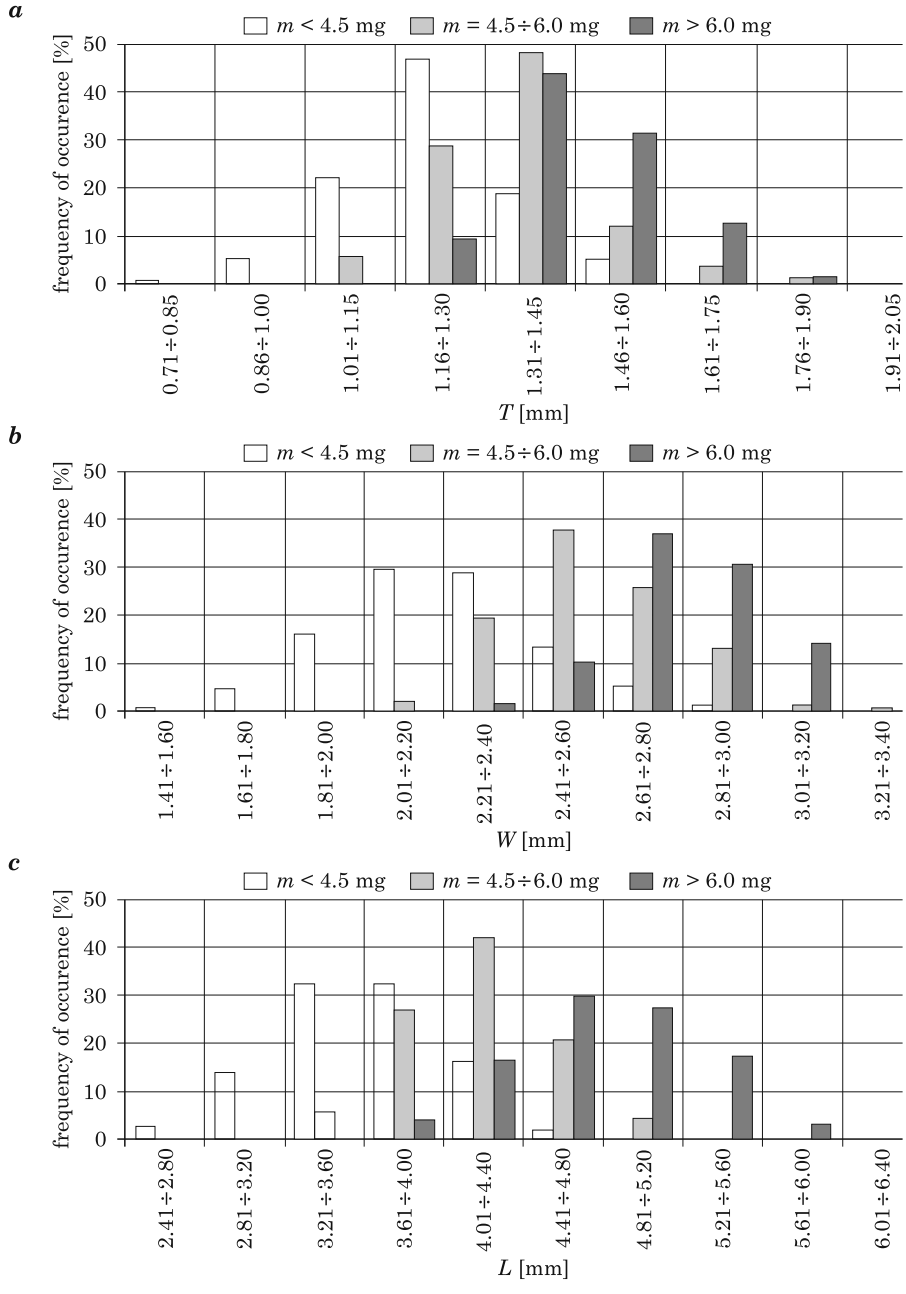

Fig. 2. Distribution of seed fractions based on seed dimensions: *a* – thickness, *b* – width, *c* – length

Conclusions

1. European larch seeds harvested from seed plantations (PN) differed significantly from the material obtained from seed stands (WDN) in all physical parameters and indicators, excluding critical transport velocity. In comparison with WDN seeds, PN seeds were characterized by smaller thickness, width, length, angle of sliding friction, weight, coefficient of sliding friction, arithmetic and geometric mean diameter, specific weight and volume, but higher aspect ratio, sphericity index and density.

2. Seed length and seed weight were the most correlated parameters of European larch seeds (correlation coefficient of approximately 0.8). The relationships among seed weight vs. critical transport velocity, seed thickness and seed width, among seed density vs. critical transport velocity and seed thickness, and among seed dimensions also produced high values of the correlation coefficient (above 0.4).

3. European larch seeds are most effectively separated with the use of mesh screens with round openings (seeds are separated based on width) and/or cylindrical grain graders (seeds are separated based on length). The above devices can separate more than 80% of heavy seeds and up to 7% of light seeds, and they can be effectively used to improve germination efficiency and germination rates of selected seed fractions.

References

ANISZEWSKA M. 2009. *Three-phase extraction of European larch seeds in the local kiln and laboratory*. Annals of Warsaw University of Life Sciences – SGGW. Agriculture, Agricultural and Forest Engineering, 53: 73–78.

ANISZEWSKA M. 2010. *Analysis of opening cones of selected coniferous trees*. Annals of Warsaw University of Life Sciences – SGGW. Agriculture, Agricultural and Forest Engineering, 55: 57–64.

BART-PLANGE A., BARYEH E.A. 2003. *The physical properties of Category B cocoa beans*. Journal of Food Engineering, 60: 219–227.

BONFIL C. 1998. *The effects of seed size, cotyledon reserves, and herbivory on seedling survival and growth in Quercus rugosa and Q. laurina (Fagaceae)*. American Journal of Botany, 85(1): 79–87.

BURACZYK W. 2010. *Seed characteristics and morphological features of Scots pine (Pinus sylvestris L.) seedlings*. Leśne Prace Badawcze, 71(1): 13–20 (in Polish with English abstract).

CASTRO J. 1999. *Seed mass versus seedling performance in Scots pine: a maternally dependent trait.* New Phytologist, 144: 153–161.

CASTRO J., REICH P.B., SÁNCHEZ-MIRANDA Á., GUERRERO J.D. 2008. *Evidence that the negative relationship between seed mass and relative growth rate is not physiological but linked to species identity: a within-family analysis of Scots pine*. Tree Physiology, 28: 1077–1082.

CHOSZCZ D., KONOPKA S., ZALEWSKA K. 2010. *Characteristics of physical properties of selected varieties of spelt*. Inżynieria Rolnicza, 4(122): 23–28 (in Polish with English abstract).

CZERNIK Z. 1983a. *Studies of geometrical features of seeds of Scotch pine, Norway spruce and European larch*. Sylwan, 7: 31–40 (in Polish with English abstract).

CZERNIK Z. 1983b. *Studies of aerodynamical features of seeds of Scotch pine, Norway spruce and European larch*. Sylwan, 9/10: 31–40 (in Polish with English abstract).

CZERNIK Z. 1993. *Studies of Geometrical Properties of Silver Fir Seeds*. Sylwan, 8: 57–64 (in Polish with English abstract).

HEBDA T., MICEK P. 2007. *Geometric features of grain for selected corn varieties*. Inżynieria Rolnicza, 5(93): 187–193 (in Polish with English abstract).

JAWORSKI A. 2011. *Hodowla lasu*. Tom III. *Charakterystyka hodowlana drzew i krzewów leśnych*. Wyd. PWRiL, Warszawa.

JOHNSON M., VANDER WALL S.B., BORCHERT M. 2003. *A comparative analysis of seed and cone characteristics and seed-dispersal strategies of three pines in the subsection Sabinianae*. Plant Ecology, 168: 69–84.

KALINIEWICZ Z. 2013. *Analysis of frictional properties of cereal seeds*. African Journal of Agricultural Research, 8(45): 5611–5621.

KALINIEWICZ Z., GRABOWSKI A., LISZEWSKI A., FURA S. 2011. *Analysis of correlations between selected physical attributes of Scots pine seeds*. Technical Sciences, 14(1): 13–22.

KALINIEWICZ Z., MARKOWSKI P., ANDERS A., RAWA T., LISZEWSKI A., FURA S. 2012a. *Correlations between the germination capacity and selected attributes of European larch seeds (Larix decidua Mill.)*. Technical Sciences, 15(2): 229–242.

KALINIEWICZ Z., POZNAŃSKI A. 2013. *Variability and correlation of selected physical attributes of small-leaved lime (Tilia cordata Mill.) seeds*. Sylwan, 157(1): 39–46 (in Polish with English abstract).

KALINIEWICZ Z., TYLEK P., MARKOWSKI P., ANDERS A., RAWA T., ZADROŻNY M. 2012b. *Determination of shape factors and volume coefficients of seeds from selected coniferous trees*. Technical Sciences, 15(2): 217–228.

KALKAN F., KARA M. 2011. *Handling, frictional and technological properties of wheat as affected by moisture content and cultivar*. Powder Technology, 213: 116–122.

KHAN M.L. 2004. *Effects of seed mass on seedling success in Artocarpus heterophyllus L., a tropical tree species of north-east India*. Acta Oecologica, 25: 103–110.

KHAN M.L., SHANKAR U. 2001. *Effect of seed weight, light regime and substratum microsite on germination and seedling growth of Quercus semiserrata Roxb*. Tropical Ecology, 42(1): 117–125.

KUSIŃSKA E., KOBUS Z., NADULSKI R. 2010. *Impact of humidity on physical and geometrical properties of Slavic varieties of rye grains*. Inżynieria Rolnicza, 4(122): 151–156 (in Polish with English abstract).

MARKOWSKI M., ŻUK-GOŁASZEWSKA K., KWIATKOWSKI D. 2013. *Influence of variety on selected physical and mechanical properties of wheat*. Industrial Crops and Product, 47: 113–117.

MATZIRIS D. 1998. *Genetic Variation in Cone and Seed Characteristics in a Clonal Seed Orchard of Aleppo Pine Grown in Greece*. Silvae Genetica, 47(1): 37–41.

MIKOLA J. 1980. *The effect of seed size and duration of growth on the height of Scots pine (Pinus sylvestris L.) and Norway spruce (Picea abies (L.) Karst.) provenances and progenies at the nursery stage*. Silva Fennica, 14(1): 84–94.

MOHSENIN N.N. 1986. *Physical properties of plant and animal materials*. Gordon and Breach Science Public, New York.

MURAT E. 2002. *Szczegółowa hodowla lasu*. Wyd. Oficyna Edytorska „Wydawnictwo Świat", Warszawa.

Nasiennictwo leśnych drzew i krzewów iglastych. 1995. Red. A. ZAŁĘSKI. Wyd. Oficyna Edytorska „Wydawnictwo Świat", Warszawa.

OMOBUWAJO T.O., SANNI L.A., BALAMI Y.A. 2000. *Physical properties of sorry (Hibiscus sabdariffa) seeds*. Journal of Food Engineering, 45: 37–41.

OYELADE O.J., ODUGBENRO P.O., ABIOYE A.O., RAJI N.L. 2005. *Some physical properties of African star apple (Chrysophyllum alibidum) seeds*. Journal of Food Engineering, 67: 435–440.

PARKER W.C., NOLAND T.L., MORNEAULT A.E. 2006. *The effects of seed mass on germination, seedling emergence, and early seedling growth of eastern white pine (Pinus strobus L.)*. New Forests, 32: 33–49.

PRADHAN R.C., MEDA V., NAIK S.N., TABIL L. 2010. *Physical properties of Canadian grown flaxseed in relation to its processing*. International Journal of Food Properties, 13: 732–743.

Quero J.L., Villar R., Marañón T., Zamora R., Poorter L. 2007. *Seed-mass effects in four Mediterranean Quercus species (Fagaceae) growing in contrasting light environments*. American Journal of Botany, 94(11): 1795–1803.

Rabiej M. 2012. *Statystyka z programem Statistica*. Wyd. Helion, Gliwice.

Sabor J. 1984. *Relation between the weight and the germination capacity of seed of silver fir*. Sylwan, 4: 59–69 (in Polish with English abstract).

Sarnowska G., Więsik J. 1998. *Wyłuszczarnia w Czarnej Białostockiej*. Część III. *Czyszczenie i separacja nasion*. Przegląd Techniki Rolniczej i Leśnej, 1: 19–21.

Seiwa K. 2000. *Effects of seed size and emergence time on tree seedling establishment: importance of developmental constraints*. Oecologia, 123: 208–215.

Shankar U. 2006. *Seed size as a predictor of germination success and early seedling growth in 'hollong' (Dipterocarpus macrocarpus Vesque)*. New Forests, 31: 305–320.

Sivacioğlu A. 2010. *Genetic variation in seed cone characteristics in a clonal seed orchard of Scots pine (Pinus sylvestris L.) grown in Kastamonu-Turkey*. Romanian Biotechnological Letters, 15(6): 5695–5701.

Sivacioğlu A., Ayan S. 2010. *Variation in cone and seed characteristics in clonal seed orchard of Anatolian black pine [Pinus nigra Arnold subsp. pallasiana (Lamb.) Holmboe]*. Journal of Environmental Biology, 31: 119–123.

Turna I., Güney D. 2009. *Altitudinal variation of some morphological characters of Scots pine (Pinus sylvestris L.) in Turkey*. African Journal of Biotechnology, 8(2): 202–208.

Tylek P. 1999. *Problems of pneumatic selection of forest tree seeds*. Sylwan, 12: 65-72 (in Polish with English abstract).

Tylek P. 2004. *Selected physical features and storting criteria for European larch seeds*. Sylwan, 4: 27–33 (in Polish with English abstract).

Zdybel A., Gawłowski S., Laskowski J. 2009. *Influence of moisture content on some physical properties of rye grains*. Acta Agrophysica, 14(1): 243–255 (in Polish with English abstract).

Technical Sciences 17(2), 2014, 135–148

MODIFICATION OF THE PATHFINDER ALGORITHM FOR CALCULATING GRANULAR BEDS WITH VARIOUS PARTICLE SIZE DISTRIBUTIONS

Waldemar Dudda, Wojciech Sobieski

Department of Mechanics and Machine Design
University of Warmia and Mazury in Olsztyn

Received 19 May 2014, accepted 18 June 2014, available on line 18 June 2014

K e y w o r d s: PathFinder code, porous media, granular beds, tortuosity.

A b s t r a c t

This paper discusses a new approach to analyzing fluid flow through a granular bed. The analysis involves the determination of a set of geometric parameters characterizing a granular bed based on information about the location and diameter of all bed particles. The above task has been achieved with the use of the PathFinder numeric code developed by the authors. The study proposes a new algorithm for calculating the parameters of granular beds composed of spherical particles with various diameters in the PathFinder program. The algorithm has been verified with the use of independent tools and implemented in the new version of the PathFinder code. The modified algorithm's effect on flow path tortuosity has been analyzed. Path length is used to determine tortuosity, a key parameter of pore geometry that is difficult to calculate. Comparative calculations were performed in a granular bed generated by the Discrete Element Method in the PFC^{3D} program.

Introduction

Granular porous media comprising spherical or quasi-spherical particles play an important role in various technological and engineering processes. Due to the widespread occurrence of porous media, mathematical models describing the behavior of a granular medium, also known as a granular bed, or its interactions with the environment are of great practical significance. Models predicting resistance (pressure loss) during fluid flow through granular media have attracted particular interest. Despite many years of research, a satisfactory solution to the problem has not yet been proposed (SOBIESKI, TRYKOZKO 2011), and continuous attempts are being made to develop a single universal

* Correspondence: Waldemar Dudda, Katedra Mechaniki i Podstaw Konstrukcji Maszyn, Uniwersytet Warmińsko-Mazurski, ul. Oczapowskiego 11, 10-917 Olsztyn, phone: 48 89/523 32 40, e-mail: waldemar.dudda@uwm.edu.pl

theory. A well designed and executed experiment continues to be the most reliable method of investigating porous media (SOBIESKI, TRYKOZKO 2014a, SOBIESKI, TRYKOZKO 2014b).

This paper is related to a novel research method, described in detail by (SOBIESKI et al. 2012, SOBIESKI, LIPIŃSKI 2014), which relies on a specific combination of microscopic and macroscopic mathematical and physical models for analyzing fluid flow through granular beds. The models are combined with the PathFinder (PathFinder Project 2013, SOBIESKI, LIPIŃSKI 2014) numeric code to calculate a set of geometric parameters of granular beds based on information about the location and diameters of all particles in that bed. Data for calculations in the PathFinder program can be obtained indirectly by developing a virtual bed model with the use of the Discrete Element Method, or directly by generating tomographic scans of the bed sample and analyzing the resulting images. The objective of this study was to describe the new algorithm, whereas the remaining problems have been omitted due to space constraints. The adopted approach could obstruct understanding of the discussed problem, and detailed information about the tortuosity algorithm (SOBIESKI, ZHANG 2012) and the PathFinder program (SOBIESKI, LIPIŃSKI 2014, PathFinder Project 2013) can be found in previous publications.

The previous versions of the PathFinder program (up to version IV.0, inclusive) were developed on the assumption that particles in granular beds are spherical and have constant diameter. In consequence, the triangle defined by centroids of adjacent spheres is roughly equilateral. Therefore, it can be assumed that the center of gravity, S_{gc}, of surface (flow segment) A_p (intersected by the "tortuous flow path") will overlap the center of gravity, S_{tc}, of triangle ABC whose coordinates are defined by the following dependencies (CEWE 2010):

$$\begin{aligned} x_{tc} &= \frac{1}{3}(x_A + x_B + x_C) \\ y_{tc} &= \frac{1}{3}(y_A + y_B + y_C) \\ z_{tc} &= \frac{1}{3}(z_A + z_B + z_C) \end{aligned} \tag{1}$$

where the values in parentheses represent the coordinates of sphere centroids [m] and, consequently, the coordinates of the vertices of triangle ABC.

The determination of the centroid of a triangle composed of three adjacent spheres is a very important consideration in algorithms for calculating the tortuosity of a porous medium (BEAR 1972)

$$\tau = \frac{L_p}{L_0} \tag{2}$$

where: τ – tortuosity [m/m], L_p – ratio of the actual path length inside channels [m], L_0 – thickness of the porous medium [m].

In addition to porosity and specific surface area, the tortuosity of a medium is one of the key parameters characterizing the spatial structure of porous media. In analyses of granular beds, tortuosity is used in the Kozeny-Carman equation (CARMAN 1997, KOZENY 1927, SOBIESKI, ZHANG 2014).

The study proposes a new algorithm for calculating the parameters of granular beds composed of spherical particles with various diameters in the PathFinder program.

Methodology

When spherical particles, including particles with the same radius, are unevenly distributed in a medium, the coordinates of centroid S_{gc} of figure A_p do not match the coordinates of the center of gravity, S_{tc}, of triangle ABC (Fig. 1). The variations in the location of the above points will be even greater when the radii of three spherical particles are different.

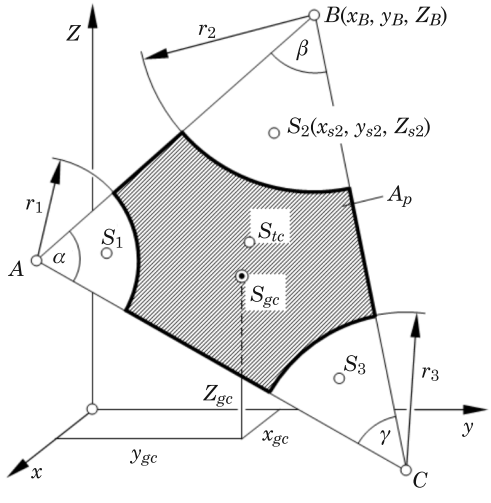

Fig. 1. Surface A_p and its center of gravity, S_{gc}

To solve the problem, a procedure for determining the coordinates of the center of gravity of the shaded region A_p (Fig. 1) has to be developed. The area of the shaded region represents the difference between the area of triangle ABC and the total area of three circular sectors with radii r_1, r_2, r_3 and angles α, β and γ. When the area of each figure and the coordinates of their centers of gravity are known, the coordinates of the center of gravity of surface A_p can be determined with the use of the summation method (LEYKO 2010), which is widely used in mechanics and mathematics:

$$\begin{aligned} x_{gc} &= \frac{A_t\, x_{tc} - A_1\, x_{S1} - A_2\, x_{S2} - A_3\, x_{S3}}{A_t - A_1 - A_2 - A_3} \\ y_{gc} &= \frac{A_t\, y_{tc} - A_1\, y_{S1} - A_2\, y_{S2} - A_3\, y_{S3}}{A_t - A_1 - A_2 - A_3} \\ z_{gc} &= \frac{A_t\, z_{tc} - A_1\, z_{S1} - A_2\, z_{S2} - A_3\, z_{S3}}{A_t - A_1 - A_2 - A_3} \end{aligned} \tag{3}$$

where A_1, A_2 and A_3 represent the area of circular sectors where centers of gravity are located at points $S_1(x_{S1}, y_{S1}, z_{S1})$, $S_2(x_{S2}, y_{S2}, y_{S2})$, $S_3(x_{S3}, y_{S3}, z_{S3})$, respectively.

The area of triangle ABC can be determined using Heron's formula (CEWE 2010):

$$A_t = \sqrt{p(p - AB)(p - BC)(p - CA)} \tag{4}$$

where parameter p, determined by dependence

$$p = \frac{1}{2}(AB + BC + CA) \tag{5}$$

is half that triangle's circumference. The length of the triangle's sides is determined based on the coordinates of the triangle's vertices:

$$\begin{aligned} AB &= \sqrt{(x_A - x_B)^2 + (y_A - y_B)^2 + (z_A - z_B)^2} \\ BC &= \sqrt{(x_B - x_C)^2 + (y_B - y_C)^2 + (z_B - z_C)^2} \\ CA &= \sqrt{(x_C - x_A)^2 + (y_C - y_A)^2 + (z_C - z_A)^2} \end{aligned} \tag{6}$$

The area of circular sectors is defined by geometric dependencies (CEWE 2010):

$$A_1 = \frac{1}{2} r_1 \alpha$$

$$A_2 = \frac{1}{2} r_2 \beta \tag{7}$$

$$A_3 = \frac{1}{2} r_3 \gamma$$

where α, β and γ are vertex angles expressed in radians. Vertex angles are calculated from trigonometric functions when the formulas are transformed to find the area of the triangle (CEWE 2010):

$$\sin \alpha = \frac{2A_t}{AB \cdot AC}$$

$$\sin \beta = \frac{2A_t}{BA \cdot BC} \tag{8}$$

$$\sin \gamma = \frac{2A_t}{CA \cdot CB}$$

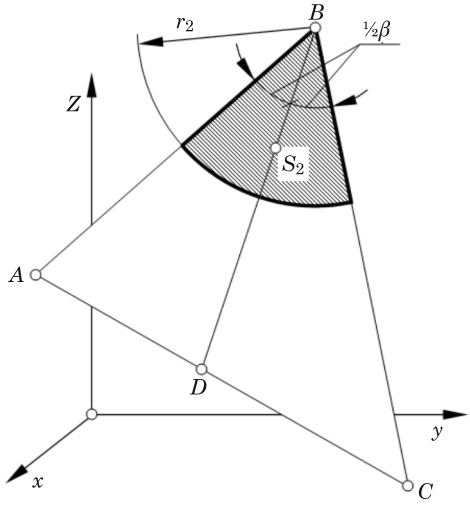

Fig. 2. Location of the center of gravity, S_2, of a circular sector with a centroid at point B

The coordinates of points S_1, S_2 and S_3 have to be calculated to determine the coordinates of point S_{gc} with the use of formula (3). A method for determining coordinates x_{S2}, y_{S2} and z_{S2}, which describe the location of the center of gravity, S_2, of a circular segment with radius r_2 and centroid at point B, is described below. The first step involves the calculation of the coordinates of point D (Fig. 2). Those coordinates are used to determine the bisector of angle β where the center of gravity, S_2, is located. The coordinates of point D are determined based on the coordinates of point A and the coordinates of displacement vector $\overrightarrow{AD}$ based on the following relationship:

$$\begin{bmatrix} x_D \\ y_D \\ z_D \end{bmatrix} = \begin{bmatrix} x_A + x_{AD} \\ y_A + y_{AD} \\ z_A + z_{AD} \end{bmatrix} \tag{9}$$

Segment BD is the bisector of angle β, therefore, the dependence between the lengths of the below segments holds true for triangle ABC:

$$\frac{AD}{AC} = \frac{AB}{CB} \tag{10}$$

When the dependence describing the length of segment AC

$$AC = AD + DC \tag{11}$$

is substituted into equation (10) and when simple transformations are performed, the length of segment AD is expressed as:

$$AD = \frac{AC \cdot AB}{BC + AB} \tag{12}$$

The vector of displacement from point A to point D can be expressed as follows:

$$\overrightarrow{AD} = \overrightarrow{AC^0} \cdot AD = \frac{\overrightarrow{AC}}{AC} \cdot AD = \overrightarrow{AC}\,\frac{AD}{AC} \tag{13}$$

and its coordinates are equal to:

$$\begin{bmatrix} x_{AD} \\ y_{AD} \\ z_{AD} \end{bmatrix} = \begin{bmatrix} x_C - x_A \\ y_C - y_A \\ z_A - z_A \end{bmatrix} \cdot \frac{AD}{AC} \tag{14}$$

Dependence (12) is substituted into formula (14), and the result is substituted into equation (9) to produce formulas for calculating the coordinates of point D:

$$\begin{bmatrix} x_D \\ y_D \\ z_D \end{bmatrix} = \begin{bmatrix} x_A \\ y_A \\ z_A \end{bmatrix} + \begin{bmatrix} x_C - x_A \\ y_C - y_A \\ z_C - z_A \end{bmatrix} \cdot \frac{AB}{BC + AB} \tag{15}$$

The next step involves the determination of the coordinates of point S_2.

The coordinates of point S_2 are calculated based on the coordinates of point B and the coordinates of displacement vector $\overrightarrow{BS_2}$. The searched coordinates are expressed by the following dependence:

$$\begin{bmatrix} x_{S_2} \\ y_{S_2} \\ z_{S_2} \end{bmatrix} = \begin{bmatrix} x_B + x_{BS_2} \\ y_B + y_{BS_2} \\ z_B + z_{BS_2} \end{bmatrix} \tag{16}$$

Centroid S_2 of the circular sector is located on bisector B_D, and its distance from point B (centroid of the circular sector) is defined by the following geometric dependence:

$$BS_2 = \frac{4}{3} r_2 \frac{\sin \frac{1}{2}\beta}{\beta} \tag{17}$$

where vertex angle β is expressed in radians.

The vector of displacement from point B to point S_2 can be expressed as follows:

$$\overrightarrow{BS_2} = \overrightarrow{BD}^0 \cdot BS_2 = \frac{\overrightarrow{BD}}{BD} \cdot BS_2 = \overrightarrow{BD} \frac{BS_2}{BD} \tag{18}$$

therefore, its coordinates are equal to:

$$\begin{bmatrix} x_{BS_2} \\ y_{BS_2} \\ z_{BS_2} \end{bmatrix} = \begin{bmatrix} x_D - x_B \\ y_D - y_B \\ z_D - z_B \end{bmatrix} \cdot \frac{BS_2}{BD} \tag{19}$$

and the length of segment BD is determined based on the following dependence:

$$BD = \sqrt{(x_D - x_B)^2 + (y_D - y_B)^2 + (z_D - z_B)^2} \tag{20}$$

Dependence (17) is substituted into (19) in view of dependence (20). The result is substituted into equation (16) to obtain (after simple transformations) the coordinates of centroid S_2 of the circular sector in the following form:

$$\begin{bmatrix} x_{S_2} \\ y_{S_2} \\ z_{S_2} \end{bmatrix} = \begin{bmatrix} x_B \\ y_B \\ z_B \end{bmatrix} + \begin{bmatrix} x_D - x_B \\ y_D - y_B \\ z_D - z_B \end{bmatrix} \cdot \frac{4r_2 \sin \frac{1}{2}\beta}{3\beta \sqrt{(x_D - x_B)^2 + (y_D - y_B)^2 + (z_D - z_B)^2}} \tag{21}$$

The above process is repeated for circular sectors at points C and A (Fig. 3) to obtain the coordinates of points E and H:

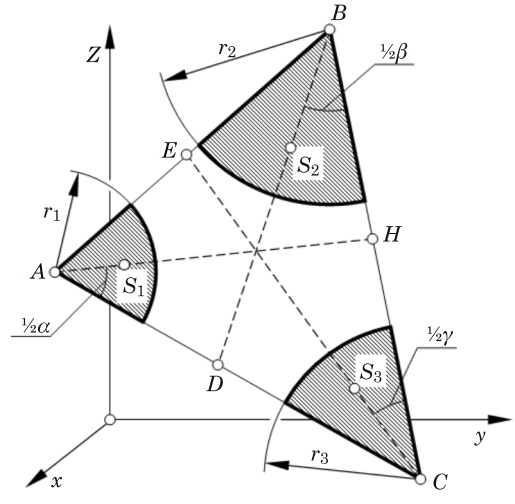

Fig. 3. Location of centroids S_1 and S_3 of the remaining circular sectors

$$\begin{bmatrix} x_E \\ y_E \\ z_E \end{bmatrix} = \begin{bmatrix} x_B \\ y_B \\ z_B \end{bmatrix} + \begin{bmatrix} x_A - x_B \\ y_A - y_B \\ z_A - z_B \end{bmatrix} \cdot \frac{BC}{CA + BC} \tag{22}$$

$$\begin{bmatrix} x_H \\ y_H \\ z_H \end{bmatrix} = \begin{bmatrix} x_C \\ y_C \\ z_C \end{bmatrix} + \begin{bmatrix} x_B - x_C \\ y_B - y_C \\ z_B - z_C \end{bmatrix} \cdot \frac{CA}{AB + CA} \tag{23}$$

and the coordinates of centroids S_3 and S_1, respectively:

$$\begin{bmatrix} x_{S_3} \\ y_{S_3} \\ z_{S_3} \end{bmatrix} = \begin{bmatrix} x_C \\ y_C \\ z_C \end{bmatrix} + \begin{bmatrix} x_E - x_C \\ y_E - y_C \\ z_E - z_C \end{bmatrix} \cdot \frac{4r_3 \sin\frac{1}{2}\gamma}{3\gamma\sqrt{(x_E - x_C)^2 + (y_E - y_C)^2 + (z_E - z_C)^2}} \quad (24)$$

$$\begin{bmatrix} x_{S_1} \\ y_{S_1} \\ z_{S_1} \end{bmatrix} = \begin{bmatrix} x_A \\ y_A \\ z_A \end{bmatrix} + \begin{bmatrix} x_H - x_A \\ y_H - y_A \\ z_H - z_A \end{bmatrix} \cdot \frac{4r_1 \sin\frac{1}{2}\alpha}{3\alpha\sqrt{(x_H - x_A)^2 + (y_H - y_A)^2 + (z_H - z_A)^2}} \quad (25)$$

The coordinates are calculated with the use of formulas (1), (21), (24) and (25), area is calculated based on equations (4) and (7), and the results are substituted into formula (3) to obtain the coordinates of the center of gravity of figure A_p.

The parameters of figure A_p, which are applied in the computational program, include its area:

$$A_F = A_t - A_1 - A_2 - A_3 \quad (26)$$

and circumference:

$$p_F = 2(p - r_1 - r_2 - r_3) + (\alpha \cdot r_1 + \beta \cdot r_2 + \gamma \cdot r_3) \quad (27)$$

where angles α, β and γ are expressed in radians.

Validation of derived dependencies

The presented algorithm was used to develop a numeric procedure in the Fortran 90 programming language. The subprogram calculates the coordinates of the centroid of figure A_p based on the input coordinates of triangle vertices and the radii of circular sectors. The procedure was implemented in the PathFinder program to determine the tortuous flow path. In the main program, the positions of three spherical particles are used to calculate the position of the fourth particle making up the tetrahedron. The position of the fourth spherical particle is calculated by determining the normal to the triangle surface intersecting the center of gravity of figure A_p. In a numerical

analysis of a bed comprising thousands of spherical particles, the position of adjacent tetrahedrons, which form the region of the tortuous flow path, is determined. The path is mapped by combining the centroids of figures A_p of adjacent tetrahedron sides. Path length is the total length of the segments combining the centroids of successive figures A_p in the region of the entire tortuous flow path. The procedure of determining the coordinates of a centroid of the current surface A_p is called before the search for every successive tetrahedron is initiated in accordance with the discussed algorithm.

The coordinate calculation procedure was verified in the AutoCAD program. The coordinates of any graphically represented flat or solid figure can be determined in the AutoCAD environment independently of the applied algorithm. The validation process was performed for a triangle with vertex coordinates $A(10,3,4)$, $B(2,20,30)$ and $C(20,30,10)$, from which circular sectors with radii R of 5, 6 and 8, respectively, had been removed (Fig. 4). The resulting figure, represented by the shaded region in Figure 4, was created with the use of an AutoCAD command. The physical properties of that region were determined in the program. A text window with the parameters of the selected region, including area, circumference and centroid coordinates, is presented in Figure 5.

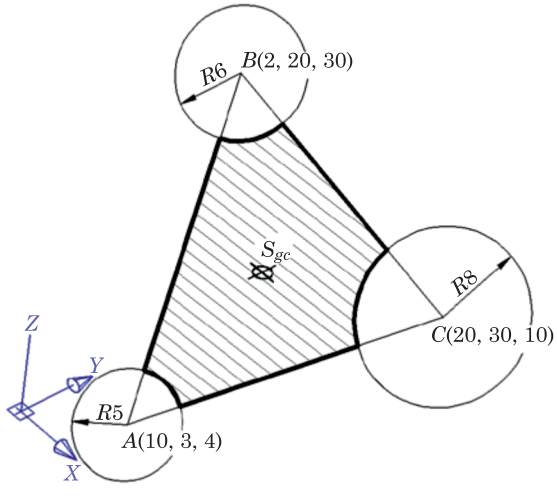

Fig. 4. Surface A_p determined in the AutoCAD program

Figure coordinates were calculated in the subprogram written in Fortran based on the dependencies derived in Chapter 2. The results are presented in Table 1. The results produced by the discussed algorithm (Table 1) and the results generated in AutoCAD are identical (Fig. 5). The derived dependencies and the numerical subprogram were thus positively validated.

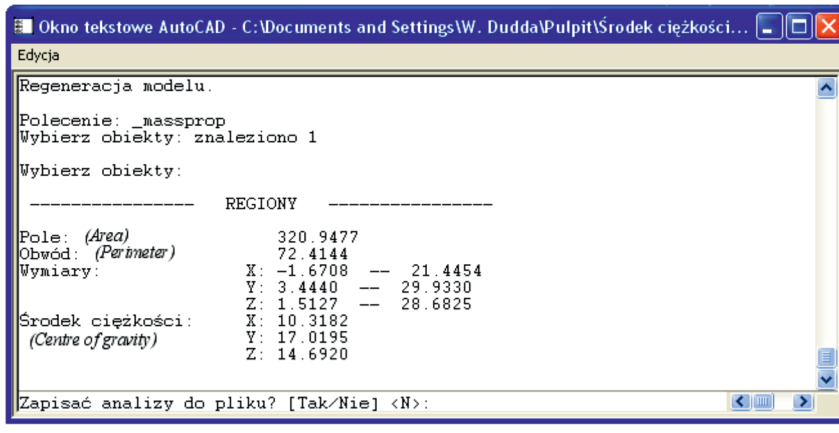

Fig. 5. Centroid coordinates determined in the AutoCAD program

Table 1

The results of geometric calculations

Coordinates of triangle centroid (x_{tc}, y_{tc}, z_{tc})	Angles (α, β, γ)	Area of circular sectors (A_1, A_2, A_3)	Coordinates of circular sector centroids [m]			Coordinates of the center of gravity (x_{gc}, y_{gc}, z_{gc})	Figure area (A_F)	Figure circumference (p_F)
			S_1 (x_1, y_1, z_1)	S_2 (x_2, y_2, z_2)	S_3 (x_3, y_3, z_3)			
[m]	[°]	[m^2]	[m]	[m]	[m]	[m]	[m^2]	[m]
10.6667	55.4537	12.0981	10.1640	3.9169	17.0806	10.31816		
17.6667	57.5555	18.0816	5.6212	19.6028	26.1772	17.01952	320.9477	72.4144
14.6667	66.9908	37.4147	5.8365	26.7035	11.4874	14.69201		

Comparison of tortuous flow paths (previous and new version)

The effect of changes in the computational algorithm on program performance was verified by performing comparative calculations in a granular bed generated by the Discrete Element Method in PFC^{3D} (LIU et al. 2008a, LIU et al. 2008b). Bed parameters and basic PathFinder settings (refer to the User's Guide (SOBIESKI, LIPIŃSKI 2014)) are presented in Table 2.

The results of both computational methods and a model ISP (in this case: a centroid) are presented in Table 3. As expected, a change in the algorithm modified the course of the path in space, including its total length, average angles between segments and tortuosity. The remaining parameters remained unchanged.

The changes in point positions were relatively small, but they significantly influenced the course of different paths. The above is illustrated by Figure 6

Table 2

Basic parameters of the flow set

Parameter	Value
Domain geometry	cylinder
Number of particles	18188 [–]
Particle diameters	5.5–7.5 [mm]
Average diameter	6.45 [mm]
Number of particles rejected from the top surface	19 [–]
Method for calculating the triangle centroid	triangle centroid / center of gravity
Characteristic dimension	l_{ave} [m]
Correction method for the Ideal Location	function
Correction based on the critical area of the triangle	yes
Critical normalized area of the triangle	3.0 [–]

where paths momentarily follow the same flow channels, then change direction and become completely separated. In some cases, previously separated paths are repeatedly merged. Even if paths follow the same flow channels, they do not overlap. Changes in three model paths for ISP = '00' (the results for this path are presented in Table 3), ISP = '– –' and ISP = '++' are presented in Figure 6. Symbols '–', '0' and '+' denote the location of the ISP relative to the centroid of the surface that constitutes the bottom wall of the bin (SOBIESKI, LIPIŃSKI 2014).

Table 3

Comparison of results

Parameter	Triangle centroid	Centre of gravity	Unit
Initial Staring Point	00		[–]
xshift / yshift	0.5 / 0.5		[–]
Number of path points	129	130	[–]
Number of path rejected points	1	0	[–]
Number of corrected triangles	0	0	[–]
Bed height	0.254938		[m]
Path length	0.315499	0.317288	[m]
Average angle between path sections	137.859292	140.183486	[°]
Tortuosity	1.237553	1.244571	[m/m]
Tortuosity determined by the formula of Yu and Li	1.632555		[m/m]
Bed volume (bulk volume)	0.004505		[m^3]
Inner surface of the solid body	2.393343		[m^2]
Specific surface of the porous body (K)	531.227627		[1/m]
Specific surface of the porous body (C)	915.918417		[1/m]
Volume of the porous body	0.002613		[m^3]
Porosity	0.420006		[m^3/m^3]

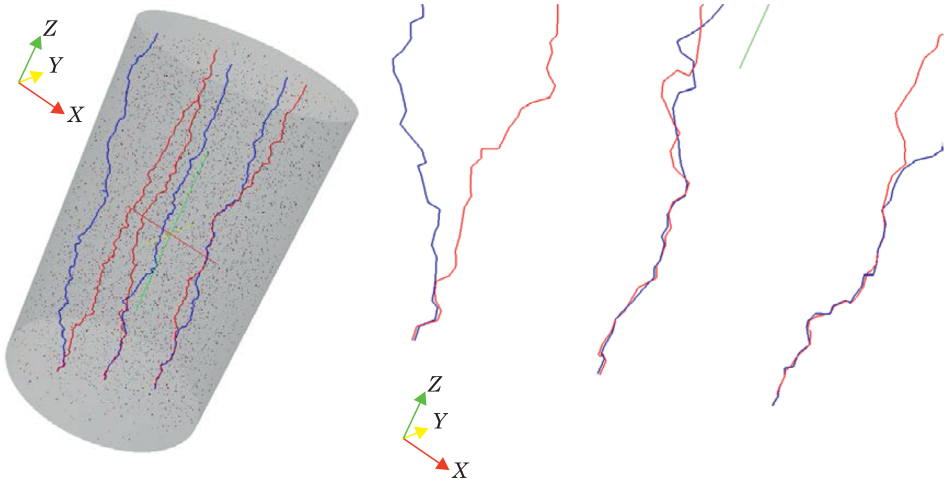

Fig. 6. Paths determined with the use of different methods: triangle centroid (blue) and center of gravity (red)

The values of the quality indicator for predicting the location of tetrahedron vertices (an important part of the algorithm for tortuosity evaluation – refer to (SOBIESKI, ZHANG 2014) are presented in Figure 7. The lower the value of the quality indicator, the greater the algorithm's efficiency in predicting the location of successive spheres surrounding the path (spheres divided by the path). The data presented in Figure 7 indicates that an algorithm based on centers of gravity often produces more satisfactory results.

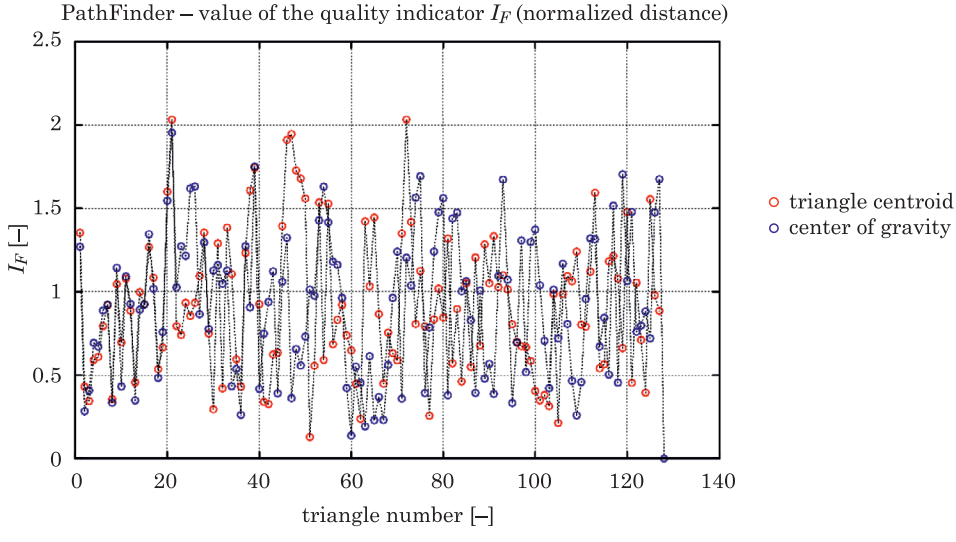

Fig. 7. Values of the quality indicator for predicting the location of tetrahedron vertices

Conclusions

The following conclusions can be formulated based on the results of the study:

– A universal algorithm was developed for calculating the center of gravity of a figure intersected by a flow path. The algorithm was verified with the use of independent computational tools (AutoCAD program) and successfully implemented in the source code of the PathFinder program.

– The new version of the computational algorithm influences only the length of the flow path, the angles between path segments and path tortuosity. The remaining parameters and indicators remain unchanged.

– The new algorithm is more logically justified, and it increases the quality of predicting the location of successive spheres. For this reason, it will be recommended as the default algorithm in the upcoming versions of the PathFinder program, beginning from version IV.1.

References

BEAR J. 1972. *Dynamics of Fluids in Porous Media*. Dover, New York.

CARMAN P.C. 1997. *Fluid Flow through a Granular Bed. Transactions of the Institute of Chemical Engineers*. Jubilee Supplement, 75: 32–48.

CEWE A., NAHORSKA H., PANCER I. 2010. *Tablice matematyczne*. Wydawnictwo Podkowa, Warszawa, p. 1-143.

KOZENY J. 1927. *Über kapillare Leitung des Wassers im Boden*. Akademie der Wissenschaften in Wien, Sitzungsberichte, 136(2a): 271–306 (in German).

LEYKO J. 2010. *Mechanika ogólna*. PWN, Warszawa. Tom 1. p. 1–392.

LIU C., ZHANG Q., CHEN Y. 2008a. *PFC^{3D} simulations of lateral pressures in model bins*. Paper No 083340, American Society of Agricultural and Biological Engineers, St. Joseph, MI.

LIU C., ZHANG Q., CHEN Y. 2008b. *PFC^{3D} simulations of vibration characteristics of bulk solids in storage bins*. Paper No 083339, American Society of Agricultural and Biological Engineers, St. Joseph, MI.

PathFinder Project 2013. On-line, http://www.uwm.edu.pl/pathfinder/index.php (available at February 7, 2014). University of Warmia and Mazury in Olsztyn.

SOBIESKI W., LIPIŃSKI S. 2014. *PathFinder User's Guide*. On-line: http://www.uwm.edu.pl/pathfinder/index.php (available at 7 February 2014). University of Warmia and Mazury in Olsztyn.

SOBIESKI W., TRYKOZKO A. 2014a. *Darcy's and Forchheimer's laws in practice*. Part 1. *The experiment*. Technical Sciences (submitted).

SOBIESKI W., TRYKOZKO A. 2014b. *Darcy's and Forchheimer's laws in practice*. Part 2. *The numerical model*. Technical Sciences (submitted).

SOBIESKI W., TRYKOZKO A. 2011. *Sensitivity aspects of Forchheimer's approximation*. Transport in Porous Media, 89(2): 155–164.

SOBIESKI W., ZHANG Q., LIU C. 2012. *Predicting Tortuosity for Airflow through Porous Beds Consisting of Randomly Packed Spherical Particles*. Transport in Porous Media, 93(3): 431–451.

SOBIESKI W., ZHANG Q. 2014. *Sensitivity analysis of Kozeny-Carman and Ergun equations*. Technical Sciences (in press).

Technical Sciences 17(2), 2014, 149–163

INFLUENCE OF MESH REFINEMENT ON RESULTS OF ELASTIC-PLASTIC FEM ANALYSIS

***Paweł Szabracki*[1], *Tomasz Lipiński*[2]**

Chair of Material and Machinery Technology
University of Warmia and Mazury in Olsztyn

Received 29 October 2013, accepted 22 April 2014, available on line 4 May 2014

K e y w o r d s: FEM analysis, local mesh refinement, elastic-plastic deformation, error optimization.

A b s t r a c t

To improve fitting of numerical results to experimental data, in the past, distances between nodes were decreased for whole mesh. A typical mesh generator for Finite Element Method (FEM) analysis ensures possibility to decrease distances between nodes for edges or surfaces of described geometries. Influence of local mesh refinement for a flat and round tensile specimen on fitting of numerical tensile simulation results to experimental data was presented in the paper. Local mesh refinement was performed for areas with the error values higher than threshold value. First iteration of flat and round mesh refinement has to improved correlation of numerical and experimental data with acceptable increase of mesh file size. Similar observations have been made for the second iteration of the flat specimen mesh. On the basis of analysis, shown that second iteration of round mesh refinement caused crucial increase of mesh file size and computation time with negligible fitting improvement.

Introduction

Finite Element Method (FEM) analysis make possible mechanical, thermal acoustic and other calculations for different geometries not restricted to normalized shapes (BÉCACHE et al. 2005, BELL et al. 2006, DUARTEM et al. 2013, DUMONT et al. 2013, KŁYSZ et al. 2013, KUHL et al. 2013, KUHL et al. 2013, MIAZIO, ZBOIŃSKI 2013, PERDUTA, PUTANOWICZ 2013, ROSSILLON, MEZIERE 2010, SZABRACKI 2012).Geometrical model in FEM analysis has to be defined with discrete elements. Preparation of the mesh describing geometrical model, built on discrete elements is very important for calculation accuracy. Typically, to build discrete model of analyzed geometry, nodes, edges, plane figures and

* Correspondence: Pawel Szabracki, Katedra Technologii Materiałów i Maszyn, Uniwersytet Warmińsko-Mazurski, ul. Oczapowskiego 11, 10-719 Olsztyn, tel.: +48 89 523 38 55, e-mail: pawel.szabracki@uwm.edu.pl

polyhedrons are used. Geometrical edges and planes have to be divided for smaller parts to achieve discrete elements. Ends of the smaller parts are called as nodes. Connected nodes are defined as edges. Connected edges form plane figures. Connected plane figures form polyhedron. The most commonly used plane figures are triangles and rectangles. On the basis of plane figures, the most commonly used three-dimensional solids used to build discrete model of analyzed geometry are tetrahedron and cuboids.

Most commonly used methods to generate mesh base on maximal distance between nodes or number of element along edge. Typical software used for preprocessing enables to define specific distance between nodes for different areas of the geometry. Literature presents three main refinement methods. *h-refinement* method is focused on the local refinement and/or coarsening of a mesh. Second method, *r-refinement* method, is used to relocate or move a mesh. *p-refinement* method is focused on local varying the polynomial degree of the basis. These strategies can be used singly or in combination. *r-refinement* is usually useful with transient problems, where elements move according to described phenomena. Many researchers improve methods of mesh refinement to modify initial mesh on the basis of error distribution or other criterion (ALEXA 2002, BABUSKA et al. 1995, BABUSKA, RHEINBOLDT 1978, BERN et a. 1999, CLARK et al. 1994, DUNCAN 1998, FLAHERTY et al. 1989, MIAZIO, ZBOIŃSKI 2013, NICOLAS, FOUQUET 2013, PERDUTA, PUTANOWICZ 2013).

Current literature trends confirms application of different refinement algorithms for practical calculations (BÉCACHE et al. 2005, BELL et al. 2006, DUARTEM et al. 2013, DUMONT et al. 2013, KOSTOFF et al. 2013, KUHL et al. 2013), what was also made for tensile test simulation in the paper.

On the basis of FEM analysis, stress and strain distributions for flat and round tensile specimens were analyzed. To perform Finite Element Analysis (FEA) of tensile specimens, meshes of the specimens has to be prepared. Mesh generation on the basis of maximal distance between nodes or number of element on the edge of geometry is not sufficient to properly describe nonlinear behavior in those areas. Nonlinear behavior requires mesh with small distance between nodes. Usually, nonlinear behavior occurs in small areas of analyzed geometry. Mesh refinement on the basis of edge and surfaces of geometry is usually not sufficient for 3D geometries. Definition of distance between nodes for whole mesh like for areas with nonlinear behavior induce creation of large mesh file with huge amount of nodes without practical importance for calculation results. Many nodes need a lot of time and computer resources for calculations and the vast majority of nodes in areas with elastic behavior are useless. As results of homogenous mesh refinement we obtain crucial increase of calculation time and many nodes useless for performed analysis. Local mesh refinement methods based on error distribution provide tools and methodology

to optimize number of nodes in mesh for performed analysis. Concerning applicability of different refinement methods, *h*-refinement methods was choosing. Methodology, which implies the use of tetrahedral and pyramids to connect the zones of different level of refinement (NICOLAS, FOUQUET 2013), was used. Literature does not present any information about influence of tensile test specimen's local refinement on the accuracy of tensile test simulation results. Especially for X2CrNiMoN25-7-4 super duplex stainless steel used to build responsible constructions working with danger substances.

FEA are cheaper than manufacturing and testing of machine and construction prototypes. To analyze complex geometries, large amount of computer hardware has to be used. Mesh refinement in specific areas, where error is to high, is important for those practical analysis. Local mesh refinement ensure optimal supplement of the mesh with additional nodes. Areas of the mesh not important for performed analysis are not modified. Concerning practical application of different numerical analysis (BÉCACHE et al. 2005, BELL et al. 2006, DUARTEM et al. 2013, DUMONT et al. 2013, KOSTOFF, CUMMINGS 2013, KUHL et al. 2013, SZABRACKI 2012, SZABRACKI et al. 2012, SZABRACKI, LIPIŃSKI 2013), aim of performed analysis was to determine influence of double mesh refinement of flat and round tensile specimen on the fitting of numerically calculated to experimental data. Results allow to define influence of refinement iterations on the accuracy of numerical results. Simple geometry (normalized round and flat tensile specimen) allows to verify methodology and will be background for usage of a presented methodology for more complex, real geometries.

Research methodology

According to standard PN-EN ISO 6892-1, tensile test can be performed for specimens with round and rectangular cross section. Tensile specimens with round and rectangular cross section are used due to the different forms of semi-finished and metallurgical products. Flat specimens with rectangular cross section are used for thin plates. Specimens with round cross sections are used for thick plates and rods. Experimentally tested tensile specimens were made of X2CrNiMoN25-7-4 super duplex stainless steel. Tensile specimens with rectangular cross section according to Figure 1 were prepared from 5 mm thick plate (water jet with abrasive cutting).

In the paper, local mesh refinement of round and rectangular specimens used for tensile test simulation were performed. Diameter of working part in round specimen is 8 mm. Rectangular cross section of flat specimen is equal 5×10 mm. The FEM simulation results were compared with experimental

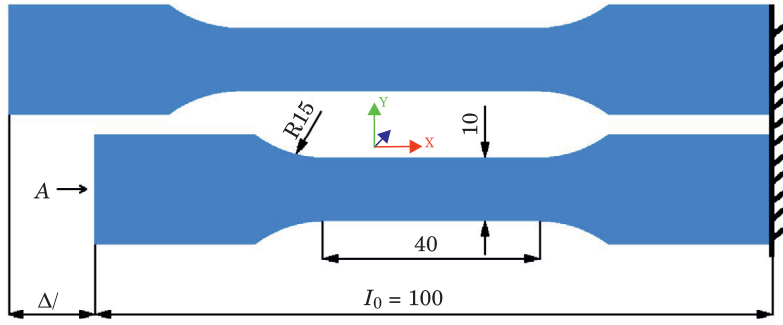

Fig. 1. Schematic presentation of tensile test simulation

tensile curve for flat (rectangular cross section) specimen (Fig. 1). Round tensile specimen was not experimentally tested. The FEM simulation results confirms possibility of usage FEA regardless of the geometry. Important part of a finite element analysis is the discrete model of analyzed geometry preparation. According to the methodology of tensile test simulation presented in the paper (SZABRACKI et al. 2012), analyzed in this paper simulations were performed for elastic and plastic deformations until Ultimate Tensile Strength (UTS) reached. Failure of the numerical specimen were defined when stresses in mesh reach UTS value. Practically, for experimental test UTS value was reached, visible neck creation starts.

FEM calculations were performed on the basis of Code Aster solver (TAYLOR 1999).The solver was developed for nuclear installations analysis. Open source code allows to improve the solver by different researchers and programmers around the world. Main advantage of the code is wide range of applications for mechanical, thermal, metallurgical and acoustic analysis.

Elastic-plastic behavior of X2CrNiMoN25-7-4 super duplex stainless steel was defined according to isotropic hardening model (1) described and presented in previous works (ALEXA 2002, NICOLAS, FOUQUET 2013, SZABRACKI et al. 2012).

$$R(p) = \sigma_i + \frac{\sigma_{i+1} - \sigma_i}{p_{i+1} - p_i}(p - p_i) \tag{1}$$

where:

$p_i = \varepsilon_i - \frac{\sigma_i}{\mathrm{E}}$

E – Young modulus

σ_i – stresses in point i of the experimental tensile curve [MPa]

ε_i – strains in point i of the experimental tensile curve [MPa]

Initial mesh, describing tensile specimen with rectangular cross section, shown in Figure 2a). The Mesh contains triangles (2D) and tetrahedrons (3D). The maximal distance between nodes was 2.5 mm. For nonlinear areas of the flat specimen geometry (connection of working and handling part of the specimen), maximal distance between nodes decreased to 1 mm. Mesh prepared according to described above criteria contains 2,054 nodes, 272 edges, 2,936 triangles and 7,298 tetrahedrons (Fig. 2a). Maximal distance between nodes in round tensile specimen decreased to 1.5 mm for handling part and 1 mm for other parts of the specimen. The maximal distance between nodes decrease has increased number of nodes in the mesh. Mesh of the round tensile specimen contains 5,238 nodes, 352 edges, 70,114 triangles and 19,642 tetrahedrons (Fig. 2b). Described above changes in mesh generation condition caused changes of the mesh files size. The file size of flat tensile specimen mesh is equal 312 KB and the file size of round tensile specimen mesh is equal to 782 KB.

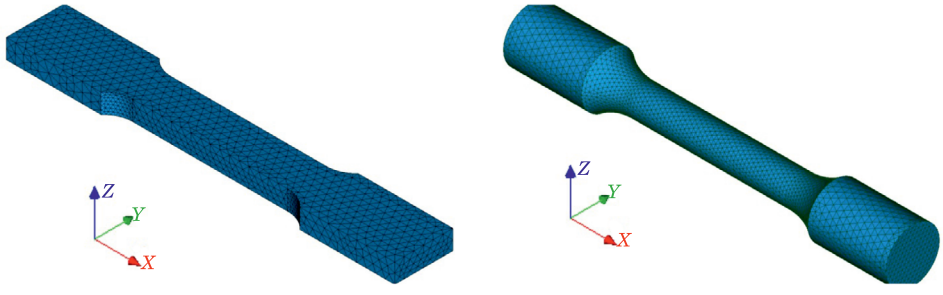

Fig. 2. Initial mesh of *a*) flat and *b*) round tensile specimen

Tensile test simulation was performed according to methodology described in the paper (SZABRACKI et al. 2012) with linear displacement of surface A (Fig. 1) along – x axis. Velocity of A surface displacement was 0.5 mm/s. Iteration step was changing during simulation. Nonlinear behavior of the material in plastic deformation areas causes decrease of iteration steps to achieve convergence threshold value. 20 convergence iterations were used as maximal acceptable number of convergence steps. If it was not enough to achieve threshold convergence value, the A surface step was decreased 2 times until convergence criterion was fulfilled. For elastic deformation area, iteration step was 0.5 mm. When highest stresses in mesh were almost equal to Yield Strength, iteration step decreased to 0.1 mm. When UTS reached, error distribution in the plane mesh elements (K) indicates the estimator of error (noted (Ω)) was defined as being the quadratic average of the site indicators of

error ($\eta(K)$) (3) (NICOLAS, FOUQUET 2013). This kind of error estimation allow to detect significant changes of calculated values (stresses, strains or others) for neighboring plane elements. Used estimator is an explicit estimator of error utilizing the residues of the balance equations and the jumps of the normal stresses to the application interfaces (NICOLAS, FOUQUET 2013). Contrary to the Zhu-Zienkiewicz estimator (AINSWORTHET et al. 1989), which uses a techniques of smoothing of the stresses a posteriori. In this case, areas with significant values evolution for neighboring nodes will be refined without modification of not significant areas.

$$\eta(\Omega) = [\sum_{K \in T} \eta(K)^2]^{\frac{1}{2}} \tag{3}$$

$$\eta(\Omega)_{\text{rel}} = \eta(\Omega)_{\min} + \eta_{\text{rel}}(\eta(\Omega)_{\max} - \eta(\Omega)_{\min}) \tag{4}$$

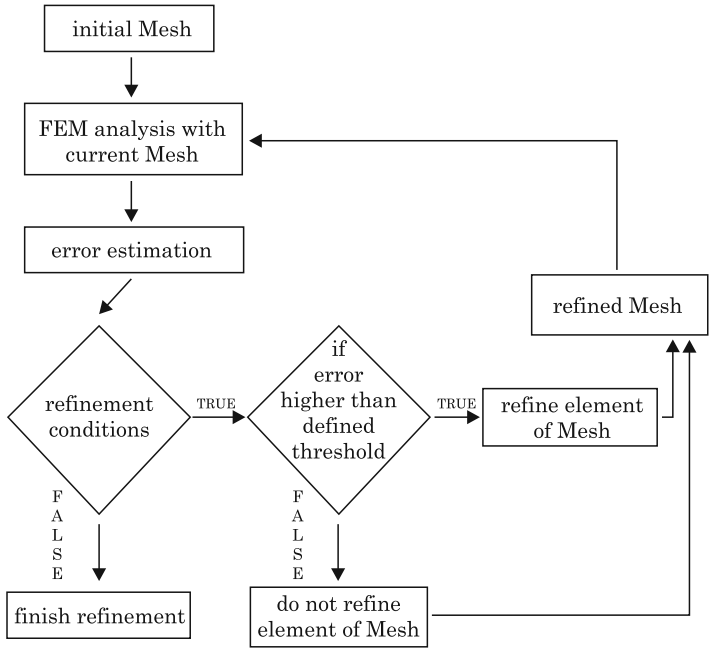

Fig. 3. Mesh refinement algorithm

For areas with error higher than threshold value, mesh refinement based on the error distribution (NICOLAS, FOUQUET 2013) in the plane mesh elements was performed. Threshold value for mesh refinement was calculated according to formula (4) with 10% relative error η_{rel} (NICOLAS, FOUQUET 2013). This value allows significantly rebuilding the mesh after each iteration step. Higher values of relative error require more refinement iteration steps. For more

complex geometries, higher relative error can be required. Normalized tensile specimens not require small steps of mesh refinement.

The mesh refined according to presented methodology was used for next iteration of tensile test simulation. Influence of mesh refinement on experimental tensile curve fitting was analyzed according to prepared algorithm (Fig. 3). For cases where more than two iterations will be needed, mesh refinement ending criterion was used, to achieve less than 2% increase of the correlation coefficient value. Due to the significant consumption of computing resources, crucial increase of the mesh file size resulting significant increase of computation time without significant improvement of the results quality were considered as condition terminating the algorithm. In the present case, more than two mesh refinement iterations was not used.

Stress and strains distributions (numerically calculated tensile curve) at the point of symmetry for round and flat tensile specimen were compared with experimental tensile curve. Pearson's correlation coefficient (5) was used to describe fitting of numerical results to experimental data (TAYLOR 1999).

$$r_{xy} = \frac{cov(xy)}{\sigma_x \sigma_y} \tag{5}$$

where:

$$\sigma_x = \sqrt{\frac{\sum_{i=1}^{n}(x_i - \bar{x})^2}{n}},$$

$$\sigma_y = \sqrt{\frac{\sum_{i=1}^{n}(y_i - \bar{y})^2}{n}}.$$

Results and analysis

Table 1 presents number of elements (0D-3D) used to build meshes of flat and round tensile specimen for initial state and after mesh refinement.

Table 1

Mesh 0D – 3D elements for different samples and refinement iterations

Iteration	Flat sample				Round sample			
	Nodes	1D	2D	3D	Nodes	1D	2D	3D
0 – Initial Mesh	2,054	272	2,936	7,298	5,238	352	7,014	19,642
1 – First refinement	7,193	372	6,656	32,179	16,732	416	14,662	76,353
2 – Second refinement	33,439	459	15,108	174,631	79,686	497	28,476	428,603

The size of flat specimen files increases from 312 KB to 2.6 MB after first refinement. The round specimen files size increases from 782 KB to 6.1 MB. Figure 4a presents error distribution for flat specimen before refinement, when UTS reached in working part. Similar error distribution in round specimen presents Figure 4b. Maximal error value, calculated according formula (3) for flat specimen is 1,285. For round specimen 918. Maximal error values are not located in the middle part of working area because of symmetry conditions and restrictions of error estimation model (3) (NICOLAS, FOUQUET 2013). According to error distribution (Fig. 4) and presented methodology, refined meshes of flat (Fig. 5a) and round (Fig. 5b) specimen were prepared.

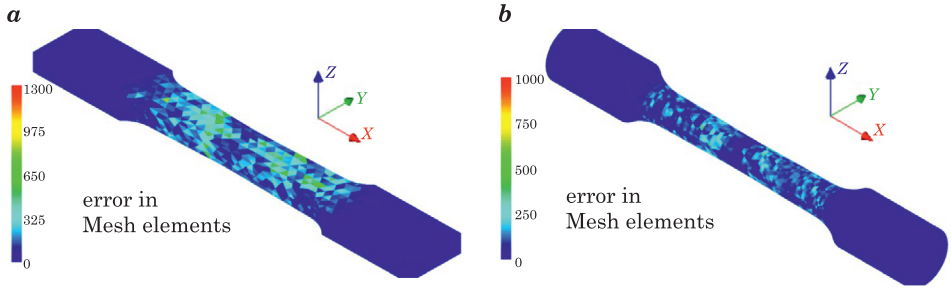

Fig. 4. Error distribution for initial mesh of *a*) flat and *b*) round specimen

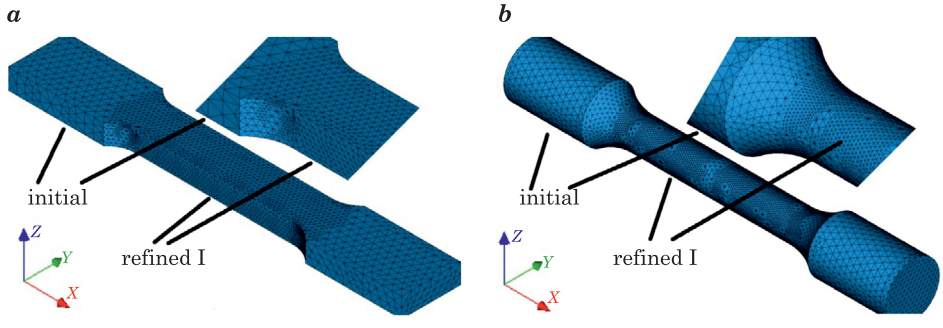

Fig. 5. Mesh after first mesh refinement iteration of *a*) flat and *b*) round specimen

On the basis of local mesh refinement method, number of nodes in middle part of flat specimen was increased (Fig. 5a – Refined I). Handling part of the mesh was not modified in this refinement iteration (Fig. 5a – Initial). Difference between handling and working part of the specimen allow to compare mesh element size before and after refinement. Mesh refinement presented in the specimen's surface is the same for whole specimen's thickness. Round

specimen's mesh refinement was observed in the working part of the specimen (Fig. 5b – Refined I). Handling part and transition zone of the specimen mesh was not refined (Fig. 5b – Initial).

Error distribution for refined mesh was presented in Figure 6. First refinement iterations of flat specimen decrease the error value for plane mesh elements (Fig. 6a). The error value for locked specimen's surface reach 25% of maximal error value in flat specimen (3). Highest values of the error were obtained for areas with highest plastic deformations (working part of the specimen). Considerable value of the error (25% of the maximal value) was reported near the transition zone (transition between working and handling part of the specimen). Described error distribution after first refinement was used to perform second mesh refinement iteration. Highest error values after first mesh refinement iteration was observed in working part of round specimen (Fig. 6b). Area near transition zone and area near locked surface of round specimen's mesh shows error about 25% of maximal value in the whole mesh. Maximal value of the error for round specimen's mesh after first refinement iteration is 266. For flat specimen's mesh after first refinement iteration calculated error is two times higher (514). Flat specimen's mesh after second refinement iteration was shown in Figure 7a. Areas called Initial represent mesh

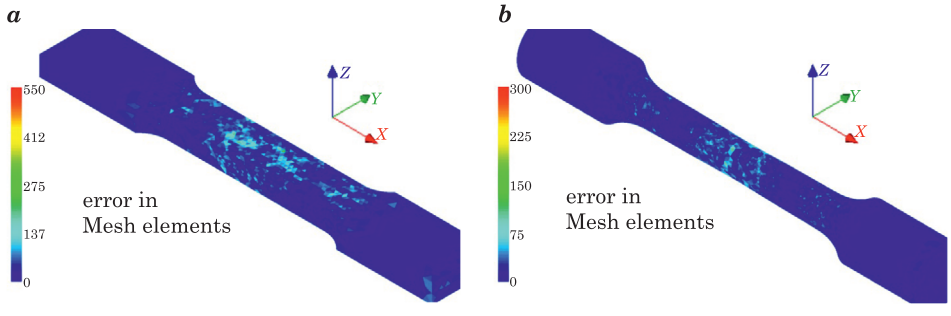

Fig. 6. Error distribution for 1 time refined mesh of *a*) flat and *b*) round specimen

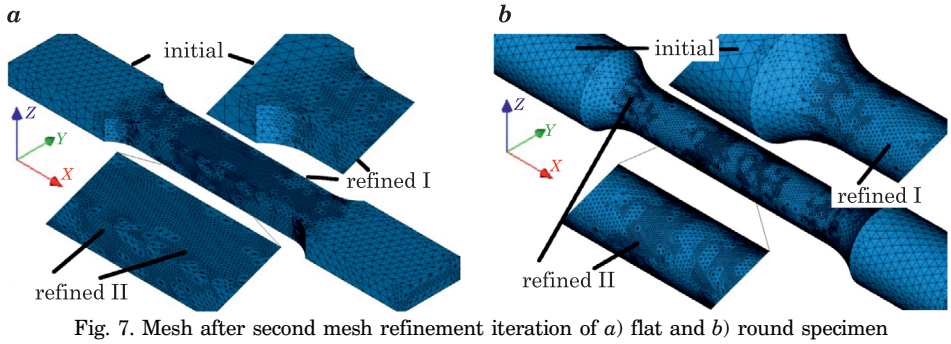

Fig. 7. Mesh after second mesh refinement iteration of *a*) flat and *b*) round specimen

before refinement. Refined I areas represent mesh not refined during second iteration. Refined II areas represent areas after both refinement iterations. Round specimen's mesh after second refinement iteration was shown in Figure 7b. Handling part of the specimen is not modified (initial mesh size).

Influence of refinement iterations on the mesh file size for flat and round tensile specimen was presented in Figure 8. First flat specimen's mesh refinement iteration has caused 8.5-fold increase of the mesh file size from 0.3 up to 2.6 MB. Second mesh refinement iteration has caused increase of the mesh file size up to 12.8 MB. This gives a 42-fold increase of the initial mesh file size. The computation time in this case was extended from 20 minutes at an initial mesh up to two hours after two flat mesh refinement iterations. The round mesh file size after first refinement iteration was increased from 0.76 up to 6.1 MB. This gives almost 8-fold increase of the file size. Second mesh refinement iteration has caused increase of the mesh file size up to 30.8 MB. This gives a 40-fold increase of the initial mesh file size. The computation time in this case was extended from 50 minutes at an initial mesh up to 32 hours after two round mesh refinement iterations. After two flat mesh refinement iterations, maximal error was 204 and 103 for round two times refined mesh. Influence of refinement iterations on the maximal error value for flat and round specimen's mesh was presented in Figure 9.

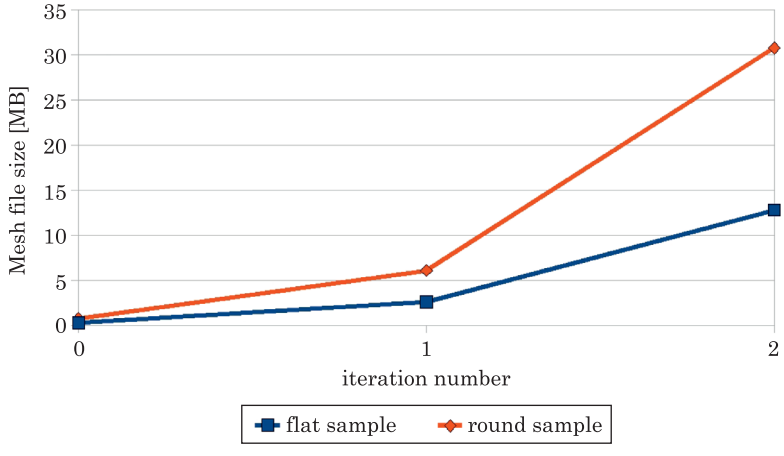

Fig. 8. Influence of mesh refinement iterations on the mesh file size

Fitting of experimental data to numerically calculate was presented as evolution of correlation coefficient value (5) for different geometries and mesh refinement iterations (Table 2). Graphical representation of fitting for initial meshes was presented in Figure 10. Double flat mesh refinement has improved fitting of numerical results to experimental data. The increase of the correlation

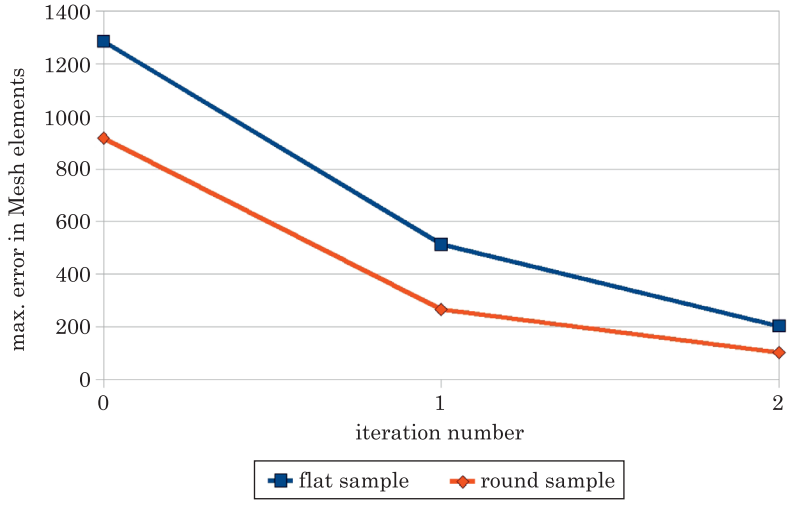

Fig. 9. Influence of mesh refinement iterations on the maximal error value in plane mesh elements

coefficient value in the analyzed range confirms this relationship. The increase of the correlation coefficient value after second flat mesh refinement iteration was 10 times lower than after first refinement. This shows smaller improvement of experimental and numerical fitting. 0.044% increase of Pearson correlation coefficient was observed after first round mesh refinement iteration. Second round mesh refinement has decreased correlation coefficient value.

Table 2

Correlation coefficient for different refinements

Iteration	Flat sample	Round sample
0	0.997654900	0.997622964
1	0.997655629	0.998062859
2	0.997655710	0.998062322

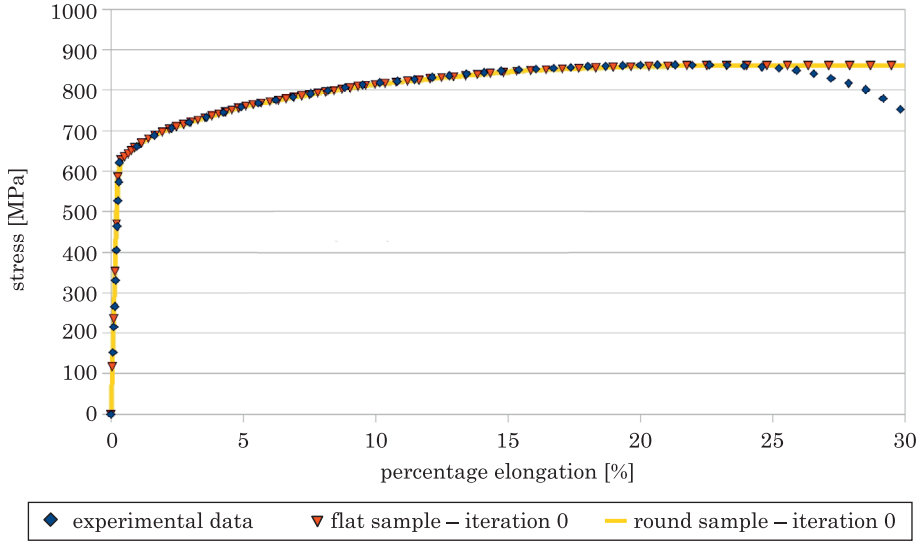

Fig. 10. Numerical and experimental tensile curve for initial meshes

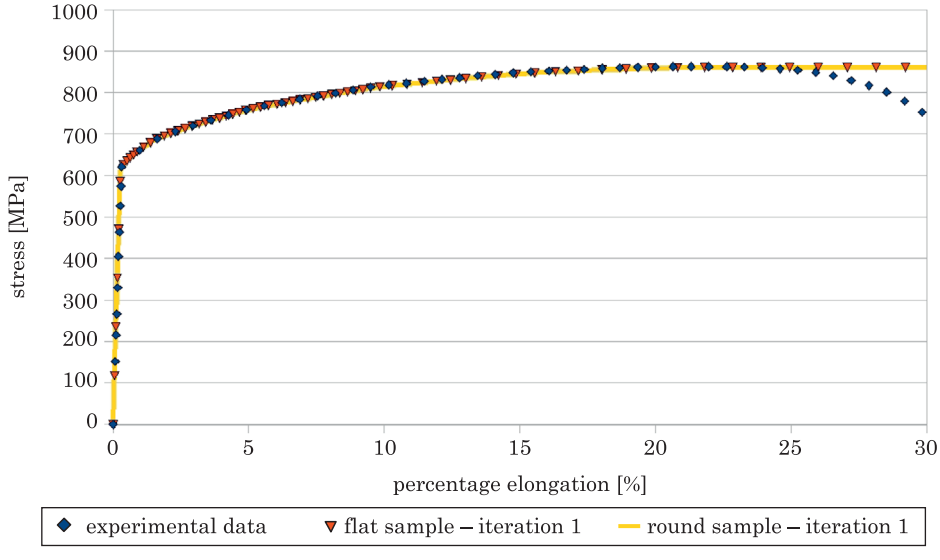

Fig. 11. Numerical and experimental tensile curve for refined mesh

For stresses 0 – UTS, results of numerical calculations coincide with experimental data. When UTS reached, numerically calculated stresses are constant and equal UTS with increasing strains. This induce difference between experimental numerically calculated stresses for percentage elongations higher

than 25%. This phenomenon was wider described in the paper (SZABRACKI et al. 2012). Small difference of correlation coefficient value between initial and refined mesh (Table 2) confirmed with negligible difference between experimental and numerically calculated results (Fig 11). Small variation of correlation coefficient value between first and second refinement iteration (Table 2) also confirmed with small differences on the tensile curve for double refined mesh (Fig. 12).

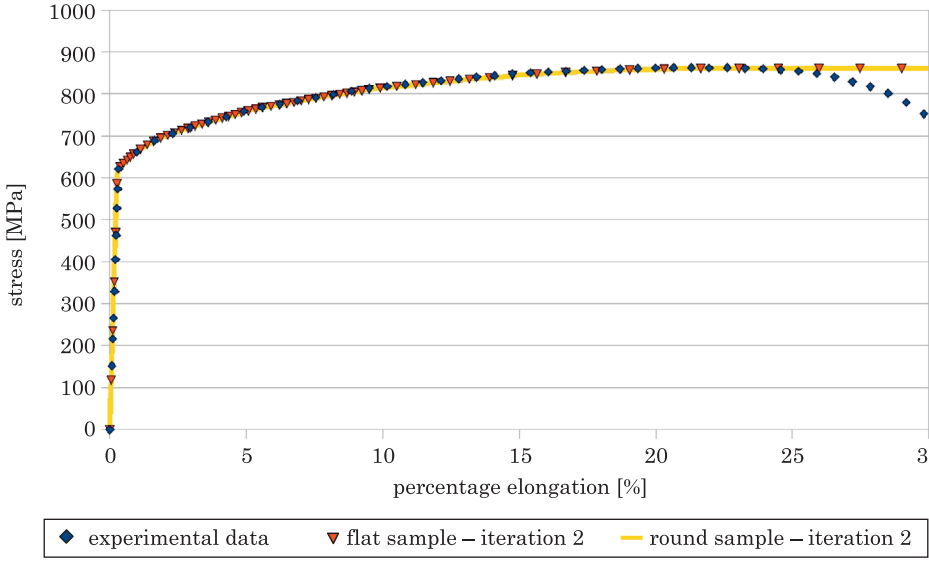

Fig. 12. Numerical and experimental tensile curve for double refined mesh

Summary

It has been shown that the local mesh refinement, performed in areas with a large error, it greatly improves the results of the fitting the experimental results with numerical results. This confirms the increase of the correlation coefficient.

Local mesh refinement allows for expansion of the mesh in areas with high error without creating unnecessary expand of the mesh in areas where error was considered to be satisfactory. This improves the matching of the results obtained at the same time and reduces the calculation time in comparison with uniform mesh refinement over the entire volume of the mesh.

Increase with ten thousandths of the correlation coefficient obtained for subsequent iterations will improve the fit too small for the analysis, and

significantly increase the computation time and computer resources needed to carry out these calculations.

First iteration of local mesh refinement performed for round and flat tensile specimens has improved fitting of numerical results to experimental data with acceptable increase of the mesh file size. Similar observations have been made for the second iteration of the flat sample local mesh refinement. Based on the analysis results have shown that second iteration of the local mesh refinement for the round specimen has increased the file size of the mesh and the computation time with slightly improved fit. There is, the limit number of iterations for which the local mesh refinement is appropriate. If the limit number of iterations was exceeded, the mesh file size and calculation time increases disproportionately to the benefits of the fitting improvement.

When error value does not exceeds about 30% of the Yield Strength no more local mesh refinement is needed. For our case, error at the level of 200–230 is acceptable for real calculations. Further refinement increase calculation costs (time and hardware) but do not improve significantly results.

Influence of local mesh refinement on the tensile test simulation results improvement was confirmed for normalized tensile specimens. This is an initial step for refinement of more complex geometries and real constructions analysis.

References

AINSWORTH M., ZHU J.Z., CRAIG A.W., ZIENKIEWICZ O.C. 1989. *Analysis of the Zienkiewicz-Zhu a-posteriori error estimator in the finite element method*. International Journal for Numerical Methods in Engineering, 28(9): 2161–2174.

ALEXA M. 2002. *Refinement operators for triangle meshes*. Computer Aided Geometric Design, 19, 169–172.

BABUSKA I., FLAHERTY J.E., HENSHAW W.D., HOPCROFT J.E., OLIGER J.E., TEZDUYAR T. 1995. *Modeling, Mesh Generation, and Adaptive Numerical Methods for Partial Differential Equations*. The IMA Volumes in Mathematics and its Applications, 75.

BABUSKA I., RHEINBOLDT W.C. 1978.*A posteriori error estimates for the finite element method.* International Journal for Numerical Methods for Engineering, 12: 1597–1615.

BÉCACHE E., JOLY P., RODRÍGUEZ J. 2005. *Space-time mesh refinement for elastodynamics. Numerical results*. Computer methods in applied mechanics and engineering, 194: 355–366.

BELL J., BERGER M., SALTZMAN J., WELCOME M. 2006. *Three-Dimensional Adaptive Mesh Refinement for Hyperbolic Conservation Laws*. SIAM Journal of Scientific Computing, 15(1): 127–138.

BERN M.W., FLAHERTY J.E., LUSKIN M. 1999. *Grid Generation and Adaptive Algorithms.* IMA Volumes in Mathematics and its Applications. Springer-Verlag New York Inc. New York.

CLARK K., FLAHERTY J.E., SHEPHARD M.S. 1994. *Applied Numerical Mathematics.* Special Issue. Adaptive Methods for Partial Differential Equations, 14.

Code–Aster. www.code-aster.org (access: 1.02.2014).

DUARTEM M., DESCOMBES S., TENAUD C., CANDEL S., MASSOT M. 2013. T*ime-space adaptive numerical methods for the simulation of combustion fronts*. Combustion and Flame, 160(6): 1083–1101.

DUMONT T., DUARTE M., DESCOMBES S., DRONNE M., MASSOT M., LOUVET V. 2013. *Simulation of human ischemic stroke in realistic 3D geometry*. Communications in Nonlinear Science and Numerical Simulation, 18(6): 1539–1557.

KŁYSZ S., SZABRACKI P., LISIECKI J. 2013. *Numeryczna symulacja testu na odporność na pękanie dla stopu aluminium stosowanego w lotnictwie*. Prace Naukowe ITWL, 32: 93–100.

KOSTOFF R.N., CUMMINGS R.M. 2013. *Highly cited literature of high-speed compressible flow research*. Aerospace Science and Technology, 26(1): 216–234.

KUHL L., BELL J.B., BECKNER V.E., BALAKRISHNAN K., ASPDEN A.J. 2013. *Spherical combustion clouds in explosions*. Shock Waves, 23(3): 233–249.

MIAZIO Ł., ZBOIŃSKI G. 2014. *hp-Adaptive finite element analysis of thin-walled structures with use of the numerical tools for detection and range assessment of boundary layers*. Recent Advances in Computational Mechanics. Taylor & Francais Group, London, pp. 57–62.

NICOLAS G., FOUQUET T. 2013. *Adaptive mesh refinement for conformal hexahedralmeshes*. Finite Elements in Analysis and Design, 67: 1–12.

PERDUTA A., PUTANOWICZ R. 2013. *Mesh Adaptation Components in FEM Framework*. 20th International Conference on Computer Methods in Mechanics, MS10, 13–14.

PN-EN ISO 6892-1. *Metallic materials – Tensile testing*. Part 1. *Method of test at room temperature*.

ROSSILLON F., MEZIERE Y. 2010. A*nalysis of fracture specimen failure of inconel 600: elastic-plastic calculations and thermo plastic energy fracture parameter*. PVP 25323.

SZABRACKI P. 2012. *Fracture behavior of nickel based alloy 600 of ductile tearing*. Tech. rep., EDF SEPTEN internal report.

SZABRACKI P., BRAMOWICZ M., LIPIŃSKI T. 2012. *Development and verication of work hardening models for X2CrNiMoN25-7-4 super duplex stainless steel after sigma phase precipitation hardening used for FEM simulations*. Journal of Power Technologies, 92(3): 166–173.

SZABRACKI P., LIPIŃSKI T. 2013. *Effect of Aging on the Microstructure and the Intergranular Corrosion Resistance of X2CrNiMoN25-7-4 Duplex Stainless Steel*. Solid State Phenomena, 203–204: 59–62.

TAYLOR J.R. 1999. *Wstęp do analizy błędu pomiarowego*. PWN, Warszawa.

Technical Sciences 17(2), 2014, 165–180

SEDIMENT TRANSPORT IN THE COASTAL ZONE

Szymon Sawczyński[1], *Leszek M. Kaczmarek*[2]

[1] Department of Mechanics and Civil Engineering Constructions
University of Warmia and Mazury in Olsztyn
[2] Department of Geotechnics
University of Technology in Koszalin

Received 27 May 2013, accepted 3 July 2014, available on line 7 July 2014

Key words: sediment transport, graded sediment, grain size distribution changes.

Abstract

The paper provides basic information on the description of sediment transport in the coastal zone of the sea. It explains the mechanisms of sediment movement under the influence of the waves and currents interactions, characteristic for the coastal zone. It presents models describing the movement of sediment in the regime of flat bottom, making their divided in accordance with the method of description of vertical structure of sediments transport. Particular emphasis is placed on modeling of graded sediment transport. It presents basis for the three-layer model of graded sediment transport. This allows, among others, the analysis of the variability of particle size distribution in the whole area of sediment movement. The model assumes that the movement of sediment is divided into three layers: bedload layer, contact load layer and outer flow region, as a result of the shear stress influence on the bottom.

Introduction

The primary factor leading to the reconstruction of the profile of the seabed is a wave caused by the wind and the return current which is caused by this wave. Wind-induced waves are generated in the deep-water off-shore area, where the seabed does not affect the nature of the waves. As a result of decreased depth, the wave undergoes a transformation process leading to the increase of the wave crest height and shortening its length, each wave through becoming shallower and longer. In the area of deepwater it is necessary to use the sinusoidal wave approximation, whereas along with the decrease of the depth, the 2nd Stokes approximation is used and then the cnoidal approximation

* Correspondence: Szymon Sawczyński, Katedra Technologii Materiałów i Maszyn, Uniwersytet Warmińsko-Mazurski, ul. Heweliusza 4, 10-724 Olsztyn, e-mail: sz.sawczynski@uwm.edu.pl

and solitary waves (DRUET, KOWALIK, 1970). In the coastal zone, for the purpose of describing sediment transport, the 2nd Stokes wave approximation is most commonly used (KACZMAREK 1999). It is characterized by shortened and steep crest and elongated and flattened through, in comparison to the sine wave.

In the coastal zone there is an interaction between the hydrodynamic forces and sediment and bathymetric profile of the bottom. The fluid stream due to friction forces, runs the sediment from the bottom and the sediment material is transferred over a certain distance. So, moving water causes the bottom sediment transport, and the spatial variability of sediment transport volume causes changes in morphology of the bottom, which in turn affects the water movement change. The question of what controls the rate and method of sediment transport and the nature of changes in the level of the bottom occupied researchers for over a century. Numerous relations between the level of bottom elevation and the rate of sediment transport and flow parameters, including a number of empirical and far less theoretical relations have been proposed. Empirical relations generally can not be applied beyond the limited conditions for which they were formulated, and the majority of theoretical propositions depends on arbitrary assumptions with only a little or no physical credibility (ALLEN 1977). Comprehensive description of such a complex system is very difficult and therefore only by successive approximations and simplifications it is possible to describe the phenomena occurring in the coastal zone of the sea. Despite that in recent years there has been a significant progress, still many issues remain unresolved.

The objective of this paper is the review of sediments transport models. It has been indicated that the primary advantage of the two- and three-layer models in comparison with classic models, based on empirical and semi-empirical relations, is the fact, that such models allows to evaluate a concentration of sediments at any level, depending on the instantaneous hydrodynamic force. The proposed three-layer theoretical model of graded sediments transport providing a complete theoretical description of the vertical structure of transportation of the sandy sediment of a various grain size. Using this model, it is possible to predict an amount of moving sandy sediments of various grain size, as well as there is a possibility to predict the size of the transport of individual fractions.

Sediment transport in the coastal zone

Hydrodynamic processes (waving and wave driven currents) are the driving force of the sediment transport and the evolution of seabed. Actual parameters of morphodynamic and lithodynamic processes depend on the kind

of sediment which residues in the seabed and on the supply of these fractions of sediment that are susceptible to the effects of water flow in the bottom layer (transportation in the form of bedload transport and suspended as a result of shear bottom stresses impact). First of all, the parameters of the litho – and morphodynamic processes depend on the wave climate, the bathymetric bottom arrangement and hydrotechnical facilities in the coastal zone of the sea.

In the traditional division (GRADZIŃSKI et al. 1986) adopted in considerations concerning the transport of sediment, the sediments are transported in three layers, starting from the lowest point: bedload, saltation and in the layer of suspended sediments. The bedload layer covers an area below the bottom of the theoretical level of very high concentration of sediment particles set in motion under the influence of the shear stress impacting the bottom surface. Shearing the bottom layer being the result of shear stress causes only a slight increase in the space between the particles of sediment. Surface friction and intermolecular collisions cause energy transfer between individual molecules of the sediment. The thickness of the bedload layer ranges from one to several tens of sediment grain diameters (NIELSEN 1992, O'DONOGHUE, WRIGHT 2003). In saltation layer with a thickness of about few centimeters, the sediment particles are transported and they are raised from the bottom as a result of turbulent pulsations and punching through the falling sediment particles on the small height above the bottom. Due to the short time of the particles staying in suspension, their transport depends on the oscillation velocity of the wave motion (GRADZIŃSKI et al. 1986). Suspension layer with a thickness of about meters covers an area over the saltation layer up to the free surface of the water column. In this layer, sediment particles reside for a period longer than the period of the wave, and their resultant transport is mainly related to the return current which is characteristic for the coastal zone of the sea. To describe the transport of sediment in suspension it is applied the theory of compensating return current (SVENDSEN 1984).

Sediment transport may take place in two basic regimes. In the regime in which the bottom is covered with bottom forms, e.g. in the form of ripples or in the regime where the bottom is flat with a mobile "carpet" of sediments or flat – stationary. The ability of occurrence of these sediment movement variants depends primarily on the type of sediments building the sea bottom and on the intensity of the waving impact on the bottom. To determine the size of the driving force causing the movement of sediment, most commonly the Shields parameter is used – $\Theta_{2.5}$, and this defines the dimensionless friction. It is assumed, that the beginning of the sediment movement occurs when $\Theta_{2.5} = 0.05$ (NIELSEN 1992).

The resultant sediment transport rate along the transverse profile of the sea coast is the result of the coexistence of wave motion asymmetry and

compensating return current. The consequence of the wave motion asymmetry is the asymmetry of orbital velocity of water at the bottom between the wave crest and the through (CHEN et al. 2010, ZHENG 2007, YHENG et al. 2008). There is a far greater impact on the bottom during the wave crest than during the through. As a result, the individual fractions of the bed sediment are more intensively transported in landward than in seaward direction (Fig. 1). Despite the fact that the duration of the wave through is longer than the crest, only small diameter grains participate in the motion. During the wave crest, the wider spectrum of sediment particles is transported.

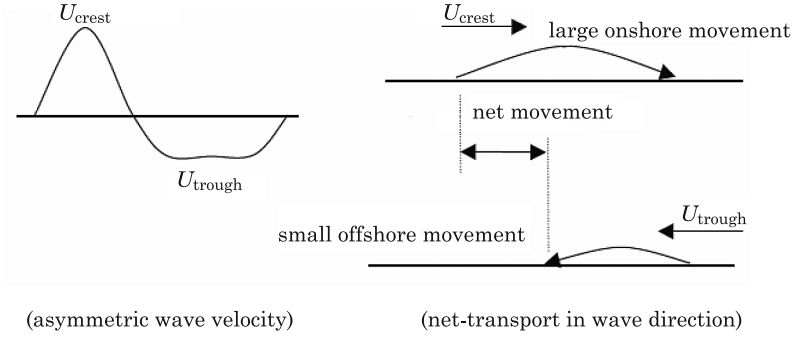

Fig. 1. Resultant sediments transport rate under the influence of the asymmetric waves
Source: HASSAN (2003).

As demonstrated by laboratory tests, carried out in the oscillatory tunnel (RIBBERINK, AL-SALEM 1994), the resultant sediment transport rate with the representative median diameter of d_{50} = 0.21 mm is in landward direction, i.e. compatible with the direction of wave propagation. For fine-grained sediment of d_{50} = 0.13 mm, RIBBERINK and CHEN (1993) obtained the opposite (from the coast) transport direction. It turns out that under conditions of strong wave functions, the resultant sediment transport changes its direction (Fig. 2). The reason for this is the fact that the suspension during the wave through (in seaward direction of the water orbital velocity) of fine grains of sediment, previously raised from the bottom during the wave crest, moves in seaward direction. Sediment particles remain in suspension for the duration of the wave through due to the low speed of their descent. The phase lag (arising as a result of the above situation) between the maximum speed of the water and the maximum concentration of sediment can be particularly well noted for the fine sediment, transported by the strong and short-term waves (DOHMEN-JANSSEN, HANES 2002, JANSSEN 1995, O'DONOGHUE, WRIGHT 2004, VAN DER A et al. 2010). As a result, both the effect of the phase lag and the impact of return current result that the resultant transport of the finest fractions of sediment is

directed towards the sea. The magnitude of the volumetric sediment transport intensity depends thus on: the intensity of the impact of wave motion on the seabed, the asymmetry of wave motion, bed sediment grain size composition, as well as on the value of the return current.

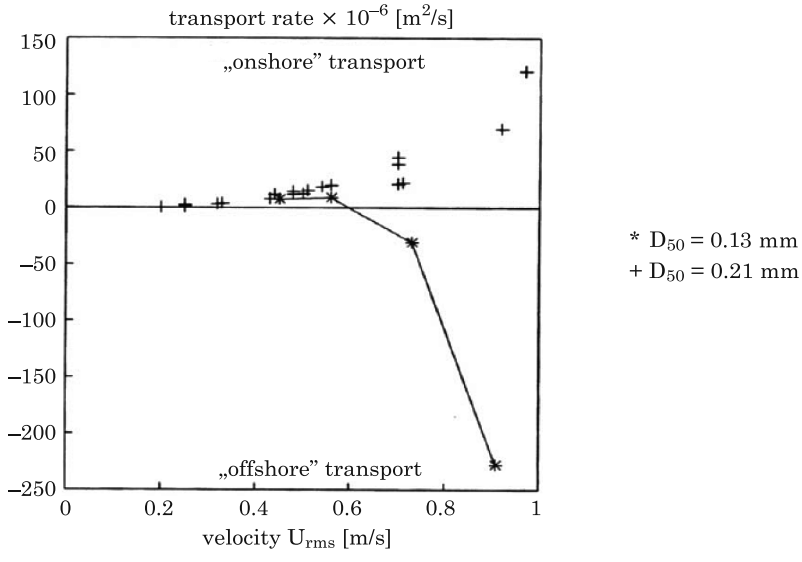

Fig. 2. Resultant sediments transport under the influence of the asymmetric waves
Source: on the basis of: (*) RIBBERINK, CHEN (1993), (+) RIBBERINK, AL-SALEM (1994); following: HASSAN (2003).

The average size of the shallow sea sediment particles decreases with increasing distance from the coast. As a result of observations (PAWLUK 1984, PAWLUK 1990) it was found, that the largest sediment sizes do occur in the area of wave shoaling and it decreases with the increase of water depth. The nature of the sediment which builds the bottom in the profile perpendicular to the shoreline is closely related to the morphology of the coastal zone. Basically, in the submerged bar throughs there are sediments with a lower median size than on the crests of submerged bars (GUILLEN, 1995), on which the sediment is not well sorted out and often characterized by bimodal particle size distributions, without shapes typical for regular bimodal distributions. Bimodal distributions with a clear dominance in the field of fine fractions and mode of coarse fractions as a form of long and flat tail – otherwise known as bimodal distributions negatively sloped – occur on slopes of submerged bars (PRUSZAK 1998). On the seaward slopes of submerged bards, the nature of sediment is usually unimodal and well sorted out. Sometimes in the distribu-

tion of sediment grain size it is possible to distinguish such a small mode within the fine fractions and dominant mode of coarse fractions (bimodal distribution positively sloped).

Modeling the sediment transportation in the flat bottom regime

The sediment transport rate, under the action of waves and currents is defined as integrated (summed by depth) product of velocity and sediment concentration. The sediment transport rate is highly variable during the period of the wave. Stationary models of sediments transport models base on the analytical or numerical solution of basic equations of momentum (amount of motion) and the continuity of the fluid and the equation mass conservation – equation of diffusion-advection. Stationary models describe the transport of bottom sediment in the simplified manner. In this case, the empirical or quasi-empirical formulas are used. They are based mainly on the characteristic parameters of the wave motion, such as: the maximum (in wave period) water velocity at the bottom or the maximum bottom friction value. Sediment transport models can be divided into three main groups, according to the criterion of how to describe the vertical structure of the sediment transport:

– models describing suspended sediment transport,

– models describing bedload sediment transport,

– two- and three-layer models, i.e. describing the transport of suspended and bedloaded sediments; possible third layer describes transition region between the layers and corresponds to the saltation layer.

Suspended sediment transport models put the emphasis on the solution of the equations of water momentum and advection – diffusion equation describing the instantaneous concentration of sediment being suspended. In case of flat bed (1DV), i.e. when only the variability of flows in vertical is taken into consideration, it is possible to express as follows:

$$\frac{\partial C}{\partial t} = \frac{\partial}{\partial z}\left(\varepsilon_s \frac{\partial C}{\partial z} + w_s C\right) \tag{1}$$

where:

$C = C(z, t)$ – instantaneous volumetric concentration of the suspended sediment [m^3/m^3],

w_s – sediment grains falling speed [m/s],

$\varepsilon_s = \varepsilon_s(z, t)$ – factor of sediment diffusion turbulence in the vertical profile [m^2/s],

whereas the volumetric concentration is possible to be defined as follows:

$$C = \frac{V_s}{V_p + V_s} \tag{2}$$

where:
V_s – volume of the ground control volume,
V_p – pores volume.

To determine the sediment concentration distribution in the vertical profile it is necessary to know the size of the concentration at reference level, i.e. at the lower limit of the modeling. In simplified models, it is generally assumed that the turbulent diffusion factor is constant in time – mostly during the wave period. In addition, it is assumed its constancy throughout the whole depth range. In addition, sometimes, additional simplification may also relate to the concentration at reference level. It can be determined using empirical or semi-empirical functions, making the concentration dependent on the friction along the bottom surface (e.g. ENGELUND, FREDSØE 1976, GLENN, GRANT 1987, GRANT, MADSEN 1986, MADSEN, GRANT 1976, ZYSERMAN, FREDSØE 1994).

A detailed review of models of suspended sediment transport in the regime of flat bottom can be found in the works: AMOUDRY, LIU (2010), DAVIES, VILLARET (2002), DAVIES et al. (1997), DOHMEN-JANSSEN (1999).

In the description of sediment transport, in the bedload layer, strong influence of interactions between sediment particles causes the necessity of a different approach to the description of transport than the concept of diffusion, used in the suspension layer. BAGNOLD (1956) introduced the postulate of "dispersion stress" in the bedload layer, which is the result of sediment grains presence in the soil and water mixture and he showed that as a result of shear of soil and water layer, due to the presence of sediment grains in the mixture, there is an additional normal (causing the relaxation of water and soil mixture) and tangential stress generated. SAYED and SAVAGE (1983), using the results of experimental researches on the mechanics of granular media, proposed the constitutive equations to describe the state of stress and strain, as well as associated relations used to describe normal and tangential stresses resulting from the momentum transfer between particles of sediment on their mutual collisions.

Holistic modeling – describing transport within the whole area of sediment movement, i.e. taking into account the total of bedload and suspended sediment transport in the regime of flat bottom, requires a description based on a two-layer model (e.g. AMOUDRY et al. 2008, ASANO 1990, BAKHTYAR et al. 2010, DONG, ZHANG 2002, LI, SAWAMOTO 1995, LIU, SHEN 2010). The first two-layer models were based on the classical bagnold approach (ASANO 1990, KOBAYASHI, SEO 1985).

KACZMAREK (1991) adapted the stationary description of sediment layer motion, proposed by SAYED and SAVAGE (1983) for wave conditions. In order to determine the instantaneous value of the sediment transport rates in bedload layer, he used the instantaneous stresses at the upper surface of the bedload layer. The resulting solution of the equations concerning movement in bedload layer was in the next step "stitched" with the solution obtained in the suspension layer, and obtained on the basis of diffusion – advective model (1DV). KACZMAREK and OSTROWSKI in 2002 joined the third layer, so-called contact load layer – between a bedload and suspension layers – using for its description the proposal of DEIGAARD (1993). Deigaard's description, adapted by KACZMAREK and OSTROWSKI (2002) enabled the analysis of the momentum exchange between the elements of water and sediment grains and the mutual exchange of momentum (by way of chaotic collisions) between grains of sediment. In turn, a more simplified version of 1DV modelling, rather more similar to the model of KACZMAREK (1991) was presented by MALARKEY et al. (2003).

The primary advantage of the two- and three-layer models in comparison with classic models (formulas), based on empirical and semi-empirical relations, is the fact, that such models allows to evaluate a concentration of sediments at any level, depending on the instantaneous hydrodynamic force. Furthermore, they allow for the description of the vertical profiles of velocity and sediment concentration throughout the entire area of sediment motion.

To describe the transport of sediments in the vertical profile, the various models are used, e.g. UNIBEST-TC (BOSBOOM et al. 1998, RENIERS et al. 1995) and CROSMOR2000 (VAN RIJN 2000, VAN RIJN, WIJNBERG 1996) to describe the bedload transport they use the quasi-stationary model of RIBBERINK (1998), while for the description of the suspended transport – model of van RIJN (1993) providing the size of averaged transport volume within the period of the wave. COSMOS model (NAIRN, SOUTHGATE 1993, SOUTHGATE, NAIRN 1993) is based on the Bailard's model (1981), BEACH models (O'CONNOR, NICHOLSON 1989, O'CONNOR et al. 1998), CIRC (RIVERO, SANCHEZ-ARCILLA 1993, SIERRA, SANCHEZ-ARCILLA 1999) use the model of WATANABE (1980). These models, except the CROSMOR2000 model do not take into account the graded sediment. In CROSMOR2000 model, it is a priori assumed that some diameters of sediment grains move within the bedload layer – to the coast and other within the suspension layer – from the coast. Such an approach does not take into account the fact, that along with the increase of the waving impact on the bottom, the range of sediment diameters, transported from the coast in the suspension is changed. Among others, for this reason, CROSMOR2000 model does not describe the changes in grain size distribution in the coast cross profile which is the result of the storm activity.

Modeling of graded sediment transport

Graded sediment description is performed using the results of the granulometric analysis, while the following relationship applies:

$$\sum_{i=1}^{N} n_i = 1 \tag{3}$$

where:

n_i – value describing the percentage size (fractional) of the i-th fraction in the mixture of sediment which builds the bottom,

N – number of fractions in the mixture.

The biggest simplification used in the modeling of graded sediment transport is the assumption that the intensity of transport (q) of all fractions of the sediment is the sum of independent transport intensities ($n_i q_i$) of individual fractions (BIEGOWSKI 2006):

$$q = \sum_{i=1}^{N} n_i q_i \tag{4}$$

The values of q [m^2/s] and q_i [m^2/s] mean the grain skeleton flow intensity (excluding the porosity) of a given flow volume per unit width and time. Value of qi is the transport rate of homogenous sediment with a diameter of the i-th fraction. It is assumed that this value does not depend on the presence of other fractions in the mixture. Thus, the equation (4) means, that the simplified model of mixture was adopted, assuming no interaction between the different fractions of the sediment. In fact, the sediment fractions interact with each other and the contribution of the various factions in the intensity of sediment transport varies in relation to the situation when there is no interaction between the fractions.

HASSAN (2003) presented the possibility to implement a quasi – stationary model, proposed by BAILARD (1981), to describe the intensity of graded sediment transport. It is assumed the sediment transport intensity in the bedload layer depends on the representative diameter (median d_{50}) of the sediment of the bottom. However, in the suspension layer, because of the variable fall velocity, depending on the particle diameter, the flow of sediment transport depends on the diameter of individual sediments fractions. Thus, with respect to the suspended sediment transport rate, there is a simplification described by the equation of (4).

Within the frames of the simplification, described by the equation of (4), RIBBERINK (1998) made the volume of individual deposit fractions transport

dependent on the dimensionless friction, the most frequently described by the Shields parameter, determined for each diameter of the sediment. In turn, DOHMEN-JANSSEN (1999) has adopted the RIBBERINK'S (1998) quasi-stationary model of graded sediments transport and she also introduced a modification, taking into account the effect of the phase shift between suspended sediment concentration and instantaneous velocity of water. In this way, it was possible to achieve the simplified, two-way selective description of sediments transport, wherein the coarser fractions move towards the coast, and finer fraction move away from the coast.

However, the quasi-stationary models of graded sediments transport (BAILARD 1981, RIBBERINK 1998) insufficiently describe the intensity of sediment transport due to hydrodynamic forcing. What's more, they very poorly describe the bidirectional effect of sediments transport within the coastal zone of the sea (BIEGOWSKI 2006). In the last case, in the calculations carried out with model of DOHMEN-JANSSEN (1999), it is possible to obtain better results, although the best results are obtained only when the particle size of the sediment is described with four fractions (HASSAN 2003). This description makes it obviously impossible to characterize a natural sediment, deposited on the bottom of the sea.

The three-layer model of graded sediments transport

Complete description of sediment transport, i.e. the description of grain heterogeneous sediment transport within the entire area of motion may be made on the basis of the three-layer model of graded sediments transport (KACZMAREK et al. 2004). The model assumes that the movement of sediment is carried out in three layers (Fig. 3): bedload layer, contact load layer and outer flow region, as a result of the shear stress influence on the bottom. In the area of each layer there is a different character of the deposits movement and the momentum exchange between the water and sediment particles and therefore, they are described with various equations. At the contact of layers, there is a "stitching" of solutions, so as to ensure the continuity of sediment movement description.

The model assumes that all fractions in the bedload layer move at the same speed in the form of a dense water and soild mixture and sediments sorting is carried out in this layer. It was assumed that the interactions between the sediment fractions are so strong, that finer fractions are slowed down by the coarser ones, and finally all fractions move at the same speed. Thus, this layer does not apply to the simple summation of transport flow for individual fractions, treated as the homogeneous sediment.

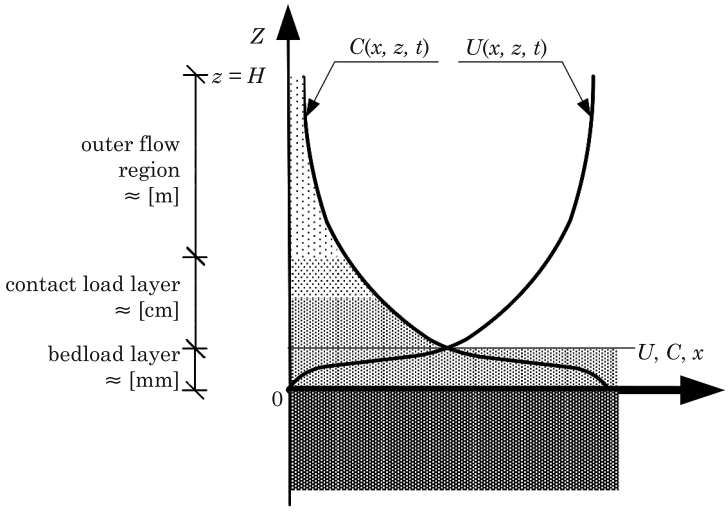

Fig. 3. Scheme of the three-layer sediment transport model

The intensity of sediment transport in the bedload layer (KACZMAREK et al. 2004) towards the coast (for the duration of wave crest) q_{bx}^{+} and away from the coast q_{bx}^{-} respectively equals (see SAWCZYŃSKI 2012, SAWCZYŃSKI et al. 2011):

$$q_{bx}^{+} = \frac{1}{T}\int_{0}^{T_c}\left(\int_{0}^{\delta_{br}^{+}} u_{br}^{+}(z',t)\; c_{br}^{+}(\mathrm{z'},\mathrm{t})\; dz'\right)dt \tag{5}$$

and

$$q_{bx}^{-} = \frac{1}{T}\int_{T_c}^{T}\left(\int_{0}^{\delta_{br}^{-}} u_{br}^{-}(z',t)\; c_{br}^{-}(\mathrm{z'},\mathrm{t})\; dz'\right)dt \tag{6}$$

where:

T_c, T – wave crest duration, wave period,
$\delta_{bx}^{+/-}$ – bedload layer thickness,
$u_{bx}^{+/-}$ – sediment velocity in the bedload layer,
$c_{bx}^{+/-}$ – sediment concentration in the bedload layer,
z' – elevation, while z' axis directed vertically down.

The mathematical modeling takes into account the fact that the most intensive vertical sorting takes place in the process of raising grains in the contact load layer over the bottom. In the contact load layer, turbulent and

chaotic pulsations of collision between particles cause very strong differentiation transportation of individual fractions of the sediment. Very close to the bottom – in a sublayer, where in the distribution of the i-th fraction of sediments, the slip speed is strongly revealed – there is a very strong interaction between the individual fractions, resulting in mutual chaotic collisions. In a further distance from the bottom, these interactions between fractions are subject to weakening. However, the concentration of the i-th fraction is so high as to cause turbulence suppression, while this suppression is dependent on the grain diameter di. It was assumed, that each i-th fraction, as a result of interactions, moves with its own speed, and it is characterized by its own concentration. Coarser fractions velocities and concentrations, calculated in the contact load layer are greater than the size of which would have these fractions if the bottom is homogenous and made of only one, corresponding fraction. This increase in speed in the mixture is the result of interactions between fractions where coarser ones are accelerated by the finer ones.

The intensity of sediment transport in the contact load layer (KACZMAREK et al. 2004) towards the coast q_{cx}^{+} and away from the coast q_{cx}^{-} may be respectively described as (see SAWCZYŃSKI 2012, SAWCZYŃSKI et al. 2011):

$$q_{cx}^{+} = \sum_{i=1}^{N} n_i \left(\frac{1}{T} \int_0^{T_c} \left(\int_0^{\delta_{br}^{+}} u_{ci}^{+}(z,t)\ c_{ci}^{+}(\mathrm{z,t})\ dz \right) dt \right) \tag{7}$$

and

$$q_{cx}^{-} = \sum_{i=1}^{N} n_i \left(\frac{1}{T} \int_{T_c}^{T} \left(\int_0^{\delta_{br}} u_{ci}^{-}(z,t)\ c_{ci}^{-}(\mathrm{z,t})\ dz \right) dt \right) \tag{8}$$

where:

δ_{br} – contact load layer thickness,
n_i – percentage content of the i-th fraction,
$u_{ci}^{+/-}$ – velocity of the i-th fraction in the contact load layer,
$c_{ci}^{+/-}$ – concentration of the i-th fraction in the contact load layer.

In the outer layer, over the contact load layer, it is assumed that there is no change in the particle size distribution of the transported sediment. The vertical distribution of concentration in this layer is described by a power function.

The transport flow in the outer layer (KACZMAREK et al. 2004) can be expressed with the following formulas (see SAWCZYŃSKI 2012, SAWCZYŃSKI et al. 2011):

$$q_{ox}^{-} = \int_{\delta_{cr}}^{H} U_{ox}^{-}(z) C_0(z) dz \tag{9}$$

$$q_{oy} = \int_{\delta_{cr}}^{H} U_{oy}(z) C_0(z) dz \tag{10}$$

where, C_0 means the averaged in time value of suspended sediment mixture concentration and U_{ox}^{-} and U_{oy} are current velocities, resulted from waving (in the coastal zone of the sea) of the respectively return current (directed towards the sea) and alongshore current, generated as a result of waves propagation at the angle to the cross profile of the coast.

BIEGOWSKI (2006) in his doctoral dissertation, using a three-layer model of graded sediments transport, conducted, among others, the analysis of grain distribution variability on the profile, exhibiting at the same time a usefulness of the model. He explained the essence of formation of a various grain distributions (unimodal and bimodal) during a short-term storm, depending on the position of the calculation point on the profile (from the sea or from the coast) and the occurring phenomenon of erosion or accumulation as a result of the bi-directional stream of deposits. This bi-directional flow is related to the transport of sediment at the bottom, faced towards the coast as a result of the asymmetry of wave motion and transport of sediments carried away into the sea by the return current.

Summary and conclusions

As a result of the review of sediments transport models, presented in this paper, it has been indicated that the primary advantage of the two- and three-layer models in comparison with classic models (formulas), based on empirical and semi-empirical relations, is the fact, that such models allows to evaluate a concentration of sediments at any level, depending on the instantaneous hydrodynamic force. Furthermore, they allow for the description of the vertical profiles of velocity and sediment concentration throughout the entire area of sediment motion. The three-layer theoretical model of graded sediments transport details the bedload, contact load layer and outer flow region. Character of interactions between water and sediments is different in each of the above layers and that is why they are described in different equations, while at the contact between the layers there is a stitching of solutions, providing a complete theoretical description of the structure of transportation of the sandy sediment of a various grain size. Using this model,

it is possible to predict an amount of moving sandy sediments of various grain size, as well as there is a possibility to predict the size of the transport of individual fractions. As a result, the knowledge of grain size may be crucial, e.g. in planning and conducting works associated with artificial sand supply. The silt material extracted from the navigation channel is often used to reinforce the edge in the vicinity of ports and therefore knowledge of the particle size distribution is very important. Based on the three-layer model of graded sediment transport, it is possible to determine the bathymetry changes taking place under the influence of variations in the flow of sediment transport of non-uniform grain size, and to determine the mutual impact of changes in grain size of sediments and evolution of the bottom profile.

References

ALLEN J.R.L. 1977. *Fizyczne procesy sedymentacji*. PWN, Warszawa.

AMOUDRY L., HSU T.J., LIU P.L.-F. 2008. *Two-phase model for sand transport in sheet flow regime.* Journal of Geophysical Research, 113, C03011, doi:10.1029/2007JC004179.

ASANO T. 1990. *Two-plane flow model on oscillatory sheet-flow*. Proc. 22nd Int. Conf. Coast. Eng., ASCE, p. 2372–2384.

BAGNOLD R.A. 1956. *The Flow of Cohesionless Grains in Fluids*. Phil. Trans. Roy. Soc., Ser. A, 249: 235–297.

BAILARD J.A. 1981. *An energetics total load sediment transport model for a plane sloping beach.* J. Geophys. Res., 86(C11): 10938–10954.

BAKHTYAR R., BARRY D.A., YEGANEH-BAKHTIARY A., LI L., PARLANGE J.-Y., SANDER G.C. 2010. *Numerical simulation of two-phase flow for sediment transport in the inner-surf and swash zones*. Advances in Water Resources, 33(3): 277–290.

BIEGOWSKI J. 2006. *Dynamika osadów morskich o niejednorodnym uziarnieniu w świetle teorii i eksperymentu*. PhD thesis, IBW PAN.

BOSBOOM J., KLOPMAN G., RENIERS A, STIVE M.J.F. 1998. *Analytical model for wave-related sediment transport in flat bed sheet flow regime*. Proc. 26th ICCE, ASCE, Reston VA, p. 2573–2586.

CHEN X.W., ZHENG J.H., ZHANG C., YANG X. 2010. *Evaluation of diffraction predictability in two phase averaged wave models*. China Ocean Engineering, 24(2): 235–244.

DAVIES A.G., RIBBERINK J.S., TEMPERVILLE A., ZYSERMAN J.A. 1997. *Comparisons between sediment transport models and observations made in wave and current flows above plane beds.* Coastal Engineering, 31: 163–198.

DAVIES A.G., VILLARET C. 2002. *Prediction of sand transport rates by waves and currents in the coastal zone.* Cont. Shelf Res., 22(18–19): 2725–2737.

DEIGAARD R. 1993. *Modelling of sheet flow: dispersion stresses vs. the diffusion concept*. Prog. Rep., 74, Inst. Hydrodyn. and Hydraulic Eng., Tech. Univ. Denmark, p. 65–81.

DOHMEN-JANSSEN M.C. 1999. *Grain size influence on sediment transport in oscillatory flow*. FEBO-DRUK BV, Enschede, The Netherlands.

DOHMEN-JANSSEN C.M., HANES D.M. 2002. *Sheet flow dynamics under monochromatic nonbreaking waves.* Journal of Geophysical Research, 107(C10), doi:10.1029/2001JC001045.

DONG P., ZHANG K., 2002. *Intense near-bed sediment motions in waves and currents.* Coastal Eng., 45(2): 75–87.

DRUET C., KOWALIK Z. 1970. *Dynamika morza*. Wydawnictwo Morskie, Gdańsk.

ENGELUND F., FREDSØE J. 1976. *A sediment transport model for straight alluvial channel.* Nordic Hydrology, 7.

GLENN S.M., GRANT W.D. 1987. *A suspended sediment stratification correction for combined wave and current flows*. J. Geophys. Res., 92(C8): 8244–8264.

GRADZINSKI R., KOSTECKA A., RADOMSKI A., UNRUG R. 1986. *Zarys sedymentologii*. Wydawnictwo Geologiczne, Warszawa.

GRANT W.D., MADSEN O.S. 1986. *The continental-shelf bottom boundary layer*. Annu. Rev. Fluid Mech., 18: 265–305.

GUILLEN J. 1995. *Sediment response in a littoral system, Island of Terschelling, The Netherlands*. Report 90–20, Dep. Of Phys. Geography, Univ of Utrecht, The Netherlands.

HASSAN W.N. 2003. *Transport of size-graded and uniform sediments under oscillatory sheet-flow conditions*. PhD Thesis, Univ. of Twente, The Netherlands.

JANSSEN C.M. 1995. *Sand Transport in Oscillatory Sheet-flow. A literature review*. Communications on Hydraulic and Geotechnical Engineering, Rep. No. 95–6, Delft Univ. of Technology, Faculty of Civil Engineering.

KACZMAREK L.M. 1991. *Mathematical model for oscillating sheet flow*. Proc. Euromech 262 Colloquium on Sand Transport in Rivers, Estuaries and the Sea, A.A. Balkema/Rotterdam/Brookfield, p. 197–202.

KACZMAREK L.M. 1999. *Moveable Sea Bed Boundary Layer and Mechanics of Sediment Transport*. IBW PAN, Gdańsk.

KACZMAREK L.M., BIEGOWSKI J., OSTROWSKI R. 2004. *Modelling cross-shore intensive sand transport and changes of grain size distribution versus field data*. Coastal Engineering, 51: 501–529.

KACZMAREK L.M., OSTROWSKI R. 2002. *Modelling intensive near-bed sand transport under wave-current flow versus laboratory and field data*. Coastal Engineering, 45(1): 1–18.

KOBAYASHI N., SEO S.N. 1985. *Fluid and sediment interaction over a plane bed*. J. Hydraul. Eng., 111(6): 903–921.

LI L., SAWAMOTO M. 1995. *Multi-phase model on sediment transport in sheet-flow regime under oscillatory flow*. Coastal Eng. Jpn., 38(2): 157–178.

LIU C., SHEN Y.M. 2010. *A three dimensional k-ε-Ap* model for water-sediment movement. International Journal of Sediment Research, 25(1): 17–27.

MADSEN O.S., GRANT W.D. 1976. *Quantitative description of sediment transport by waves*. Proc. 12th Int. Conf. Coast. Eng., ASCE, p. 1093–1112.

MALARKEY J., DAVIES A.G., LI Z. 2003. *A simple model of unsteady sheet flow sediment transport*. Coastal Eng., 48(3): 171–188.

NAIRN R.B., SOUTHGATE H.N. 1993. *Deterministic profile modeling of nearshore processes*. Part 2. *Sediment transport and beach profile development*. Coastal Eng., 19: 57–96.

NIELSEN P. 1992. *Coastal bottom boundary layers and sediment transport*. Advanced Series on Ocean Engineering, 4.

O'CONNOR B.A., NICHOLSON J. 1989. *Modelling changes in coastal morphology*. In: *Sediment Transport Modeling*. Ed. S.S.Y. Wang. ASCE, pp. 160–165.

O'CONNOR B.A, PAN S., NICHOLSON J., MACDONALD N., HUNTLEY D.A. 1998. *A 2D model of waves and undertow in sufr zone*. Proc. Coastal Eng. ASCE, p. 286–296.

O'DONOGHUE T., WRIGHT S. 2004. *Flow tunnel measurements of velocities and sand flux in oscillatory sheet flow for well-sorted and graded sands*. Coastal Engineering, 51(11–12): 1163–1184.

PAWLUK K. 1984. *Segregacja materiału osadowego*. Prace wewnętrzne IBW PAN, Gdańsk.

PAWLUK K. 1990. *Materiał piaszczysty strefy brzegowej*. Studia i Materiały Oceanograficzne, 55.

PRUSZAK Z. 1998. *Dynamika brzegu i dna morskiego*. IBW PAN Gdańsk.

RENIERS A.J.H.M., ROELVINK J.A., WALSTRA D.J.R. 1995. *Validation study of UNIBEST-TC; validation against the LIP 11D experiment*. Report H2130, Delft Hydraulics.

RIBBERINK J.S. 1998. *Bed load transport for steady flows and unsteady oscillatory flows*. Coastal Engineering, 34: 59–82.

RIBBERINK J.S., AL-SALEM A. 1994. *Sediment transport in oscillatory boundary layers in cases of rippled beds and sheet flow*. Journal Geoph. Res., 99(C6): 2707–2727.

RIBBERINK J.S., CHEN Z. 1993. *Sediment transport of fine sand under asymmetric oscillatory flow*. Report H840, part VII, WL-Delft Hydraulics.

RIVERO F.J., SANCHEZ-ARCILLA A. 1993. *Propagation of linear gravity waves over slowly varying depth an currents*. In: *Waves'93* Eds. O.T. Magoon, J.M. Hamsley, Proc. 2nd International Symposium Ocean Wave Measurement and Analysis, New Orleans, ASCE, p. 518–532.

SAWCZYŃSKI S. 2012. *Bathymetry changes and sediment sorting within coastal structures: a case of the silting-up of navigation channels*. PhD thesis, University of Technology in Koszalin (in Polish).

SAWCZYŃSKI S., KACZMAREK L.M., BIEGOWSKI J. 2011. *Bathymetry changes and sand sorting during silting up of the channels*. Part 2. *Modelling versus laboratory data*. Technical Sciences, 14(2): 171–192.

SAYED M., SAVAGE S.B. 1983. *Rapid gravity flow of cohesionless granular materials down inclined chute*. J. Applied Mathematics and Physics (ZAMP), 34: 84–100.

SIERRA J.P., SANCHEZ-ARCILLA A. 1999. *CIIRC-LIM runs for Egmond Pilot Experiment*. Report RR-CIIRC/AHC-99-1, University of Catalunya, Spain.

SOUTHGATE H.N., NAIRN R.B. 1993. *Deterministic profile modelling of nearshore processes*. Part 1. *Waves and currents*. Coastal Engineering, 19(1–2): 27–56.

SVENDSEN I.A. 1984. *Mass flux and undertow in a surf zone*. Coastal Engineering, 8: 347–365.

ZHENG J.H. 2007. *Depth-dependent expression of obliquely incident wave induced radiation stress*. Progress in Natural Science, 17(9): 1067–1073.

ZHENG J.H., MASE H., DEMIRBILEK Z., LIN L. 2008. *Implementation and evaluation of alternative wave breaking formulas in a coastal spectral wave model*. Ocean Engineering, 35(11–12): 1090–1101.

VAN DER A D.A., O'DONOGHUE T., RIBBERINK J.S. 2010. *Measurements of sheet flow transport in acceleration-skewed oscillatory flow and comparison with practical formulations*. Coastal Engineering, 57Ł 331–342.

VAN RIJN L.C. 1993. *Principles of sediment transport in rivers, estuaries and coastal seas*. Aqua Publications, The Netherlands.

VAN RIJN L.C. 2000. *General view on sand transport by currents and waves*. Z2899.30, Delft Hydraulics, Delft, The Netherlands.

VAN RIJN L.C., WIJNBERG K.M. 1996. *One-dimensional modelling of individual waves and wave-induced longshore currents in the surf zone*. Coastal Engineering, 28: 121–145.

WATANABE A., RIHO Y., HORIKAWA K. 1980. *Beach profiles and on-offshore sediment transport*. Proc. 17 Conf. Coastal Eng. ASCE.

ZYSERMAN J.A., FREDSØE J. 1994. *Data analysis of bed concentration of suspended sediment*. J. Hydraul. Res., 120(9): 1021–1042.

Guide for Autors

Introduction

Technical Sciences is a peer-reviewed research Journal published in English by the Publishing House of the University of Warmia and Mazury in Olsztyn (Poland). Journal is published continually since 1998. Until 2010 Journal was published as a yearbook, in 2011 and 2012 it was published semiyearly. From 2013, the Journal is published quarterly in the spring, summer, fall, and winter.

The Journal covers basic and applied researches in the field of engineering and the physical sciences that represent advances in understanding or modeling of the performance of technical and/or biological systems. The Journal covers most branches of engineering science including biosystems engineering, civil engineering, environmental engineering, food engineering, geodesy and cartography, information technology, mechanical engineering, materials science, production engineering etc.

Papers may report the results of experiments, theoretical analyses, design of machines and mechanization systems, processes or processing methods, new materials, new measurements methods or new ideas in information technology.

The submitted manuscripts should have clear science content in methodology, results and discussion. Appropriate scientific and statistically sound experimental designs must be included in methodology and statistics must be employed in analyzing data to discuss the impact of test variables. Moreover there should be clear evidence provided on how the given results advance the area of engineering science. Mere confirmation of existing published data is not acceptable. Manuscripts should present results of completed works.

There are three types of papers: a) research papers (full length articles); b) short communications; c) review papers.

The Journal is published in the printed and electronic version. The electronic version is published on the website ahead of printed version of Technical Sciences.

Technical Sciences does not charge submission or page fees.

Types of paper

The following articles are accepted for publication:

Reviews

Reviews should present a focused aspect on a topic of current interest in the area of biosystems engineering, civil engineering, environmental engineering, food engineering, geodesy and cartography, information technology, mechanical engineering, materials science, production engineering etc. They should include all major findings and bring together reports from a number of sources. These critical reviews should draw out comparisons and conflicts between work, and provide an overview of the 'state of the art'. They should give objective assessments of the topic by citing relevant published work, and not merely present the opinions of individual authors or summarize only work carried out by the authors or by those with whom the authors agree. Undue speculations should also be avoided. Reviews generally should not exceed 6,000 words.

Research Papers

Research Papers are reports of complete, scientifically sound, original research which contributes new knowledge to its field. Papers should not exceed 5,000 words, including figures and tables.

Short Communications

Short Communications are research papers constituting a concise description of a limited investigation. They should be completely documented, both by reference list, and description of the experimental procedures. Short Communications should not occupy more than 2,000 words, including figures and tables.

Letters to the Editor

Letters to the Editor should concern with issues raised by articles recently published in scientific journals or by recent developments in the engineering area.

Contact details for submission

The paper should be sent to the Editorial Office, as a Microsoft Word file, by e-mail: techsci@uwm.edu.pl

Referees

Author/authors should suggest, the names, addresses and e-mail addresses of at least three potential referees. The editor retains the sole right to decide whether or not the suggested reviewers are used.

Submission declaration

After final acceptance of the manuscript, the corresponding author should send to the Editorial Office the author's declaration. Submission of an article implies that the work has not been published previously (except in the form of an abstract or as part of a published lecture or academic thesis or as an electronic preprint), that it is not under consideration for publication elsewhere, that publication is approved by all authors and tacitly or explicitly by the responsible authorities where the work was carried out, and that, if accepted, it will not be published elsewhere in the same form, in English or in any other language.

To prevent cases of ghostwriting and guest authorship, the author/authors of manuscripts is/are obliged to: (i) disclose the input of each author to the text (specifying their affiliations and contributions, i.e. who is the author of the concept, assumptions, methods, protocol, etc. used during the preparation of the text); (ii) disclose information about the funding sources for the article, the contribution of research institutions, associations and other entities.

Language

Authors should prepare the full manuscript i.e. title, abstract and the main text in English (American or British usage is accepted). Polish version of the manuscript is not required.

The file type

Text should be prepared in a word processor and saved in doc or docx file (MS Office).

Article structure

Suggested structure of the manuscript is as follows:

Title
Authors and affiliations
Corresponding author
Abstract
Keywords
Introduction
Material and Methods
Results and Discussion

Conclusions
Acknowledgements (*optional*)
References
Tables
Figures

Subdivision — numbered sections

Text should be organized into clearly defined and numbered sections and subsections (optionally). Sections and subsections should be numbered as 1. 2. 3. then 1.1 1.2 1.3 (then 1.1.1, 1.1.2, ...). The abstract should not be included in numbering section. A brief heading may be given to any subsection. Each heading should appear on its own separate line. A single line should separate paragraphs. Indentation should be used in each paragraph.

Font guidelines are as follows:
– Title: 14 pt. Times New Roman, bold, centered, with caps
– Author names and affiliations:12 pt. Times New Roman, bold, centered, italic, two blank line above
– Abstract: 10 pt. Times New Roman, full justified, one and a half space. Abstract should begin with the word Abstract immediately following the title block with one blank line in between. The word Abstract: 10 pt. Times New Roman, centered, indentation should be used
– Section Headings: Not numbered, 12 pt. Times New Roman, bold, centered; one blank line above
– Section Sub-headings: Numbered, 12 pt. Times New Roman, bold, italic, centered; one blank line above
– Regular text: 12 pt. Times New Roman, one and a half space,full justified, indentation should be used in each paragraph

Title page information

The following information should be placed at the first page:

Title

Concise and informative. If possible, authors should not use abbreviations and formulae.

Authors and affiliations

Author/authors' names should be presented below the title. The authors' affiliation addresses (department or college; university or company; city, state and zip code, country) should be placed below the names. Authors with the same affiliation must be grouped together on the same line with affiliation information following in a single block. Authors should indicate all affiliations with a lower-case superscript letter immediately after the author's name and in front of the appropriate address.

Corresponding author

It should be clearly indicated who will handle correspondence at all stages of refereeing and publication, also post-publication process. The e-mail address should be provided (footer, first page). Contact details must be kept up to date by the corresponding author.

Abstract

The abstract should have up to 100-150 words in length. A concise abstract is required. The abstract should state briefly the aim of the research, the principal results

and major conclusions. Abstract must be able to stand alone. Only abbreviations firmly established in the field may be eligible. Non-standard or uncommon abbreviations should be avoided, but if essential they must be defined at their first mention in the abstract itself.

Keywords

Immediately after the abstract, author/authors should provide a maximum of 6 keywords avoiding general, plural terms and multiple concepts (avoid, for example, 'and', 'of'). Author/authors should be sparing with abbreviations: only abbreviations firmly established in the field may be eligible.

Abbreviations

Author/authors should define abbreviations that are not standard in this field. Abbreviations must be defined at their first mention there. Author/authors should ensure consistency of abbreviations throughout the article.

Units

All units used in the paper should be consistent with the SI system of measurement. If other units are mentioned, author/authors should give their equivalent in SI.

Introduction

Literature sources should be appropriately selected and cited. A literature review should discuss published information in a particular subject area. Introduction should identify, describe and analyze related research that has already been done and summarize the state of art in the topic area. Author/authors should state clearly the objectives of the work and provide an adequate background.

Material and Methods

Author/authors should provide sufficient details to allow the work to be reproduced by other researchers. Methods already published should be indicated by a reference. A theory should extend, not repeat, the background to the article already dealt within the Introduction and lay the foundation for further work. Calculations should represent a practical development from a theoretical basis.

Results and Discussion

Results should be clear and concise. Discussion should explore the significance of the results of the work, not repeat them. A combined Results and Discussion section is often appropriate.

Conclusions

The main conclusions of the study may be presented in a Conclusions section, which may stand alone or form a subsection of a Results and Discussion section.

Acknowledgements

Author/authors should include acknowledgements in a separate section at the end of the manuscript before the references. Author/authors should not include them on the title page, as a footnote to the title or otherwise. Individuals who provided help during the research study should be listed in this section.

Artwork
General points

– Make sure you use uniform lettering and sizing of your original artwork

– Embed the used fonts if the application provides that option
– Aim to use the following fonts in your illustrations: Arial, Courier, Times New Roman, Symbol
– Number equations, tables and figures according to their sequence in the text
– Size the illustrations close to the desired dimensions of the printed version

Formats

If your electronic artwork is created in a Microsoft Office application (Word, PowerPoint, Excel) then please supply 'as is' in the native document format

Regardless of the application used other than Microsoft Office, when your electronic artwork is finalized, please 'Save as' or convert the images to one of the following formats (note the resolution requirements given below):

EPS (or PDF): Vector drawings, embed all used fonts

JPEG: Color or grayscale photographs (halftones), keep to a minimum of 300 dpi

JPEG: Bitmapped (pure black & white pixels) line drawings, keep to a minimum of 1000 dpi or combinations bitmapped line/half-tone (color or grayscale), keep to a minimum of 500 dpi

Please **do not**:
– Supply files that are optimized for screen use (e.g., GIF, BMP, PICT, WPG); these typically have a low number of pixels and limited set of colors
– Supply files that are too low in resolution
– Submit graphics that are disproportionately large for the content

Color artwork

Author/authors should make sure that artwork files are in an acceptable format (JPEG, EPS PDF, or MS Office files) and with the correct resolution. If, together with manuscript, author/authors submit color figures then Technical Sciences will ensure that these figures will appear in color on the web as well as in the printed version at no additional charge.

Tables, figures, and equations

Tables, figures, and equations/formulae should be identified and numbered consecutively in accordance with their appearance in the text.

Equations/mathematical and physical formulae should be presented in the main text, while tables and figures should be presented at the end of file (after References section). Mathematical and physical formulae should be presented in the MS Word formula editor.

All types of figures can be black/white or color. Author/authors should ensure that each figure is numbered and has a caption. A caption should be placed below the figure. Figure must be able to stand alone (explanation of all symbols and abbreviations used in figure is required). Units must be always included. It is noted that figure and table numbering should be independent.

Tables should be numbered consecutively in accordance with their appearance in the text. Table caption should be placed above the table. Footnotes to tables should be placed below the table body and indicated with superscript lowercase letters. Vertical rules should be avoided. Author/authors should ensure that the data presented in tables do not duplicate results described in figures, diagrams, schemes, etc. Table must be able to stand alone (explanation of all symbols and abbreviations used in table is required). Units must be always included. As above, figure and table numbering should be independent.

References

References: All publications cited in the text should be presented in a list of references following the text of the manuscript. The manuscript should be carefully checked to ensure that the spelling of authors' names and dates of publications are exactly the same in the text as in the reference list. Authors should ensure that each reference cited in the text is also present in the reference list (and vice versa).

Citations may be made directly (or parenthetically). All citations in the text should refer to:

1. Single author

The author's name (without initials, with caps, unless there is ambiguity) and the year of publication should appear in the text

2. Two authors

Both authors' names (without initials, with caps) and the year of publication should appear in the text

3. Three or more authors

First author's name followed by et al. and the year of publication should appear in the text

Groups of references should be listed first alphabetically, then chronologically.

Examples:

"... have been reported recently (ALLAN, 1996a, 1996b, 1999; ALLAN and JONES, 1995). KRAMER et al. (2000) have recently shown..."

The list of references should be arranged alphabetically by authors' names, then further sorted chronologically if necessary. More than once reference from the same author(s) in the same year must be identified by the letters "a", "b", "c" etc., placed after the year of publication.

References should be given in the following form:

KUMBHAR B.K., AGARVAL R.S., DAS K. 1981. *Thermal properties of fresh and frozen fish.* International Journal of Refrigeration, 4(3), 143–146.

MACHADO M.F., OLIVEIRA F.A.R., GEKAS V. 1997. *Modelling water uptake and soluble solids losses by puffed breakfast cereal immersed in water or milk*. In Proceedings of the Seventh International Congress on Engineering and Food, Brighton, UK.

NETER J., KUTNER M.H., NACHTSCHEIM C.J., WASSERMAN W. 1966. *Applied linear statistical models* (4th ed., pp. 1289–1293). Irwin, Chicago.

THOMSON F.M. 1984. *Storage of particulate solids*. In M. E. Fayed, L. Otten (Eds.), Handbook of Powder Science and Technology (pp. 365–463). Van Nostrand Reinhold, New York.

Citation of a reference as 'in press' implies that the item has been accepted for publication.

Note that the full names of Journals should appear in reference list.

Submission checklist

The following list will be useful during the final checking of an article prior to the submission. Before sending the manuscript to the Journal for review, author/authors should ensure that the following items are present:

– Text is prepared with a word processor and saved in DOC or DOCX file (MS Office). One author has been designated as the corresponding author with contact details: e-mail address

– Manuscript has been 'spell-checked' and 'grammar-checked'

– References are in the correct format for this Journal

– All references mentioned in the Reference list are cited in the text, and vice versa

– Author/authors does/do not supply files that are too low in resolution

– Author/authors does/do not submit graphics that are disproportionately large for the content